Research Report
KTC-99-22

LABORATORY TESTING AND ANALYSIS OF JOINTS FOR RIGID PAVEMENTS

by

Chelliah Madasamy
Visiting Research Professor

Issam E. Harik
Professor of Civil Engineering

David L. Allen
Transportation Research Engineer

and

L. John Fleckenstein
Principal Research Investigator

Kentucky Transportation Center
College of Engineering
University of Kentucky
Lexington, Kentucky

in cooperation with
Kentucky Transportation Cabinet
Commonwealth of Kentucky

and

Federal Highway Administration
U.S. Department of Transportation

May 1999

Technical Report Documentation Page

1. Report No. KTC-99-22	2. Government Accession No.	3. Recipient's Catalog No.

4. Title and Subtitle

Laboratory Testing and Analysis of Joints for Rigid Pavements

5. Report Date
May 1999

6. Performing Organization Code

7. Author(s)
Chelliah Madasamy, Issam E. Harik, David L. Allen, L. John Fleckenstein

8. Performing Organization Report No.
KTC-99-22

9. Performing Organization Name and Address

Kentucky Transportation Center
College of Engineering
University of Kentucky
Lexington, KY 40506-0281

10. Work Unit No. (TRAIS)

11. Contract or Grant No.
KYSPR-96-171

12. Sponsoring Agency Name and Address
Kentucky Transportation Cabinet
State Office Building
Frankfort Kentucky 40622

13. Type of Report and Period Covered
Final

14. Sponsoring Agency Code

15. Supplementary Notes
Publication of this report was sponsored by the Kentucky Transportation Cabinet

16. Abstract

The primary objective of this study was to analyze the concrete pavement system under nonlinear temperature distribution and vehicle wheel loading. The jointed concrete pavement system consists of concrete slabs with transverse and longitudinal joints, dowel bars (across transverse joints), tie bars (across longitudinal joints), subbase and subgrade soil. Under the loading conditions the pavement structural system may fail by cracking of the concrete slab, loss--of-support of slab due to temperature induced curling, closing and opening of joints, and failure of load transfer devices such as dowel bars, etc. In order to understand the cause of these failures or to achieve an economical design, the state of stress in the pavement system should be determined. It is very difficult to predict the stresses accurately in the pavement system with discontinuities and complex support conditions using conventional classical methods. Therefore, this project uses the ANSYS finite element software.

A literature review was performed to identify and evolve an accurate finite element model. It was found from this review that there were difficulties in incorporating the dowel-concrete interface, loss-of-support, contact conditions at the joints, nonlinear temperature distribution, etc. Since there has been no systematic comparison between the experiment and theoretical analysis in the past, the present study conducted the following laboratory testing to determine the respective stiffness quantities: (1) Doweled concrete blocks under bending and shear load, (2) Concrete blocks with tie bars under bending and shear load, (3) Concrete blocks with aggregate interlock joints under shear load, and (4) Concrete blocks with sealed joints under shear load The stiffness values derived from these testing procedures is to be used in the evolution of a finite element model for the concrete pavement system.

In addition to this, it is recommended that field measurement of temperature distribution through the thickness of the slab be performed. Finally, a full-scale field testing using FWD is also recommended. The test results obtained from this full-scale testing could be used to assess the validity of the finite element model.

17. Key Words	18. Distribution Statement
Pavement Joints Rigid Pavements	Unlimited

19. Security Classif. (of this report)	20. Security Classif. (of this page)	21. No. of Pages	22. Price
Unclassified	Unclassified		

TABLE OF CONTENTS

EXECUTIVE SUMMARY

The primary objective of this study was to analyze the concrete pavement system under nonlinear temperature distribution and vehicle wheel loading. The jointed concrete pavement system consists of concrete slabs with transverse and longitudinal joints, dowel bars (across transverse joints), tie bars (across longitudinal joints), subbase and subgrade soil. Under the loading conditions the pavement structural system may fail by cracking of the concrete slab, loss--of-support of slab due to temperature induced curling, closing and opening of joints, and failure of load transfer devices such as dowel bars, etc. In order to understand the cause of these failures or to achieve an economical design, the state of stress in the pavement system should be determined. It is very difficult to predict the stresses accurately in the pavement system with discontinuities and complex support conditions using conventional classical methods. Therefore, this project uses the ANSYS finite element software.

A literature review was performed to identify and evolve an accurate finite element model. It was found from this review that there were difficulties in incorporating the dowel-concrete interface, loss-of-support, contact conditions at the joints, nonlinear temperature distribution, etc. Since there has been no systematic comparison between the experiment and theoretical analysis in the past, the present study conducted the following laboratory testing to determine the respective stiffness quantities. The stiffness values derived from these testing procedures is to be used in the evolution of a finite element model for the concrete pavement system.

- Doweled concrete blocks under bending and shear load
- Concrete blocks with tie bars under bending and shear load
- Concrete blocks with aggregate interlock joints under shear load
- Concrete blocks with sealed joints under shear load

In addition to this, it is recommended that field measurement of temperature distribution through the thickness of the slab be performed. Finally, a full-scale field testing using FWD is also recommended. The test results obtained from this full-scale testing could be used to assess the validity of the finite element model.

1.0 INTRODUCTION

1.1 General

The American Association of State Highway and Transportation Officials (AASHTO) is currently developing a mechanistically-based rigid pavement design model. It is understodd that this model is based on a three-dimensional finite element analysis. A design procedure based on this model is to be published in the 2002 version of the *"AASHTO Pavement Design Guide"*. It is currently anticipated that Kentucky will adopt all or part of this design system for rigid pavements. However, to adopt this system, it would be most beneficial if the model could be calibrated to Kentucky conditions. Some of those conditions would be environmental, temperature distributions in the slabs, soils, joint design and spacing, loading patterns, failure criteria as related to many of these factors, and other parameters.

The analysis and modeling of rigid pavements in Kentucky has not advanced to the point where the in-situ properties of the pavement structure can be determined. In addition, environmental effects including temperature induced curling and warping which occur during the daily temperature variations cannot be adequately evaluated. The present design procedures do not contain a mechanism to evaluate the doweled joints. These areas are generally associated with the majority of rigid pavement distresses and should be evaluated. This study was initiated to provide background data (developed from a laboratory testing program) to determine many of the joint parameters necessary to analyze rigid pavement behavior.

Pavement design may be defined as *the determination of structural, material and drainage characteristics and dimensions of the pavement/subgrade structure(including all components of the pavement) through direct analytical consideration of the traffic and climatic loads that the pavement/subgrade structure is expected to be subjected to over a selected design period.*

In general, a jointed plain concrete pavement system can be divided into a number of components, namely, concrete slab, transverse and longitudinal joints, load transfer devices (dowel bars) and tie bars, subbase and subgrade soil supporting the slab. This pavement system may be subjected to the following loading conditions: vehicle wheel loads, self-weight of the slab, and environmental loadings (temperature and moisture). Under the above loading conditions the pavement system may experience cracking of the concrete slab, loss of support of slab due to temperature induced curling, closing and opening of joints along transverse and longitudinal directions, and failure of load transfer devices such as dowel bars.

Plain concrete pavement systems, as shown in Figure 1.1, are commonly constructed with joints, dowel bars and tie bars. The presence of such structural discontinuities create difficulties while analyzing the pavements using conventional methods. This is further complicated by the presence of nonlinear temperature distribution through the thickness, in addition to complex support conditions. To analyze such complex systems, one has to adopt numerical technique such as the

finite element method (FEM) for an accurate prediction of behavior of jointed pavements. The application of FEM for the analysis of pavements require a prior estimation of the stiffnesses of dowel bars, tie bars, joints with aggregate interlock, and also the interface friction between slab and subgrade. FEM has been applied to the analysis of pavements by many researchers in the past and some of the works which are relevant to the present study are discussed in the following sections.

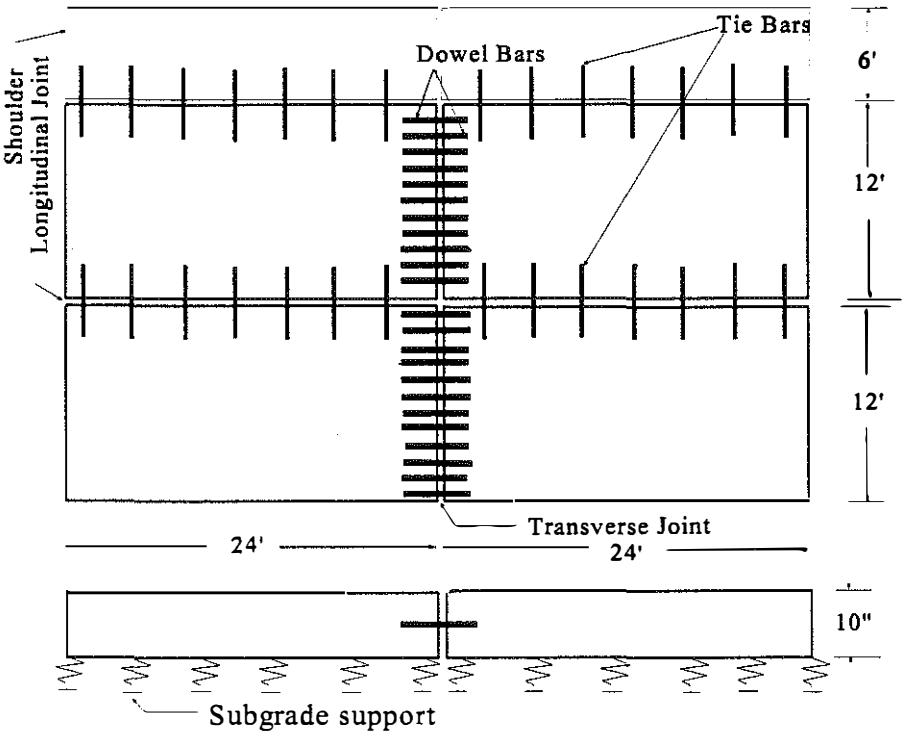

Figure 1.1 Jointed Plain Concrete Pavement

Recently, some research works have been performed to apply fiber composite dowel bars as an alternative to steel dowels in concrete pavements. The fiber composite dowels have been found to perform better in corrosive environments and also gives longer fatigue life. However, there was no improvement in the shear load-transfer capacity with fiber composite dowels over steel dowels.

1. 2 Two Dimensional Analysis Models

Traditionally plain steel or epoxy coated steel has been used for dowel bars in concrete pavements. Grieef (1996) conducted experiments to determine the feasibility of using Isorod®, a glass fiber reinforced plastic, as dowels in concrete pavements. A total of eight push-off specimens were tested with either steel or Isorod® dowels that were either partially bonded or not bonded to the concrete. The tested specimens were designed to apply a pure shear load to the dowels to determine their behavior and strength. From the experiments, it is found that the Isorod® dowels are not as stiff as the steel dowels in the pre-kinking stage and also experienced a decrease in load-carrying capacity after kinking began.

Khazanovich and Ioannides (199*) described the incorporation of the two-parameter, Kerr and Zhemochkin-Sinitsyn-Shtaerman subgrade models into finite element code ILLI-SLAB. The two conventional idealizations, namely the dense liquid and elastic solid, are also available in the program library. The size of the loaded area has been found as an important parameter.

Kukreti (1992) et al. presented a finite element procedure for the dynamic analysis of rigid airport pavements with discontinuities. The analysis procedure considers the dynamic interaction between aircraft and a rigid pavement. The rigid pavement is modeled as a series of discontinuous, thin-plate, finite elements resting on a viscoelastic foundation. At the discontinuities, load-transfer devices are modeled as vertical springs, the stiffness of which depends on the dowel properties and the dowel-concrete-interaction. The viscoelastic foundation is modeled by distributed springs and dashpots. The moving aircraft loads are represented by masses supported by linear spring and dashpot systems, which have specified horizontal velocities and accelerations.

Ioannides and salsilli-murua (1989) presented a closed-form solution to the problem of a slab-on-grade under combined temperature and wheel loading, derived on the basis of finite element results. This solution is in the form of a multiplication factor to be applied to the Westergaard equation to determine the maximum combined tensile stresses in the slab under edge loading. In addition, a sound engineering approach to numerical, experimental, and field data interpretation is proposed, founded on the principles of dimensional analysis.

Mirambell (1990) presented an analytical model capable of predicting temperature and stress distributions due to thermal and mechanical loads in concrete pavements as well as thermal actions to be considered in design. Temperature distribution in concrete pavements are, in general, nonlinear and induce self-equilibrated stress distributions. Such stress distributions depend on the physical and thermal properties of concrete, geographical location of the pavement and existing environmental conditions (solar radiation, air temperature, wind speed, etc...). On the other hand, temperature gradients across slab depth, associated with thermal effects, also induce prescribed curvatures to the slab, which can generate continuity stresses depending on boundary conditions.

Harik et al. (1994) developed an analysis technique to be used in conjunction with the finite element programs for the study of rigid pavements subjected to temperature loading. The pavement is idealized as a thin isotropic plate resting on a Winkler-type elastic foundation. Since two-dimensional elements are limited to linear temperature distribution through the thickness, the advantage of the proposed method lies in its capability to superimpose the effect of the nonlinear temperature distribution on the finite element solution. Shi et al. (1993) developed a solution of warping stresses in concrete pavement slabs resting on a Pasternak foundation. The solution is derived using the classical thin-plate theory.

Channakesava et al. (1993) developed a finite element method for the nonlinear static analysis of jointed concrete pavements. In this method, the pavement slab was modeled using 3D-solid elements and subgrade was modeled using spring elements. They have analyzed pavements under thermal gradient and wheel loadings. The nonlinearities due to cracking and yielding of concrete, and loss of support have been properly accounted. The dowel bars were modeled using beam elements and the interaction between dowel and concrete was modeled using interface spring elements. The interface spring stiffness was computed using a detailed FEM model of a small concrete block with one dowel bar under shear load. Although this model does not consider the

subgrade in detail, it can capture the stress patterns induced by nonlinear temperature conditions through the thickness and cracking of concrete. This method does not account for the inertia effects of wheel loading. The size of the finite element model by this method is less compared to Zaghioul and White (1993).

Choubane and Tia (1995) have performed an experimental and analytical study to develop a method for the analysis of pavements under nonlinear thermal loadings. They have indicated that the temperature distributions were mostly nonlinear and can be represented fairly well by a quadratic equation. The pavement system was analyzed using rectangular plate bending elements to model slab, and linear and rotational springs to model the load transfer devices. The stresses due to the nonlinear component of temperature were computed externally and superimposed on the results from the other loading conditions by FEM. The measured strains were found to be close to the computed results. Although the analytical method is simple and economical to use, it does not account for the nonlinearities associated with cracking of concrete, loss of support due to temperature induced curling.

Zaman et al. (1993) have developed a FEM algorithm for analyzing the dynamic response of rigid airport pavements subjected to warping due to temperature gradients and traversing aircraft. This pavement was modeled using thin plate elements supported on uniformly distributed springs and dashpots representing the viscoelastic foundation. At the transverse joints, dowel bars were modeled by grid elements. They have studied the effect of transverse joint, temperature gradient and the modulus of subgrade. However the effect of a nonlinear temperature distribution can't be accounted for using this method.

Zaman and Alvapillai (1995) have developed FEM for the dynamic analysis of jointed concrete pavements. The concrete slab was modeled using plate bending elements and the subgrade was modeled using spring and dashpot system. The dowel bars were modeled using plane frame elements and the interaction between concrete and dowel bars was modeled by contact elements. The results of the analysis have been compared with the analytical results available in the literature. Although this method considers the dynamic interaction effects of aircraft and pavement, it does not account for the nonlinearities due to cracking of concrete. Nonlinear temperature distribution through the thickness can't be accounted for with the plate element.

Taheri and Zaman(1995) developed a dynamic analysis procedure based on a finite element algorithm to study the response of rigid airport pavements to a traversing aircraft and a temperature gradient along the depth. The rigid pavement is modeled as a thin plate finite elements. The subgrade medium is idealized as a viscoelastic foundation. The traversing aircraft is modeled by spring and dashpot suspension systems.

Nishizawa et al. (1989) developed a refined dowel element for the linear static FEM analysis of jointed concrete pavements. Aggregate interlocking was modeled using shear springs and plate bending elements to model slabs. They have concluded that the refined dowel element performs better than the spring and bar element for various dowel diameters. Results of the analysis have been found to agree with model and full-scale experiments. This method does not consider the thermal loadings and nonlinearity induced by cracking of concrete and loss of support due to curling.

Guo et al. (1995) developed a component dowel bar model for the linear static analysis of

pavement by FEM. Plate bending element was used to model the pavement slab. The dowel bar was modeled by three segments of beam: two bending segments embedded in concrete and one shear-bending segment in the joint. A comparison of results of analytical and experimental results showed that the component dowel bar model can be used to reasonably simulate the behavior of dowel load-transfer systems. This method does not account for the thermal loadings, nonlinearities associated with the cracking of concrete and loss of support due to curling.

The study of factors that affect dowel looseness in jointed concrete pavements was performed by Buch and Zollinger (1996). The laboratory investigation revealed the influence of aggregate type, texture and shape, bearing stress (dowel diameter and crack width), load magnitude, and number of load cycles on the magnitude of dowel looseness and the subsequent loss in load transfer efficiency across saw-cut joints. A discussion is included on the development of an empirical-mechanistic dowel looseness prediction model based on the experimental results. The sequential use of the dowel looseness prediction model and its relationship to load transfer efficiency allows the design engineer to predict load transfer characteristics of a joint, based on calculated (or measured) dowel looseness.

A recent search of the archives at the Waterways Experiment Station revealed that shortly before his untimely death in 1950, Westergaard had contracted with the Ohio River Division Laboratories of the Corps of Engineers to develop an analytical solution to the problem of edge load transfer in PCC pavements. A young Greek engineer, Mikhail S.Skarlatos, worked on the project with Westergaard and produced an elegant formulation for this problem based on Westergaard's 1923 paper. The Skarlatos solution was never implemented in practical design, however, due to a number of factors, including Westergaard's death and repatriation to Greece of Skarlatos, who continues to practice civil engineering. Using the commercial mathematical software Mathematica and statistical software SigmaStat and TBLCURVE, closed-form solutions akin to those by Westergaard were derived in this study for the maximum responses on the unloaded side of a PCC pavement slab edge capable of a degree of load transfer.

Nishizawa et al. (1996) has developed a curling stress equation for transverse joint edge of a concrete pavement slab based on an FEM analysis. In the design of concrete pavement, curling stresses caused by the temperature difference between the top and bottom surfaces of the slab should be calculated at the transverse joint edge in some cases. However, no such equation has been developed in the past. Accordingly, a curling stress equation was developed based on stress analysis using the finite element method. In this analysis, a concrete pavement and its transverse joint were expressed by means of a thin plate-Winkler foundation model and a spring joint model, respectively. Multiregression analysis was applied to the results of the FEM numerical calculation and, consequently, a curling stress equation was obtained.

Lee and Lee (1996) used the ILLI-SLAB finite element program to analyze the critical comer stresses of concrete pavements under different loading conditions. Subsequently, the effects of a finite slab size, different gear configurations, a widened outer lane, a tied concrete shoulder, and a second bonded or unbonded layer were considered. Based on the principles of dimensional analysis and experimental designs, the dominating mechanistic variables were carefully identified and verified. A new regression technique (Projection pursuit regression) was used to develop prediction models to account for these theoretical differences and to instantly estimate the critical comer stresses.

Evaluation of the AASHTO rigid pavement design model using the long-term pavement performance data base was performed by Darter et al. (1996). The evaluation included determining the adequacy of predicting the number of heavy axle loads required to cause a given loss of serviceability. The results indicate that the original 1960 equation generally over predicts the number of 18kip axle repetitions. Their work improves predictions considerably.

Jiang et al. (1996) carried out a study on the analysis of current state rigid pavement design practices in the United States. Pavement types, design methodologies, and reliability levels are included, along with many design inputs. Ioannides and Korovesis (1990) conducted an FEM investigation on the behavior of jointed or cracked pavement systems equipped with a pure-shear load transfer mechanism, such as aggregate interlock. A dimensional analysis was used in the interpretation of data, leading to a general definition of the relative joint stiffness of the pavement system in terms of its structural characteristics. The investigation demonstrated that deflection load transfer efficiency is related to stress load transfer efficiency and that this relationship is sensitive to the size of the applied loading. Pure shear load transfer devices are shown to be particularly desirable under a combined externally applied and thermal loading condition, since they offer no additional restraint to longitudinal curling.

Ioannides et al. (1990) developed mechanistic-empirical algorithms for more realistic estimates of anticipated faulting in concrete pavements. A factor influencing faulting is the dowel-concrete bearing stress, for which an improved method of determination is presented. Ioannides and Korovesis (1992) provided an in-depth synthesis of knowledge acquired over the last several decades pertaining to the analysis and design of doweled slab-on-grade pavement systems. This task relies extensively on the application of dimensional analysis for the interpretation of finite element data pertaining to the behavior of doweled joints. A design procedure is developed that follows, for the first time, the determination of the dowel diameter and spacing required to achieve a desired level of load transfer, or a threshold value of dowel-concrete bearing stress. An efficient and general method for the backcalculation of the modulus of dowel reaction, K, from deflection data is also suggested.

Hall et al. (1995) developed improved guidelines for determining k value from a variety of methods , including correlations with soil type, soil properties, and other tests; backcalculation methods; and plate-bearing test methods. Guidelines for seasonal adjustment to k, and adjustments for embankments and shallow rigid layers were also developed. Chou (1995) has established relationships between joint efficiency and load transfer for jointed plain concrete pavements using the finite element method ILLI-SLAB program. Efforts were made to show that the relationships depend not only on a/l but also on L/l, where L is the size of the square concrete slabs. FEM have been used to estimate load transfer from measured deflections of FWD tests.

Tabatabaie and Barenberg (1980) developed a finite element program ILLI-SLAB based on the classical theory of medium-thick plates on a Winkler foundation for the analysis of one and two layered concrete pavements with joints or cracks on a Winkler foundation, or both. The model is capable of evaluating the effect of various load transfer systems such as dowel bars, aggregate interlock, and keyways on the stresses and deflections in concrete pavements. Furthermore, the model, which provides several options, can be used for analysis of a number of problems such as jointed reinforced concrete pavements with cracks, continuously reinforced concrete pavements, concrete slab with a stabilized base or an overlay, concrete shoulders, and slabs with varying

thicknesses and varying support conditions.

Larralde and Chen (1986) presented a method to estimate the mechanical deterioration of highway rigid pavements caused by repetitive traffic loading. In the method, erosion, fatigue, and joint faulting are recognized as mechanisms of failure in highway rigid pavements. A nonlinear analysis with finite elements is used to calculate the repetitive stresses and strains caused by traffic. Decay of slab stiffness and load transfer efficiency, as well as pumping and amount of damage, are obtained as a function of traffic volume and pavement properties.

Krauthammer and Western (1988) presented a procedure for analyzing joint shear transfer effects on pavement behavior, based on the finite element method. This approach employed an explicit-shear/stress-shear slip relationship for defining the shear transfer across a pavement joint, and the model was subjected to simulated FWD loads for the analyses. The pavement systems were classified according to four material quality groups and several shear transfer levels across the joint.

1.3 Three Dimensional Analysis Models

Zaghioul and White (1993) performed a nonlinear analysis of concrete pavements under static and dynamic loading conditions using the well-known finite element software ABAQUS. In this study, the pavement slab and subgrade were modeled using 3-D solid elements. Longitudinal and transverse joints were modeled using gap elements in which the initial joint opening was specified. The dowels and tie bars across the joints were modeled as rebar elements located at the mid-thickness of the slab. For dowel bars, the bond stress at one side was assumed to be zero to allow a relative horizontal movement between the slabs. The nonlinearity of concrete and subgrade were considered using the nonlinear material model provided in the ABAQUS software. Though it is possible, the nonlinearities due to temperature induced curling have not been taken into account in their analysis. The static and dynamic analysis results have been compared with the experimental results. They have studied the effects of moving load speed, load position, subbase course, dowel bars, joint width, axle loads and slab thickness. This method of modeling requires a very large FE mesh and hence leads to larger computer storage and more time.

Kuo et al. (1995) developed a three-dimensional finite element model for the analysis of concrete pavement support to analyze the many complex and interacting factors that influence the support provided to a concrete pavement, including foundation support (k value), base thickness, stiffness, and interface bond and friction; slab curling and warping due to temperature and moisture gradients; dowel and aggregate interlock load transfer action at joints; and improved support with a widened lane, widened base, or tied concrete shoulder. The ABAQUS general purpose software was used to develop a powerful and versatile 3-D model for analysis of concrete pavements. The 3-D model was validated by comparison with deflections and strains measured under traffic loadings and temperature variations at the AASHTO road test, the Airlington road test, and the Portland Cement Association's slab experiments.

Uddin et al. (1995) conducted a research study using the finite element code ABAQUS to investigate the effects of pavement discontinuities on the surface deflection response of a jointed plain concrete pavement-subgrade model subjected to a standard falling weight deflectometer load. Transverse joints with dowel bars are modeled using gap and beam elements for an uncracked

section, a section with cracked concrete layer, and a section with cracked concrete and cracked cement-treated base layers.

In almost all linear elastostatic programs used in backcalculation procedures, a uniform pressure distribution is assumed for the applied load. As such, the loading system of any falling weight deflectometer should be designed so that the load transferred to the pavement is uniform. This is difficult because the pressure distribution under the FWD is also affected by the pavement profile being tested. The other aspect of the FWD testing that is typically ignored is the dynamic nature of the load. The dynamic effects are related to the pulse width as well as the variation in the stiffness of the subgrade. A finite element study has been carried out by Nazarian and Bodapati (1995) to investigate the significance of these parameters on the determination of the remaining lives of pavements.

1.4. Scope of the Work

In all the previous the finite element models generated for parametric studies were not properly validated using laboratory and experimental studies. Therefore, in this work, a systematic experimental and theoretical (FEM) investigations on jointed plain concrete highway pavement systems will be conducted. The results of this study will be presented in the form of design aids for practical use.

In this present project, testing was performed on small concrete blocks in the laboratory. Futhermore, it is recommended that the following tasks be performed in the future: (1) Field testing on full pavement systems and measurement of temperature, (2) Development of structural finite element model , (3) Finite element model calibration, (4) Parametric studies, and (5) Preparation of design aids.

The laboratory work includes testing on doweled concrete blocks under bending moment and shear load to derive the respective stiffness. One end of the dowel bar is free to slide and the other end is fully bonded. The concrete blocks joined by tie bars will be tested under bending moment and shear load to derive the stiffness of tie bar embedded in the slab. Both ends of the tie bar is fully bonded to the concrete blocks, in this case. Testing will also be done on concrete blocks with aggregate interlock joints under shear load to derive their stiffness. The axial stiffness of joint sealants between the concrete blocks will be determined under axial loading.

The further field testing should include the measurement of day and night-time temperature profile along the thickness of the pavement slab. Testing on pavement slab to determine the frictional resistance provided by the subgrade to the slab under thermal deformations. Falling Weight Deflectometer (FWD) testing on the full pavement system to calibrate a possible finite element model.

The structural modeling should include a global finite element model using layered shell elements, beam elements, compression only elements for subgrade support and contact elements for modeling joints should be developed. A local model using 3-D solid elements and beam elements to study the results of laboratory testing should be developed. A feasibility analysis has already been

performed using the ANSYS finite element software to solve pavement problems reported in the literature.

The model calibration should include the derivation of stiffness quantities for dowel bars, tie bars, aggregate interlock joints, interface friction from the load deflection obtained from laboratory and field testing, incorporating the stiffness values in the global finite element model, and calibrating the model with the falling weight deflectometer test results.

The parametric studies would involve an analytical study to determine the influence of the following parameters on the structural performance of pavements: (1) size and spacing of dowel and tie bars, (2) thickness of concrete pavement slab, (3) temperature profile along the thickness of slab, (4) joint width, (5) wheel loading position, (6) subgrade modulus, and (7) shoulder width and thickness.

Upon completion of those tasks, design curves could be prepared based on the parametric studies.

2.0 LABORATORY TESTING

2.1 General

2.1.1 Dowel Bars

Dowel bars are commonly used as major load-transfer devices at transverse joints of plain concrete pavements. In practice, the size, length and spacing of dowels vary depending upon the thickness of pavements, wheel loading, etc. However, most highway pavements use a steel dowel of diameter of 1.25" to 1.75", spaced at 1-foot intervals with a length of each dowel from 18" to 24". The width of joints with dowels commonly used in highway pavements is around 3/8". Dowels are embedded in the concrete slab with full bond (non-greased) at one end and other end is unbonded (greased) and coated with epoxy to allow longitudinal movement during thermal expansion/contraction.

A dowel bar in pavements can undergo shear and bending deformations under wheel loading. Although, shear is the dominant mode of deformation, evaluation of bending stiffness of doweled systems will result in a complete description of the deformation field. Theoretical evaluation of stiffness of dowels becomes difficult due to the interaction of concrete and dowel. Therefore, in this work, independent testing was performed to estimate the stiffnesses of dowel bars, tie bars and aggregate interlock.

2.1.2 Tie Bars

Tie bars are mainly used in longitudinal joints to simulate a hinged joint. These joints relieve stresses developed due to thermal warping. Unlike dowel bars, the tie bars are usually constructed with full bond on both ends of the bar. The tie bars used in highway pavements have diameter 1/2" to 5/8", with a length of 20" to 33" and a spacing of 23" to 48". The width of the longitudinal joint is approximately 3/8". These tie bars are fully bonded to both concrete slabs, and therefore, the connected slabs are not allowed to undergo thermal expansion/contraction. The tie bars are not designed as a load-transfer device. However, they may create local tensile stresses around the bar under wheel load or thermal warping and this can lead to cracking of the concrete. Therefore, the study of the state of stress in concrete around the tie bar is very important. Also, the measurement of relative deflection at joints, and shear and bending strain distribution along the length of the tie bar can be used for accurate modeling of tie bars. A similar experimental setup as explained earlier for dowel bars, and as shown in Figs.2a-b and 3a-b, was adopted for testing concrete blocks with tie bars.

2.1.3 Specimen Preparation

The mold for casting concrete pavement specimens is shown in figure A.1. A closer look at the arrangement of dowel bar, strain gages, and filler for the joint is shown in figure A.2. The filler is removed before testing. Figure A.3 shows the molds for doweled concrete specimens without strain gages. The arrangement of the tie bar is shown in figure A.4. Concreting of the mold is shown

in figure A.5. The cylinder compressive strength of the concrete after 31 days was determined to be 4,521 psi. From the stress-strain curve, the modulus of elasticity of the concrete was calculated to be 4,464,276 psi. The specimen sizes and identification numbers for different loading situations are presented in the following sections.

2.2 Testing under shear load

In this testing, the doweled concrete blocks were subjected to shear load as shown in Fig. 2. The deflection at the dowel bar and at several locations in the concrete block was measured by LVDTs. By attaching strain gages along the dowel bar, bending strains were obtained. This testing is conducted to determine the shear stiffness of the dowel bar when one end of the bar is fully bonded to the concrete slab and the other end is free to move due to thermal loading. The moving end of the dowel bar is coated with epoxy paint to prevent locking due to corrosion. Similar testing was performed to determine the shear stiffness of the tie bar embedded in concrete. Both ends of the tie bar were fully bonded to the concrete. Tie bars are deformed bars of diameter ranging from 1/2" to 5/8". Displacements at the joint and strains in the vicinity of the dowel bar were measured. Table 2.1 describes the specimen designation for testing under shear load and Table 2.2 lists the geometric properties of the specimen measured before testing. In the test setup, shown in figure S3, springs were placed to prevent rotation of the loaded block. In figure S3, the labels for LVDT locations are as follows:

bfe = beam fixed end
js = joint spring side
ej = edge on jack side
jj = joint jack side
ec = edge near corner

Table 2.1 Specimen Designation (S-1 to S-9)

Loading : Shear
Size : 36" x 12" x 10" ; Joint Width = 1"
Half length of the Dowel bar should be greased; Rebar should not be greased.

	Dowel - 1.25" dia.			Dowel - 1.75" dia.			Rebar -1" dia.			Total Number of Specimens
SG*	No	No	Yes	No	No	Yes	No	No	Yes	
SIN**	S-1	S-2	S-3	S-4	S-5	S-6	S-7	S-8	S-9	9

*SG- Strain Gage
**SIN-Specimen Identification Number

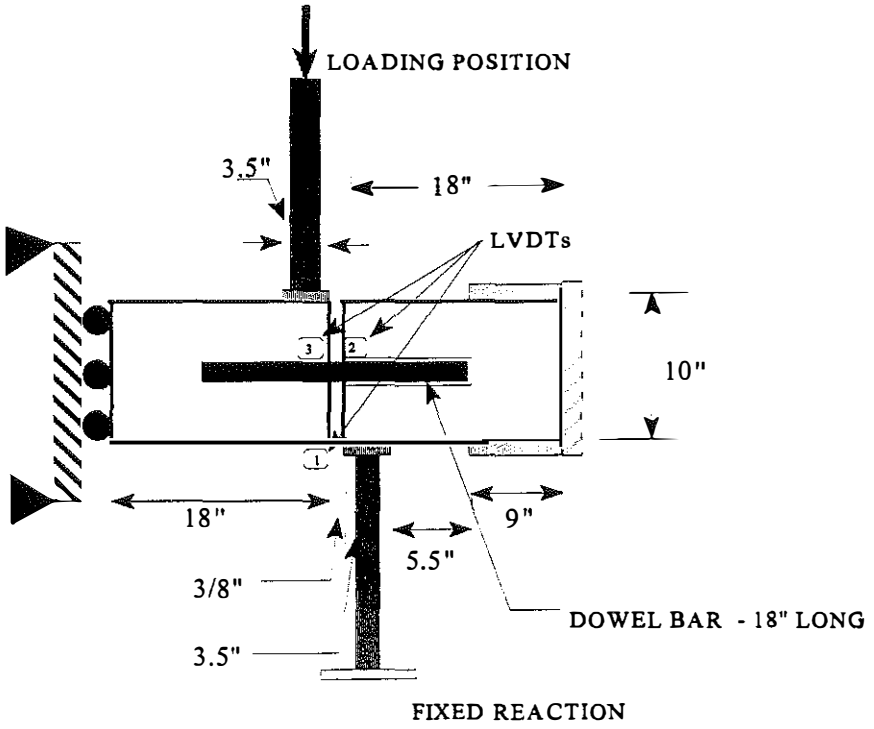

Figure 2.1 Setup for Shear Load Testing

Table 2.2

Geometric properties of shear loaded specimen (in)

Beam	Greased End			Non-Greased End		
	Height	Length	Width	Height	Length	Width
S1	12.000	17.500	9.813	12.250	17.500	9.750
S2	12.063	17.500	10.000	12.063	17.500	10.000
S3	12.000	17.563	9.875	12.063	17.500	9.875
S4	12.000	17.375	10.125	12.000	17.625	10.063
S5	12.125	17.625	10.125	12.188	17.375	10.000
S6	12.000	17.875	10.000	12.000	17.250	10.063
S7	12.000	17.500	10.000	12.000	17.625	10.125
S8	12.063	17.375	10.000	12.063	17.750	10.000
S9	12.000	17.438	10.000	12.000	17.563	9.750

2.2.1 Test Results

2.2.1a 1.25" Dowel Bars

Three specimens were tested for each dowel bar size. Every third specimen was instrumented with strain gages. The picture of the test setup for specimen S1 is shown in Figure A.6a. The load-displacement relationship for S1 is shown in Figure I.1. Displacements are plotted for locations described in Figure S3 for load levels up to 5,000 pounds. Maximum displacement of approximately 0.19" occurs at the sliding end of the pavement.

The testing arrangement for specimen S2 is shown in Figure A.6b. Figure I.2 shows the load-displacement behavior for specimen S2. Displacements at several locations as described in the figure S3 are plotted in this figure. Loading was applied to approximately 5,500 pounds. Maximum displacement at the edge near the joint was approximately 0.65", and at the joint-jack side, displacement was 0.2".

The load-displacement relationship for specimen S3 is shown in Figure I.3. The test setup is shown in Figure A.6c. Displacements at different locations, as shown in Figure, S3 are plotted. Maximum displacement at the edge near the comer is 0.475", at a failure load of 10,000 pounds. The axial strains at the top and bottom sides of the bar as described in Figure S3 is shown in Figure I.3b.

2.2.1b 1.75" Dowel Bars

The arrangement of testing for specimen S4 is shown in Figure A.7a-b. The load-displacement relationship for this specimen is shown in Figure I.4. Displacements at different locations (Fig. S3) are plotted in Figure I.4 for various loads until failure at 8,500 pounds.

The test setup for specimen S5 is shown in Figure A.7c. Figure I.5 shows the load-displacement relationship for this specimen. Displacements are plotted in this figure at various locations (Fig. S3) and loads until failure at 16,000 pounds.

The load-displacement relationship for specimen S6 is shown in Figure I.6a. Figure A.7d-e shows the arrangement of testing for this specimen. Displacements at different locations (Fig. S6)and loads are plotted in Figure I.6a until failure at 17,000 pounds. Figure I.6b shows the load-strain relationship for specimen S6 for the strain gages described in Figure I.6b.

2.2.1c 1" Rebars

The test setup for specimen S7 is shown in Figure A.8a. Figure I.7 shows the load-displacement relationship for this specimen. Displacements at different locations (Fig. S6) and loads are plotted in Figure I.7 up to failure at 8,500 pounds. Maximum displacement of 0.35" occurs at the edge-near joint.

The arrangement of testing for specimen S8 is shown in Figure A.8b. The load-displacement behavior for this specimen is shown in Figure I.8. Displacements at different locations (Fig. S6) and loads are plotted in Figure I.8 up to failure at 10,000 pounds. Maximum displacement of about 0.6"

occurs at the edge-near joint.

Figure I.9a shows the load-displacement behavior for the specimen S9. Displacements at different locations (Fig. S9) and loads are plotted in Figure I.9a up to failure at 7,500 pounds. Figure I.9b shows the load-strain relationship for specimen S9 , for the strain gages described in figure S9.

2.3 Testing under Bending Moment

Dowel bars may experience bending moments at the joints due mainly to thermal gradients and/or wheel loading. This testing was performed to determine the flexural stiffness of the dowel bar when one end of the bar is fully bonded to concrete and other end is free to move due to thermal loading. In the testing, the doweled concrete blocks were subjected to bending moment as shown in Figure 2.2. The deflection at the dowel bar level and at various locations on the concrete block were measured by LVDTs. By attaching strain gages along the dowel bar, bending strains were obtained.

Tie bars were also tested. Both ends of the tie bars were fully bonded to the concrete. Tie bars are deformed bars ranging from 1/2" to 5/8" in diameter. Displacements at the joint and strains near the bar were measured. Table 2.3 describes the specimen designation for testing under bending moment and Table 2.4 lists the geometric properties of the specimen measured before testing. Three specimens were tested for each dowel bar size and every third specimen is instrumented with strain gages. Only one size of tie bar was tested.

2.3.1 Test Results

2.3.1a 1.25" Dowel Bars

The photograph of the test setup for specimen B1 is shown in Figure A.9a. The load-displacement relationship for B1 is shown in Figure III.1a for various loads at the non-greased side, up to approximately about 2,000 pounds. Maximum displacements of approximately 1" was noted at the greased joint. Figure III.1b shows the load-displacement relationship for specimen B1 at the greased side.

The arrangement of testing for specimen B2 is shown in Figure A.9b. Figure III.2a shows the load-displacement relationship for B2 for various loads at the non-greased side up to approximately 2,500 pounds. Maximum displacement of approximately 1" was observed at the greased joint. Similarly, Figure III.2b shows the load-displacement relationship for the greased side.

Figure A.9c shows the test setup for specimen B3. The load-displacement behavior for this specimen is shown in Figure III.3a for loads at the non-greased side to approximately 2,000 pounds. Maximum displacement was approximately 1.25" at the greased joint. Figure III.3b shows the load-displacement relationship for loads at the greased side. Figure III.3c shows the load-strain relationship for this specimen for the load at the non-greased side and Figure III.3d shows the same for the load at greased side.

2.3.1b 1.75" Dowel Bars

The test setup for specimen B4 is shown in Figure A.10a. Figure III.4a shows the load-displacement behavior for this specimen for loads at the non-greased side up to approximately 9,500 pounds. Maximum displacement of about 1.1" occurs at the greased joint. Similarly, Figure III.4b shows the same for loads at the greased side.

Figure A.10b shows the testing arrangement for specimen B5. The load-displacement relationship for this specimen is shown in Figure III.5a for loads at the non-greased side up to approximately 10,000 pounds. Maximum displacement of about 0.7" occurs at the greased joint. A similar relationship for loads at the greased side is shown in Figure III.5b.

The arrangement of testing for specimen B6 is shown in Figure A.10c. Figure III.6a shows the load-displacement behavior for specimen B6 for loads at the non-greased side. Maximum displacement of 0.55" occurred at the non-greased joint for a load of approximately 7,500 lbs. Similarly, Figure III.6b shows the graph for loads at the greased side. The strain-displacement relationship for specimen B6 for loads at the non-greased side and greased side are shown in Figures III.6c and III.6d, respectively.

2.3.1c 1" Rebars

Figure A.11a shows the test setup for specimen B7. The load-displacement relationship for this specimen for loads at the non-greased and greased sides are shown in Figures III.7a and III.7b, respectively. A maximum displacement of 0.55" was observed at approximately 900 pounds.

The test setup for specimen B8 is shown in Figure A.11b. Figures III.8a and III.8b show the load-displacement relationship for this specimen for loads at the non-greased and greased sides, respectively. A maximum displacement of 0.8" occurred at a load of approximately 1,100 pounds.

The arrangement of testing for specimen B9 is shown in Figures A.11c-d. The load-displacement relationship for specimen B9 for loads at the non-greased and greased sides is shown in Figures III.9a and III.9b, respectively. A maximum displacement of 1.5" occurs at a load of approximately 1,600 pounds. The strain-displacement behavior for the this specimen for loads at the non-greased and greased sides is shown in Figures III.9c and III.9d, respectively for the strain gages shown in Figure B9.

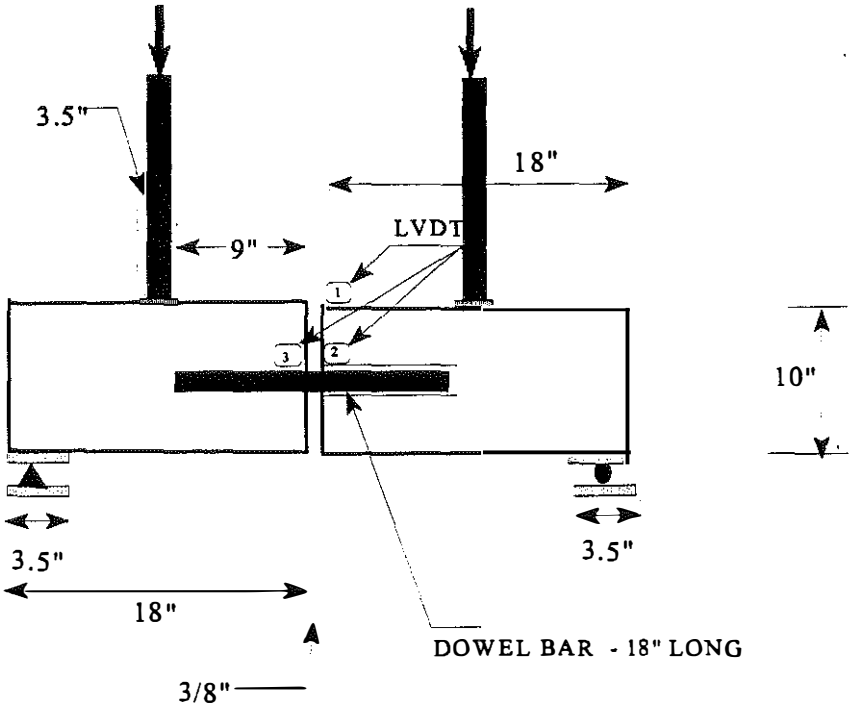

Figure 2.2 Setup for Bending Moment Testing

Table 2.3 Specimen Designation (B-1 to B-9)

Loading : Bending Size : 36" x 12" x 10" ; Joint Width = 1" Half length of the Dowel bar should be greased; Rebar should not b e greased.										
	Dowel - 1.25" dia.			Dowel - 1.75" dia.			Rebar - 1" dia.			Total Number of Specimens
SG*	No	No	Yes	No	No	Yes	No	No	Yes	
SIN**	B-1	B-2	B-3	B-4	B-5	B-6	B-7	B-8	B-9	9

*SG- Strain Gage
**SIN-Specimen Identification Number

Table 2.4 Geometric properties of the bending specimens (in)

Beam	Greased End			Non-Greased End		
	Height	Length	Width	Height	Length	Width
B1	12.000	17.750	9.938	12.000	17.250	9.875
B2	12.063	17.750	10.000	12.063	17.250	10.000
B3	12.000	17.563	10.000	12.000	17.625	10.000
B4	12.000	17.375	10.000	12.000	17.438	10.000
B5	12.000	17.500	10.000	12.000	17.250	9.938
B6	12.000	17.500	10.000	12.000	17.500	10.000
B7	12.000	17.500	10.000	12.000	17.625	10.000
B8	12.000	17.563	10.000	12.000	17.000	9.875
B9	12.000	17.500	10.000	12.000	17.500	9.875

2.4 Aggregate Interlock Testing

Many joints, whether it is a doweled or undoweled, are commonly finished with a groove cut partially at the top of slab as shown in Figure 2.3. The width of joints generally used in highway pavements is approximately 1/4" to 3/8". Part of the uncut joint can offer shear resistance due to an aggregate interlock effect. This testing was performed to determine the shear stiffness due to aggregate interlock of the cracked joint. The depth of the initial cut was approximately 2.5" (i.e. 1/4 of the slab thickness). Partially sawn joints are provided in pavements to permit free thermal expansion and contraction when crack has fully developed through the thickness of the slab. Table 2.5 describes the specimen designation for aggregate interlock testing under shear load, and Table 2.6 lists the geometric properties of the specimen measured before testing.

The shear stiffness of this aggregate interlock effect at the joint can be determined by applying a lateral load as shown in Figure 2.3. The stiffness can be derived from the relative deflection of the two blocks.

The photograph of test setup for the specimen A1 is shown in Figures A.12a-c. Figure II.1 shows the load-displacement relationship for specimen A1 for load levels up to failure at 16,000 pounds. A maximum displacement of 0.7" occurs at the edge-near end.

The arrangement of testing for specimen A2 is shown in Figures A.12d-e. Figure II.2 shows the load-displacement behavior of specimen A2 for load levels up to approximately 16,000 pounds. A maximum displacement of about 0.55" occurs at the edge-near end.

The test setup for specimen A3 is shown in Figure A.12f. Figure II.3 shows the load-displacement relationship for specimen A3. Displacements at different locations are shown for loads up to approximately 13,000 pounds. A maximum displacement of approximately 0.75" was observed at the edge-near end.

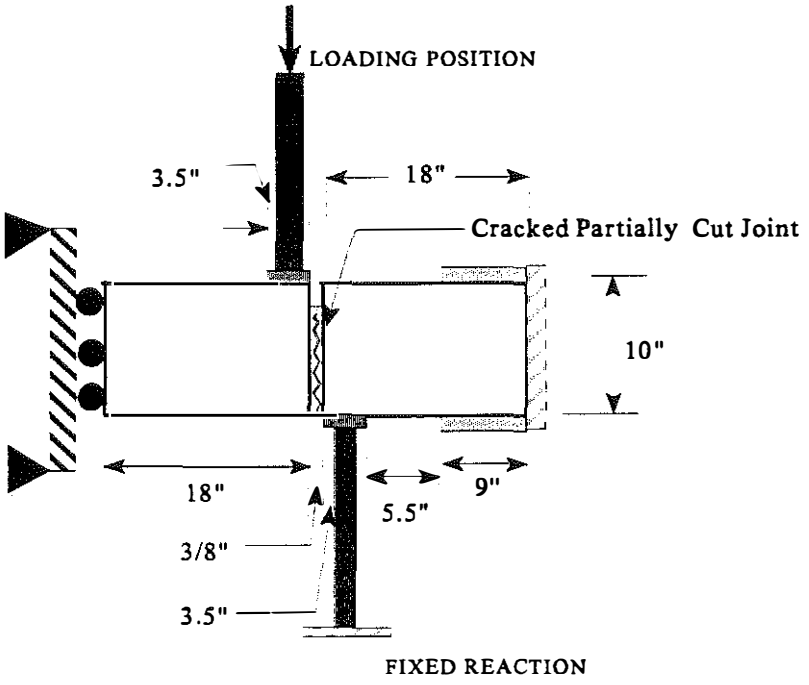

Figure 2.3 Setup for Aggregate Interlock Testing

Table 2.5 Specimen Designation (AI-1 to AI-3)

Loading : Shear Size : 36" x 12" x 10" ; Cut only at Surface; No through Joint No dowel bars; No Rebars				
				Total Number of Specimens
SIN*	AI-1	AI-2	AI-3	3

*SIN - Specimen Identification Number

Table 2.6 Geometric properties of the aggregate interlock specimen

	Loaded Side			Spring Side		
	Height	Length	Width	Height	Length	Width
A1	12.000	17.875	10.000	12.000	18.000	10.063
A2	12.125	18.000	10.125	12.000	18.000	10.250
A3	12.000	18.125	10.000	12.125	17.875	9.875

2.5 Testing under Combined Bending and Shear

This testing was performed to check the stiffness derived from independent loading situations. The setup shown in Figure 2.4 was to simulate the actual wheel load on the pavement. Subgrade is simulated by a set of springs with a spring stiffness of 5.75 pounds/inch. Table 2.5 describes the specimen designation for aggregate interlock testing under shear load, and Table 2.6 lists the geometric properties of the specimen measured before testing.

2.5.1 1.25" Dowel Bars

The test setup for specimen C1 is shown in Figure A.13a. The load-displacement behavior of the specimen is shown in Figure IV.1 for load levels up to 9,500 pounds. A maximum displacement of 1.1" occurs at the non-greased joint. The photograph of the test arrangement for specimen C2 is shown in Figure A.13b. Figure IV.2 shows the load-displacement relationship for that specimen. A maximum displacement at a load level of approximately 11,000 pounds is almost 1". For specimen C3, the load-displacement behavior is shown in Figure IV.3a for load levels up to approximately 23,000 pounds. A maximum displacement of approximately 1" was observed at the greased center. The load-strain relationship for this specimen is shown in Figure IV.3b for the strain gages shown in Figure C3.

2.5.2 1.75" Dowel Bars

The arrangement of testing for specimen C4 is shown in Figure A.14a-b. Figure IV.4 shows the load-displacement behavior of that specimen for load levels up to approximately 23,000 pounds. A maximum displacement of 1" occurs at the greased center. The test setup for specimen C5 is shown in Figure A.14c. The load-displacement relationship for that specimen is shown in Figure IV.5. A maximum displacement of about 1" occurs at a load of approximately 21,000 pounds. The photograph of the testing arrangement for specimen C6 is shown in Figure A.14d. Figure IV.6a shows the load-displacement relationship for specimen C6 for load levels up to approximately 25,000 pounds. A maximum displacement of approximately 1" occurs at the bar. The load-strain relationship for this specimen is shown in Figure IV.6b for the strain gages shown in Figure C6.

2.5.3 1" Rebars

The test setup for specimen C7 is shown in Figure A.15a. Figure IV.7 shows the load-displacement relationship for specimen C7 for load levels up to failure at approximately 3,000 pounds. A maximum displacement of approximately 0.9" was observed at the non-greased joint. The arrangement of testing for specimen C8 is shown in Figure A.15b. The load-displacement relationship for specimen C8 is shown in Figure IV.8. A maximum displacement of approximately 1" at a failure load of 7,500 pounds was observed at the non-greased joint. Figure IV.9a shows the load-displacement behavior of specimen C9. A maximum displacement of approximately 1.25" was observed at the non-greased joint spring. Loads were increased until failure at the load of about 10,000 pounds. The load-strain relationship for specimen C9 is shown in Figure IV.9b for the strain gages described in Figure C9.

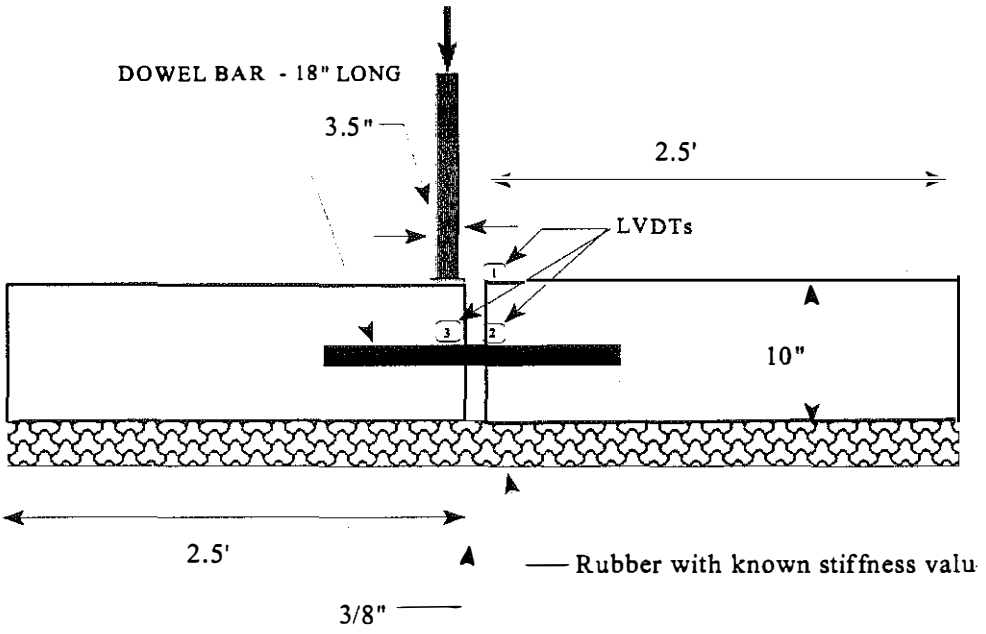

Figure 2.4 Setup for Testing under combined Loading

Table 2.7 Specimen Designation (C-1 to C-9)

Loading : Combined Shear and Bending
Size : 5' x 12" x 10" ; Joint Width = 1"
Support: Rubber, whose modulus should be between 50 pci to 300 pci
Half length of the Dowel bar should be greased; Rebar should not be greased.

	Dowel - 1.25" dia.			Dowel - 1.75" dia.			Rebar -1" dia.			Total Number of Specimens
SG*	No	No	Yes	No	No	Yes	No	No	Yes	
SIN**	C-1	C-2	C-3	C-4	C-5	C-6	C-7	C-8	C-9	9

*SG- Strain Gage
**SIN-Specimen Identification Number

Table 2.8 Geometric properties of the combined load specimen

	Greased End			Non-Greased End		
	Height	Length	Width	Height	Length	Width
C1	11.875	29.500	10.000	11.875	29.563	10
C2	11.875	29.375	10.250	12.000	29.500	10
C3	12.125	29.500	10.000	12.250	29.500	10
C4	12.875	29.750	12.000	12.000	29.250	10
C5	12.000	29.500	10.000	11.875	29.500	10
C6	12.000	29.563	10.000	12.000	29.625	10
C7	12.000	29.375	10.000	12.000	29.500	10
C8	12.000	29.750	10.000	12.000	29.375	10
C9	12.000	29.500	10.000	12.000	29.625	10

3.0 PROPOSED FIELD TESTING

3.1 General

Although this study does not include field testing, it is recommended that the following field tasks be performed in the future as funding is available. Results from these field tasks would be used in conjunction with the results of this study to validate a finite element model to predict rigid pavement behavior.

3.2 Field Testing of Friction at the Interface of Slab and Subgrade

Due to the presence of rough surfaces at the interface of slab and subgrade, friction is developed during thermal expansion/contraction. To account for the stresses developed under such conditions, the coefficient of friction should be determined through field testing.

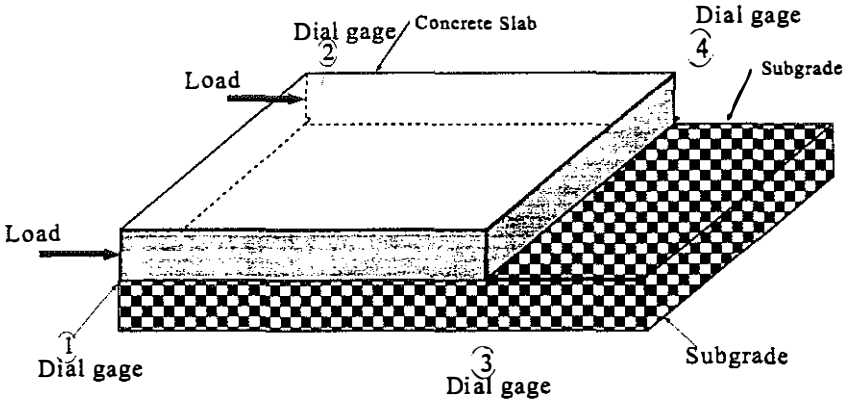

Figure 3.1 Testing Arrangement to determine Interface Friction Between Slab and Subgrade

The displacement of the concrete slab and subgrade can be measured in the field by applying (Figure 3.1) an in-plane load to a discrete slab which is not connected to adjacent slabs by dowels or tie bars. The resulting coefficient of friction could be used as a spring constant in the finite element model.

3.3 Field Measurement of Temperature Distribution

In practice, the temperature distribution in the concrete pavement slab is found to be nonlinear through the thickness direction. Due to this variation, the stress distribution through the thickness of the slab is nonlinear. To determine the stresses using the finite element method, the temperature distribution through the thickness of slab should be measured. This could be accomplished by installing thermocouples at various locations (approximately 6 to 8 locations) through the thickness of slab (Figure 3.2).

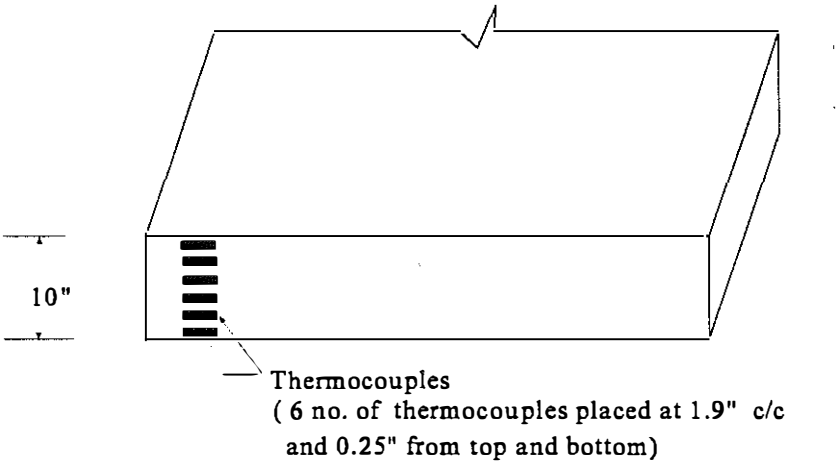

Figure 3.2 Thermocouple Locations in the Thickness

3.4 Field Testing on Plain Concrete Pavements

This testing would be required to validate the finite element model created from the stiffness parameters determined from the laboratory tests performed in this study. Falling Weight Deflectometer (FWD) could be used to measure the deflection at various locations adjacent to the joint, when a load is applied very near the joint. This test must be performed at doweled joint (Figure 3.3) and also at a tied joint (Figure 3.4). Deflection sensors and strain gages should be placed on the concrete slab to obtain the displacements and stress distribution. The results of deflection and stresses obtained from that effort would be used for validation of the finite element model results.

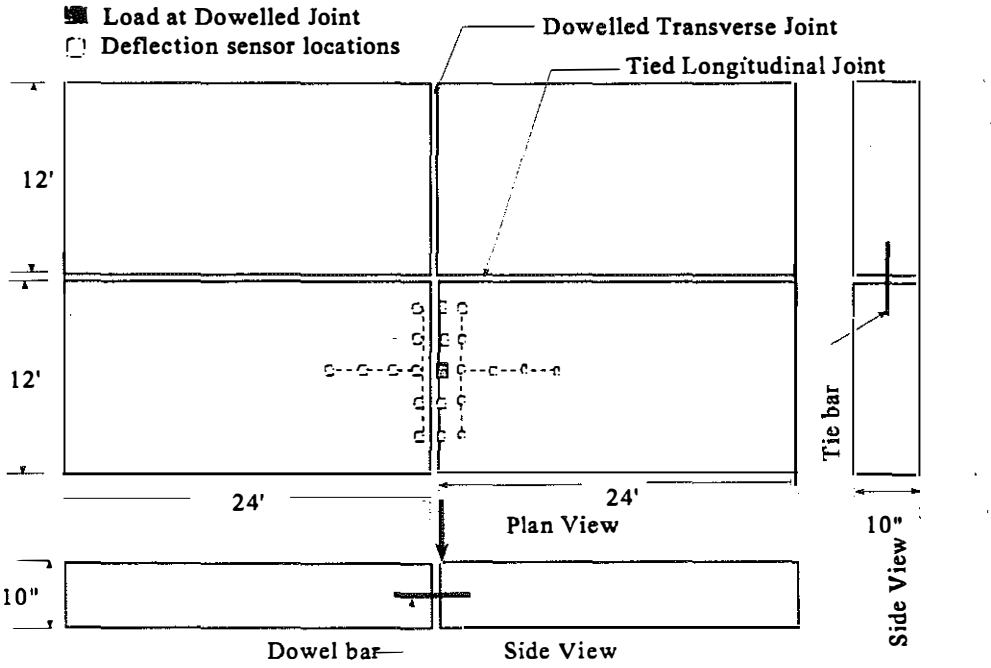

Figure 3.3 FWD Test on Dowelled Joint

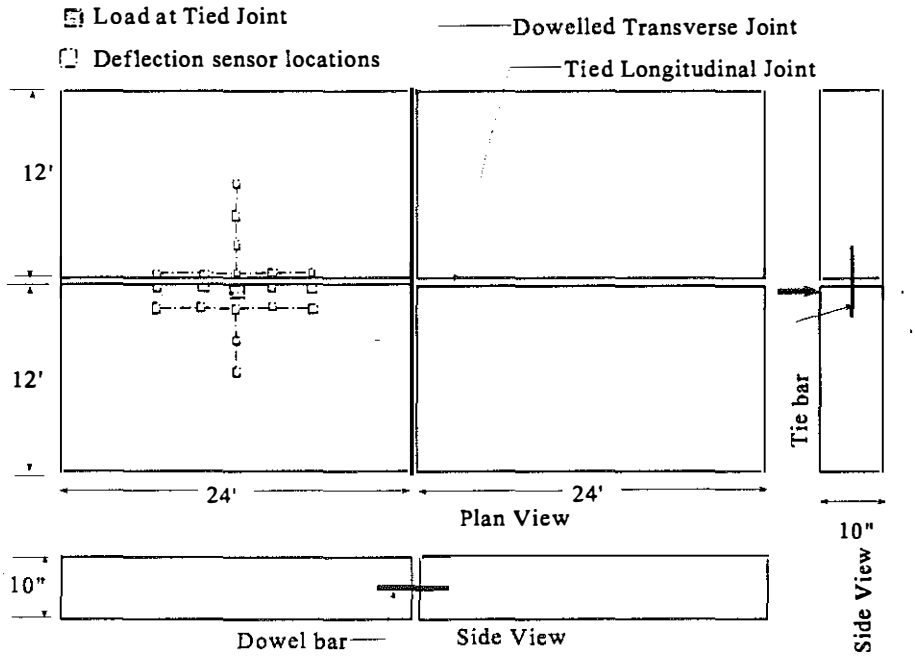

Figure 3.4 FWD Test on Tied Joint

4.0 RECOMMENDATIONS

1. It is recommended that the information and data developed in this study be used in future studies in the development of a finite element model for rigid pavements.

2. It is further recommended that future studies be conducted to collect field data for calibrating the finite element model.

References

1. N.Buch and D.G.Zollinger(1996), Development of dowel looseness prediction model for jointed concrete pavements, TRR, 1525, pp 21-27

2. C.Channakesava, F.Barzegar and G.Z.Voyiadjis(1993), Nonlinear FE analysis of plain concrete pavements with dowelled joints., J. Trans. Engrg. 119(5), pp763-781.

3. Y.T.Chou(1981), Structural analysis computer programs for rigid multi-component pavement structures with discontinuties-WESLIQUID and WESLAYER, Technical reports 1-3, U.S. Army Engrg. Waterways Experiment Station, Vicksburg, Miss.

4. Y.T.Chou(1995), Estimating load transfer from measured joint efficiency in concrete pavements, TRR No.1482, pp19-25

5. B.Choubane and M.Tia(1993) Analysis and verification of thermal-gradient effects on concrete pavement, J.Trans. Engrg., 121(1), pp75.81

6. M.I.Darter, E.Owusu-Antwi and R.Ahmed(1996), Evaluation of AASHTO rigid pavement design model using long-term pavement performance data base, TRR No.1525, pp57-71

7. S.L.Grieef(1996), GFRP dowel bars for concrete pavement, Master Thesis, University of Manitoba, Winnipeg.

8. H.Guo, J.A.Sherwood and M.B.Snyder(1995), PCC pavements, J. Trans. Engrg., 121(3), pp289-298.

9. K.T.Hall, M.I.Darter and C.M.Kuo(1995), Improved methods for selection of K value for concrete pavement design, TRR No.1505, pp128-136.

10. I.E.Harik, P.Jianping and D.Allen(1994), Temperature effects on rigid pavements, J. Trans. Engg., V.120, N.1, pp127-143.

11. A.M.Ioannides and R.A.Salsilli-murua(1989), Temperature curling in rigid pavements: An application of dimensional analysis, TRR No.1227, pp1-11.

12. A.M.Ioannides(1984), Analysis of slabs-on-grade for a variety of loading and support conditions, Ph.D thesis, Univ. of Illinois , Urbana, Ill.

13. A.M.Ioannides and M.I.Hammons(1996) Westergaard-type solution for edge load transfer problem, TRR, 1525, pp28-35

14. A.M.Ioannides and G.T.Korovesis(1990), Aggregate interlock: A pure shear load transfer

mechanism, TRR No.1286, pp14-24.

15. A.M.Ioannides, T.H.Lee and M.I.Darter(1990), Control of faulting through joint load transfer design, TRR No.1286, pp49-56

16. A.M.Ioannides and G.T.Korovesis(1992), Analysis and design of doweled slab-on-grade pavement systems, J. Trans. Engg., V.118, No.6, pp745-768

17. Y.Jiang, M.I.Darter and E.Owusu-Antwi(1996), Analysis of current state rigid pavement design practices in the United States, TRR No.1525, pp72-82

18. J.R.Keeton(1957), Load-transfer characteristics of a doweled joint subjected to aircraft wheel loads, Proc.HRB, Vol.36

19. L.Khazanovich and A.M.Ioannides (19), Finite element analysis of slabs-on-grade using higher order subgrade soil models, pp16-30

20. T.Krauthammer and K.L.Western(1988), Joint shear transfer effects on pavement behavior, J.Trans.Engg, V.114, N.5, pp505-529

21. A.R.Kukreti, M.R.Taheri and R.H.Ledesma(1992), Dynamic analysis of rigid airport pavements with discontinuties, J. Trans. Engg., V.118, N.3, pp341-360

22. C.M.Kuo, K.T.Hall and M.I.Darter(1995), Three-dimensional finite element model for analysis of concrete pavement support, TRR No.1505, pp119-127.

23. J.Larralde and W.F.Chen(1987), Estimation of mechanical deterioration of highway rigid pavements, V.113, N.2, pp193-207

24. Y.H.Lee and Y.M.Lee(1996), Corner stress analysis of jointed concrete pavements, TRR No.1525, pp44-56

25. Mirambell(1990), Temperature and stress distributions in plain concrete pavements under thermal and mechanical loads, Proc. 2 nd Int. workshop on the Desing and Rehabilitation of Concrete pavements, Siguenza, Spain.

26. S.Nazarian and K.M.Boddapati(1995), Pavement-falling weight deflectometer interaction using dynamic finite element analysis, TRR No.1482, pp33-43

27. T.Nishizawa, T.Fukuda and S.Matsuno(1989), A refined model of doweled joints for concrete pavement using FEM analysis, Proc. of 4 th Int. Conf. on concrete pavement design and rehabilitation, pp735-745, Purdue Univ.

28. T.Nishizawa, T.Fukuda, S.Matsuno and K.Himeno(1996), Curling stress equation for transverse joint edge of a concrete pavement slab based on finite element method analysis, TRR No.1525, pp 35-43

29. X.P.Shi, T.F.Fwa and S.A.Tan(1993), Warping stresses in concrete pavements on pasternak foundation, J. Trans. Engg., V.119, N.6, pp 905-913.

30. A.M.Tabatabaie and E.J.Barenberg(1980), Structural analysis of concrete pavement systems, J.Trans. Engg., V.106, N.TE5, pp493-506

31. A.M.Tabatabaie and E.J.Barenberg(1978), Finite element analysis of jointed or cracked concrete pavements, Trans. Res. Record 671, TRB, Washington D.C., pp11-19

32. M.R.Taheri and M.M.Zaman(1995), Effects of a moving aircraft and temperature differential on response of rigid pavements, Computers & Structures, V.57, N.3, pp503-511

33. S.P.Tayabji and B.E.Colley(1981), Analysis of jointed concrete pavements, FHWA, Nat. Tech. Information Service, Washington D.C.

34. M.Tia, J.M.Armaghani, C.L.Wu. S.Lei and K.L.Toye(1987), FEACONS III: computer program for the analysis of jointed concrete pavements, Trans. Res. Record 1136, TRB, Washington D.C. 12-22.

35. W.uddin, R.M.Hackett, A.Joseph, Z.Pan and A.B.Crawley(1995), Three-dimensional finite element analysis of jointed concrete pavement with discontinuties, TRR No.1482, pp26-32

36. S.Zaghioul and T.White(199), Nonlinear dynamic analysis of concrete pavements

37. M.Zaman and A.Alvapillai (1995), Contact-element model for dynamic analysis of jointed concrete pavements, J.Trans. Engrg., 121(5), pp425-433.

38. M.Zaman, M.R.Taheri and V.Khanna(1993), Dynamics of concrete pavement to temperature induced curling, TRB, 72nd Annual meeting, Jan.10-14, Washington, D.C.

39. M.Zaman, A.Alvapillai and M.R.Taheri(1993), Dynamic analysis of concrete pavements resting on a two-parameter medium, Int. J. for Num. Meth. in Engg., V.36, pp1465-1486

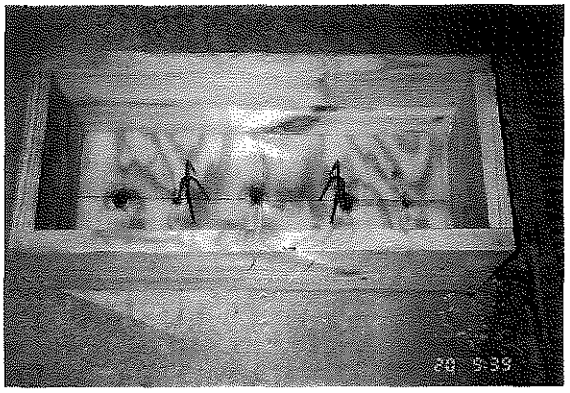

Figure A.1 Concrete Mold

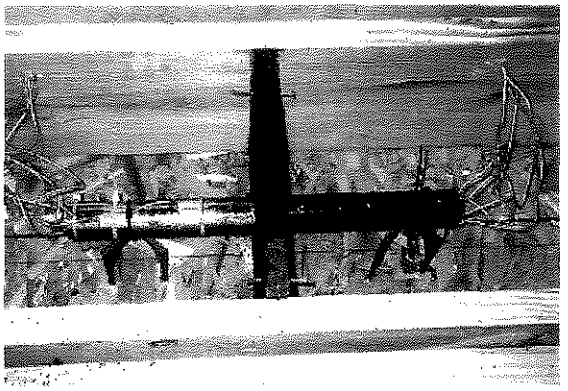

Figure A.2 Mold with Dowel bar, Strain gages, and Joint filler

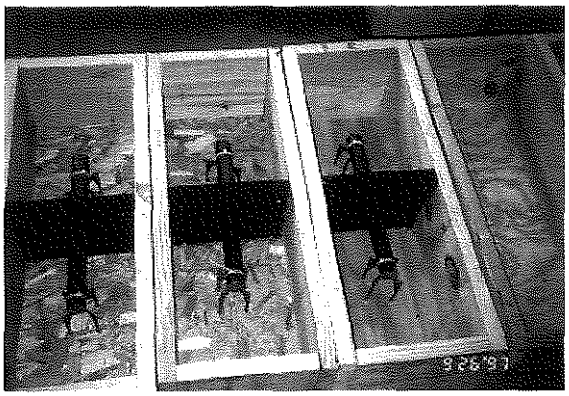

Figure A.3 Molds for Dowelled concrete Blocks

Figure A.4 Mold for Concrete Blocks joined by Tie Bar (Rebar)

Figure A.5 Concrete Blocks Casting

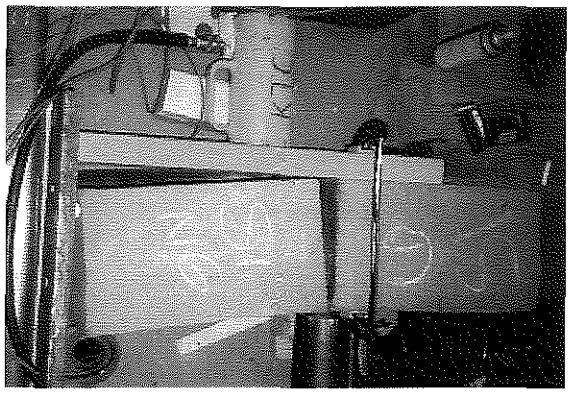

Figure A.6a Specimen S1

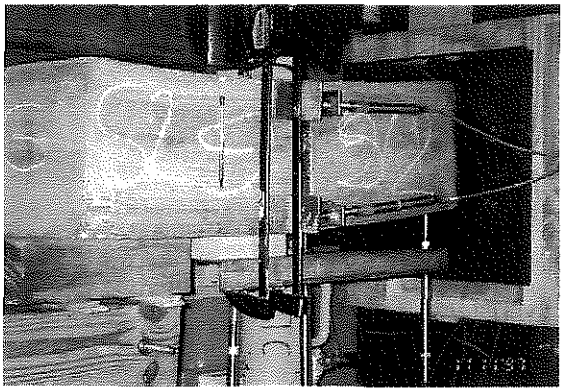

Figure A.6b Specimen S2

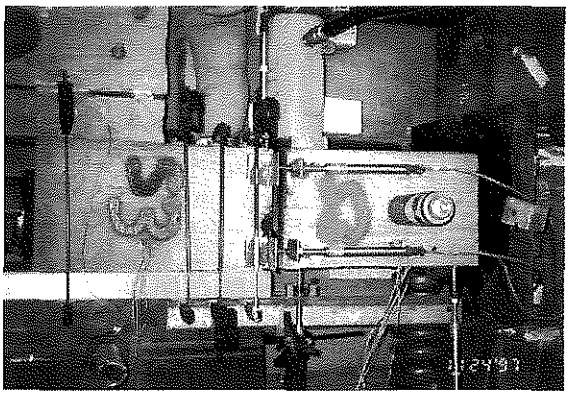

Figure A.6c Specimen S3

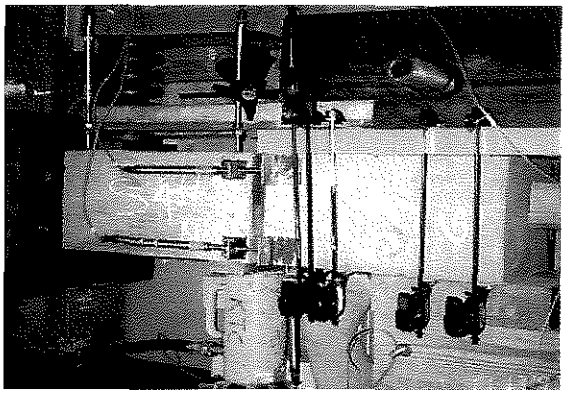

Figure A.7a Specimen S4

Figure A.7b Specimen S4 - Failure

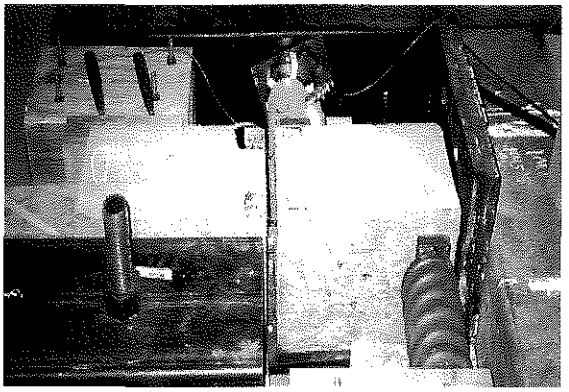

Figure A.7c Specimen S5

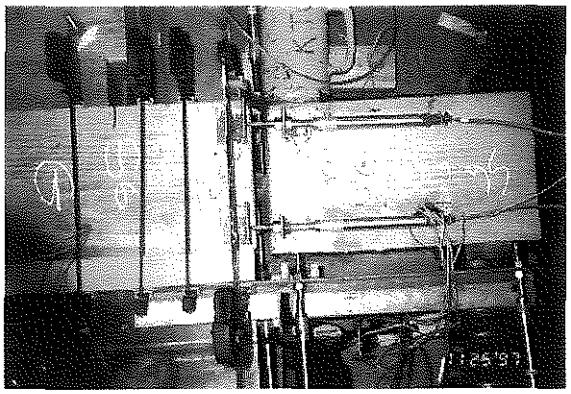

Figure A.7d Specimen S6

Figure A.7e Specimen S6 - Failure

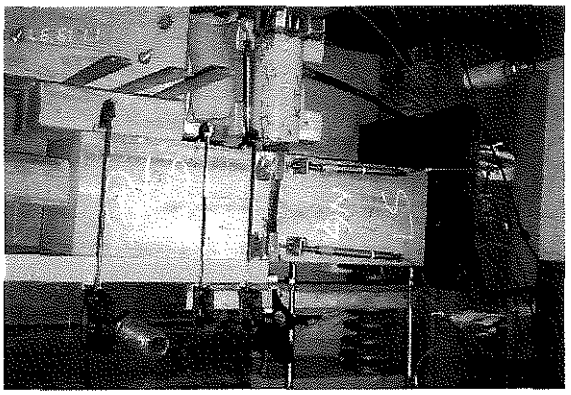

Figure A.8a Specimen S7

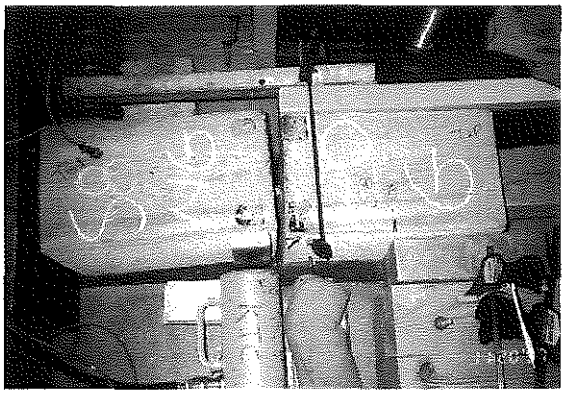

Figure A.8b Specimen S8

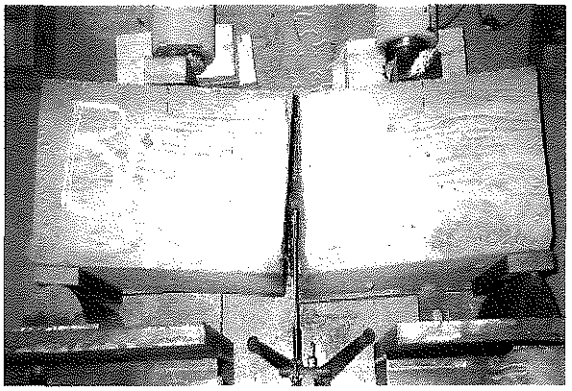

Figure A.9a Specimen B1

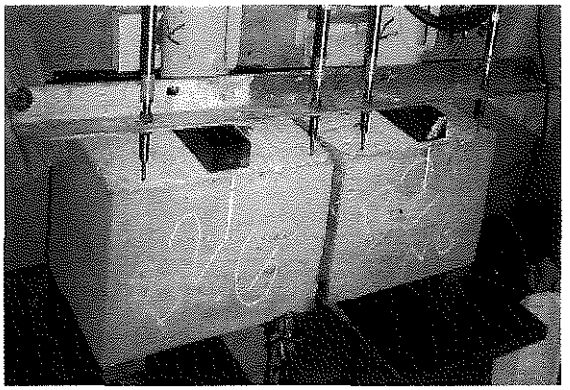

Figure A.9b Specimen B2

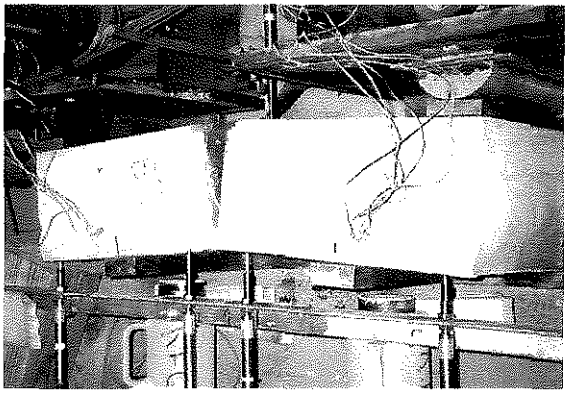

Figure A.9c Specimen B3

Figure A.10a Specimen B4

Figure A.10b Specimen B5

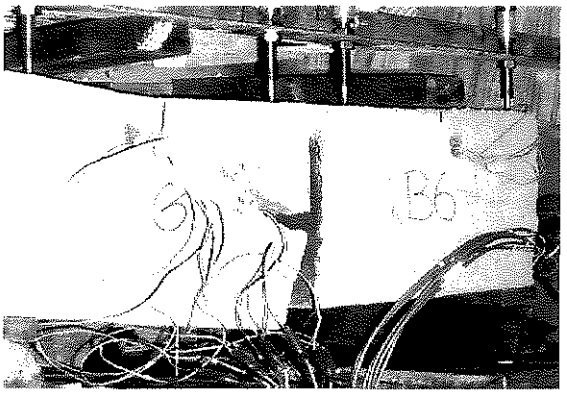

Figure A.10c Specimen B6

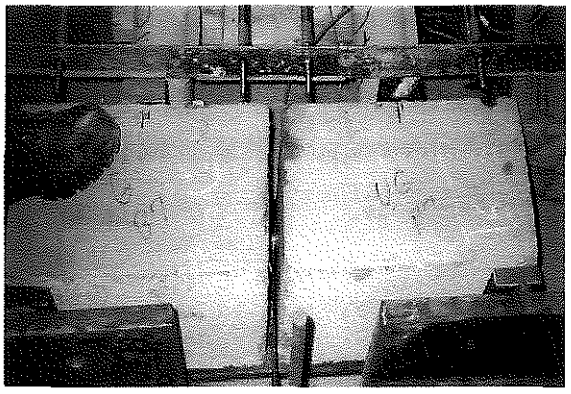

Figure A.11a Specimen B7

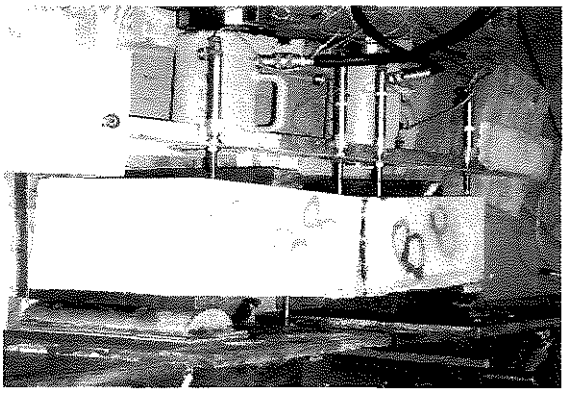

Figure A.11b Specimen B8

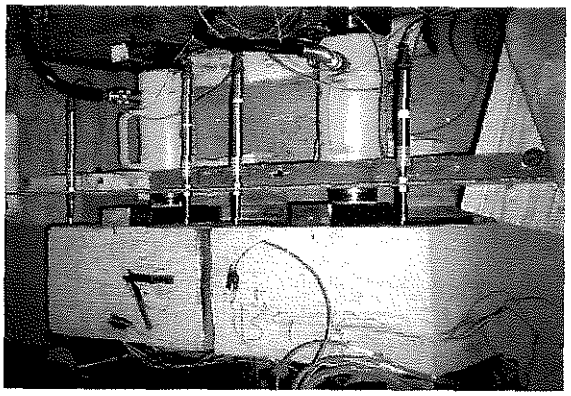

Figure A.11c Specimen B9

Figure A.11d Specimen B9-Failure

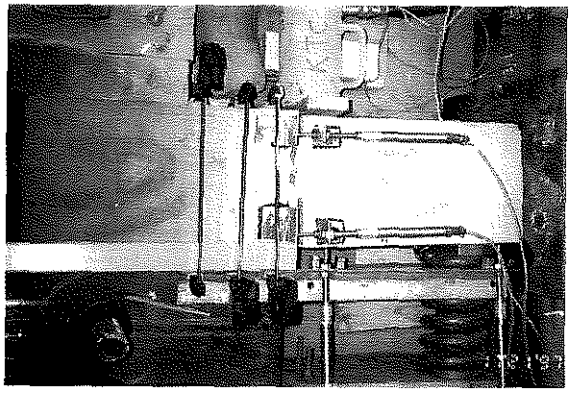

Figure A.12a Specimen A1

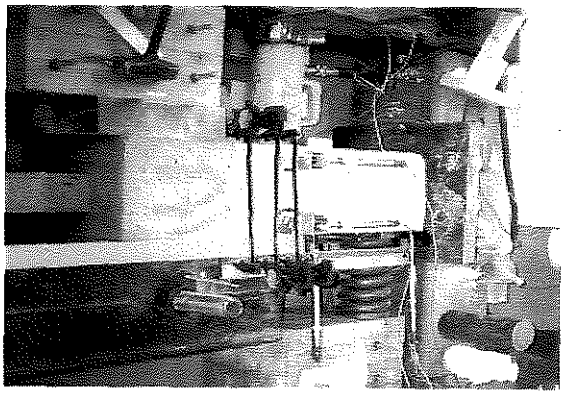

Figure A.12b Specimen A1-Another view

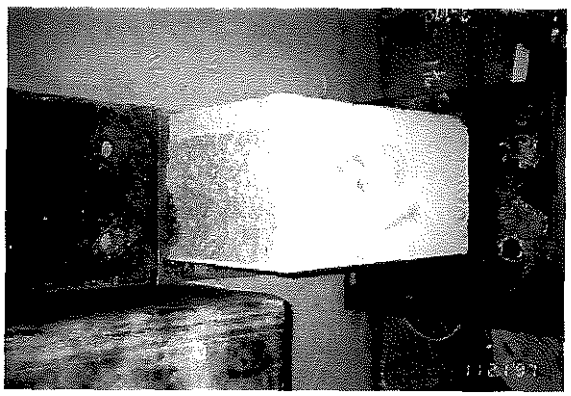

Figure A.12c Specimen A1-Cracked joint

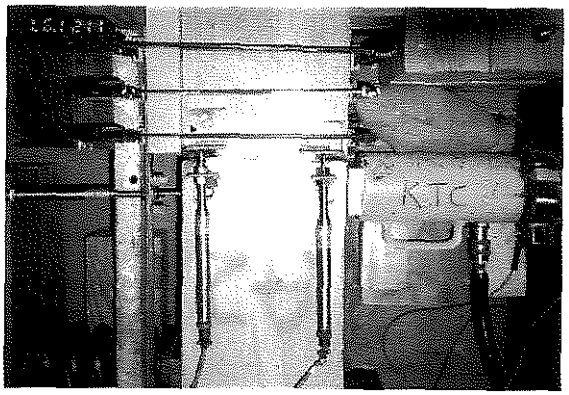

Figure A.12d Specimen A2

Figure A.12e Specimen A2 - Cracking of Joint

Figure A.12f Specimen A3 - Cracking of Joint

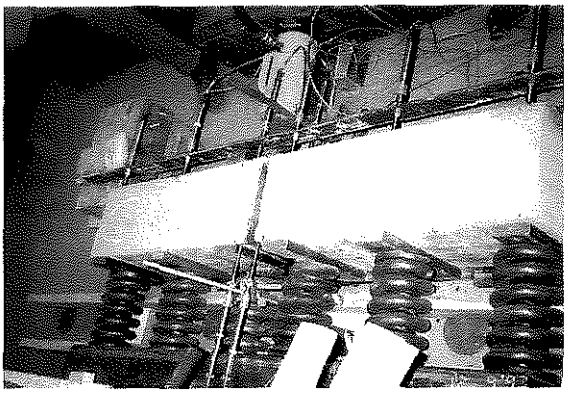

Figure A.13a Specimen C1

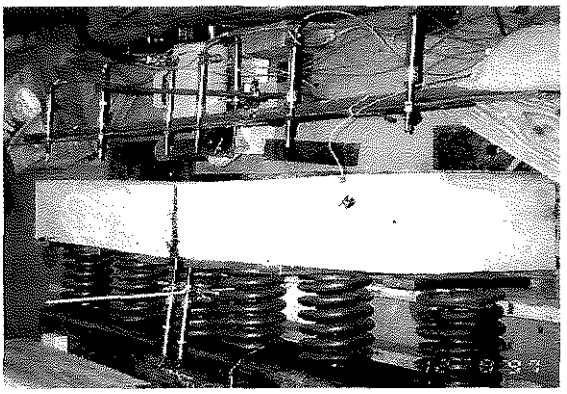

Figure A.13b Specimen C2

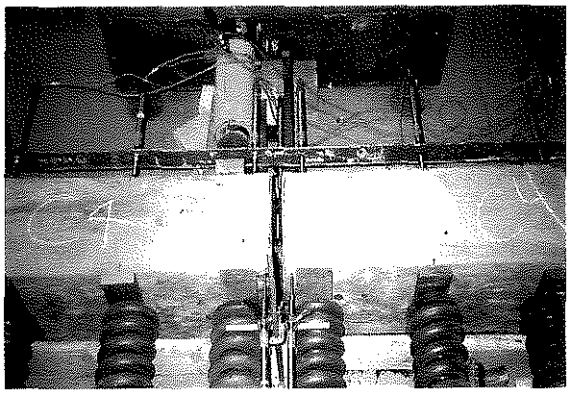

Figure A.14a Specimen C4

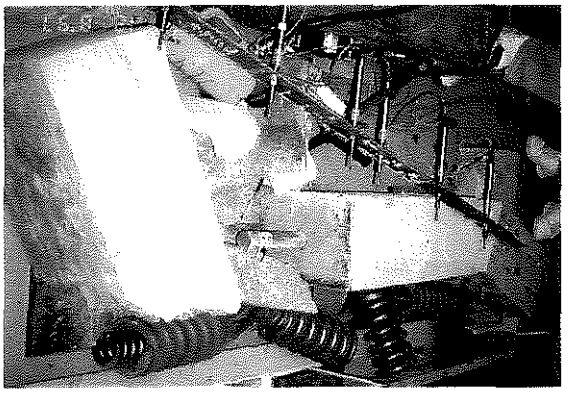

Figure A.14b Specimen C4 - Failure

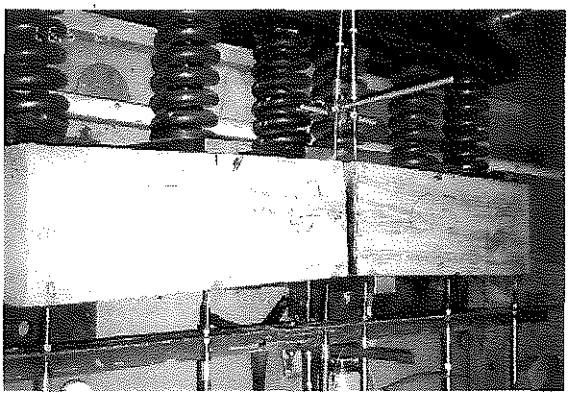

Figure A.14c Specimen C5

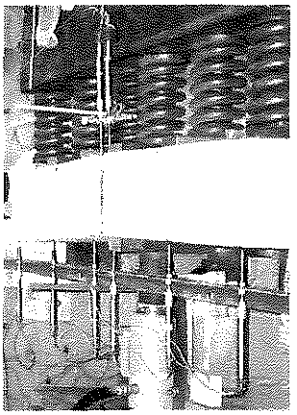

Figure A.14d
Specimen C6

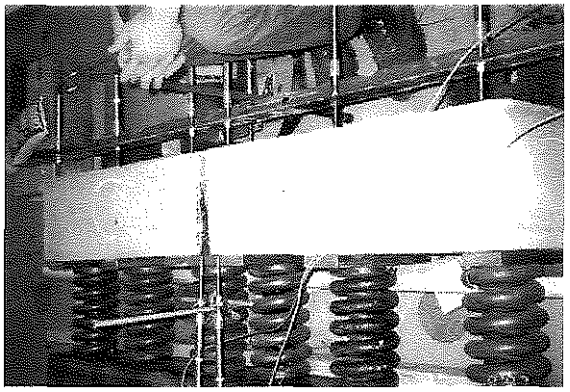

Figure A.15a Specimen C7

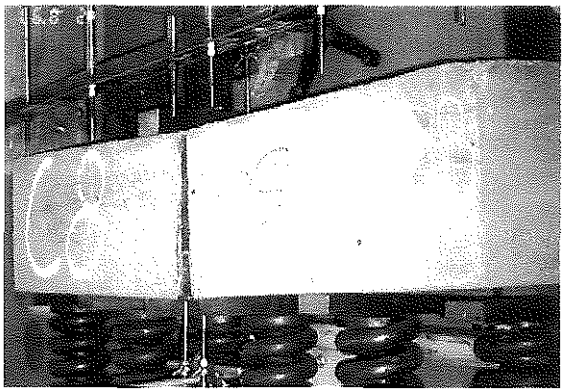

Figure A.15b Specimen C8

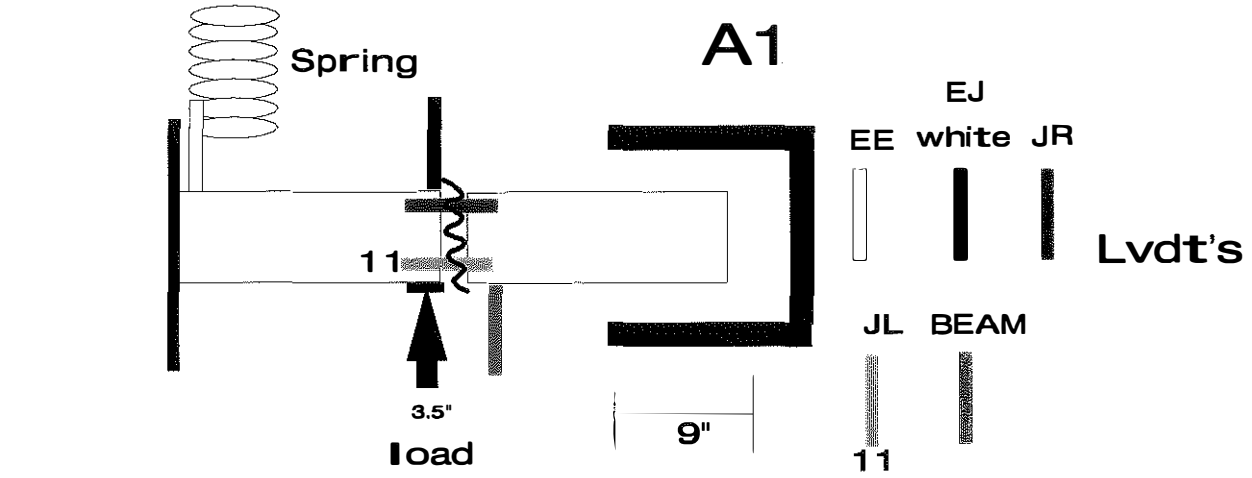
A1
Spring
11
3.5"
load
9"
EJ
EE
white
JR
Lvdt's
JL
BEAM
11

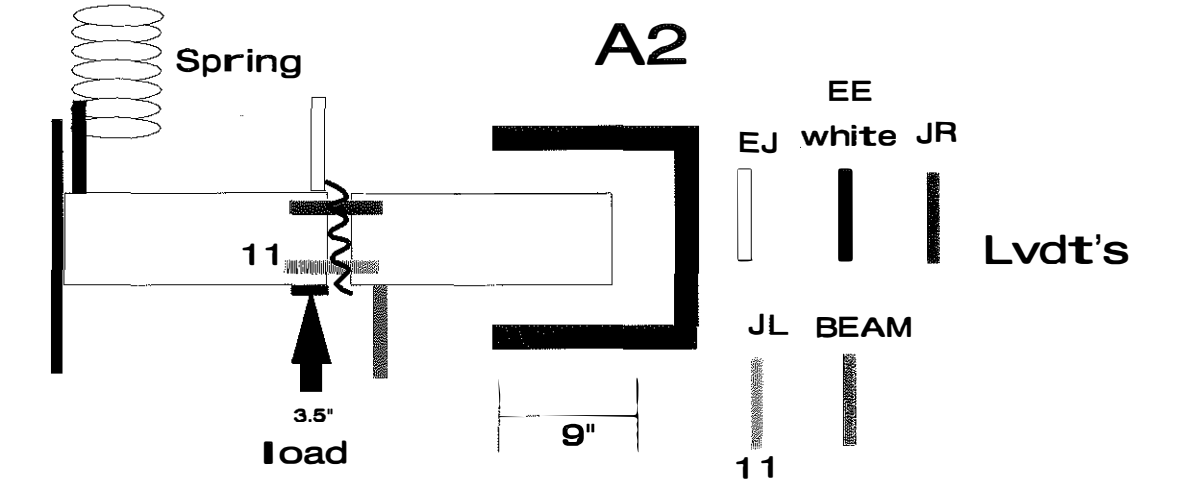
A2
Spring
11
3.5"
load
9"
EE
EJ
white
JR
Lvdt's
JL
BEAM
11

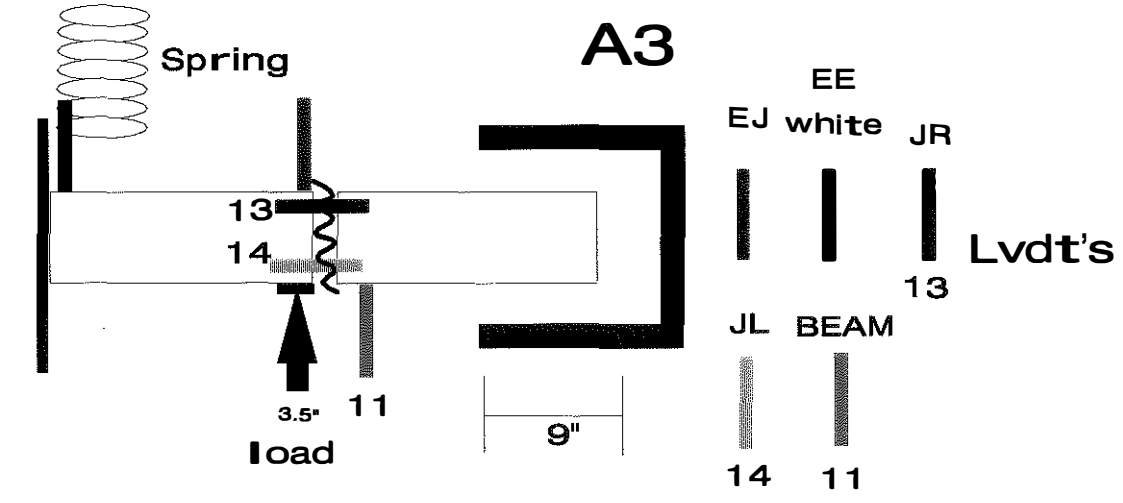
A3
Spring
13
14
3.5"
11
load
9"
EE
EJ
white
JR
13
Lvdt's
JL
BEAM
14
11

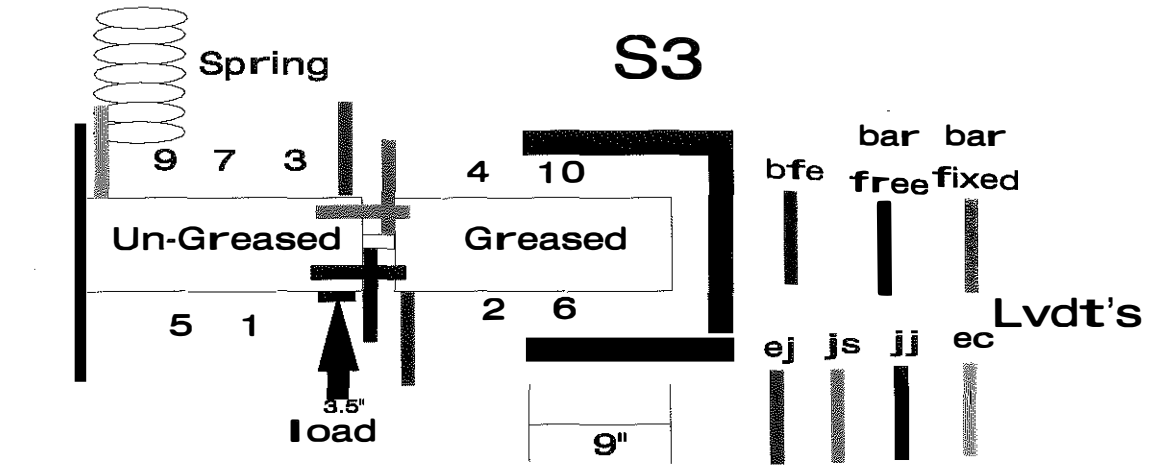
S3
Spring
9 7 3
4 10
Un-Greased
Greased
5 1
2 6
3.5"
load
9"
bfe
bar free
bar fixed
ej js jj ec
Lvdt's

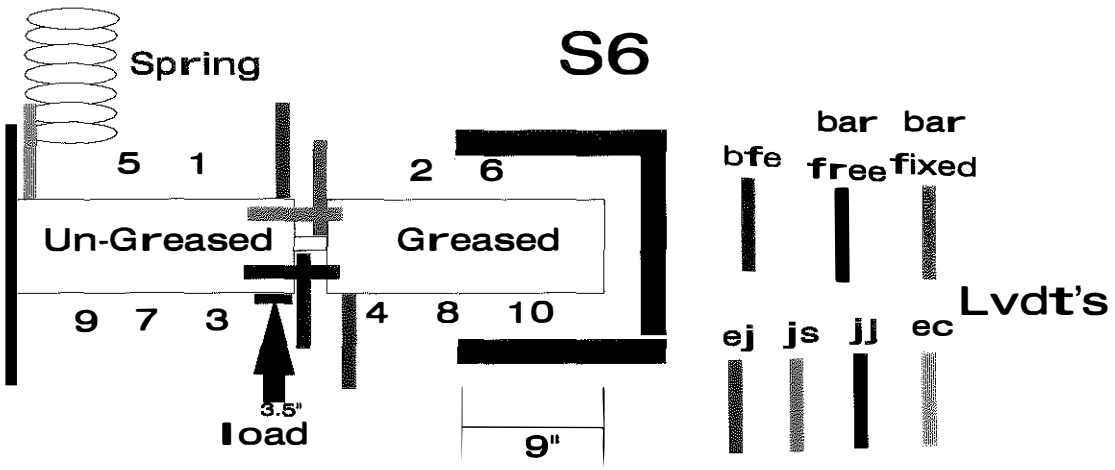
S6
Spring
5 1
2 6
Un-Greased
Greased
9 7 3
4 8 10
3.5"
load
9"
bfe
bar free
bar fixed
ej js jj ec
Lvdt's

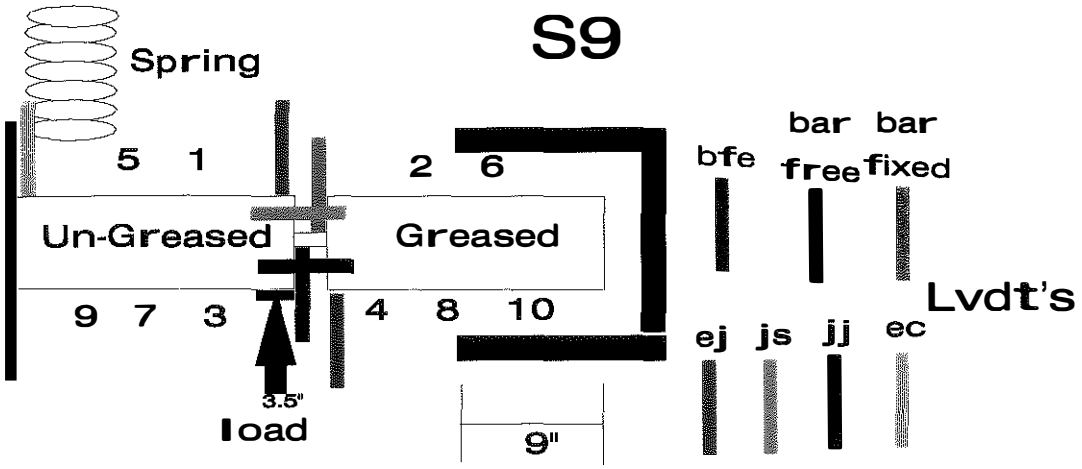
S9
Spring
5 1
2 6
Un-Greased
Greased
9 7 3
4 8 10
3.5"
load
9"
bfe
bar free
bar fixed
ej js jj ec
Lvdt's

B3

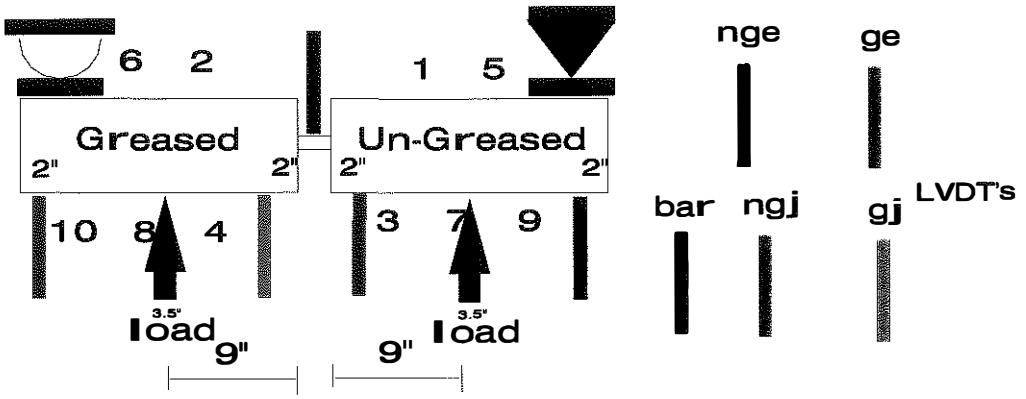
6 2
1 5
Greased
Un-Greased
2"
2"
2"
2"
10 8 4
3 7 9
3.5"
load
9"
9"
3.5"
load
nge
ge
bar
ngj
gj
LVDT's

B6

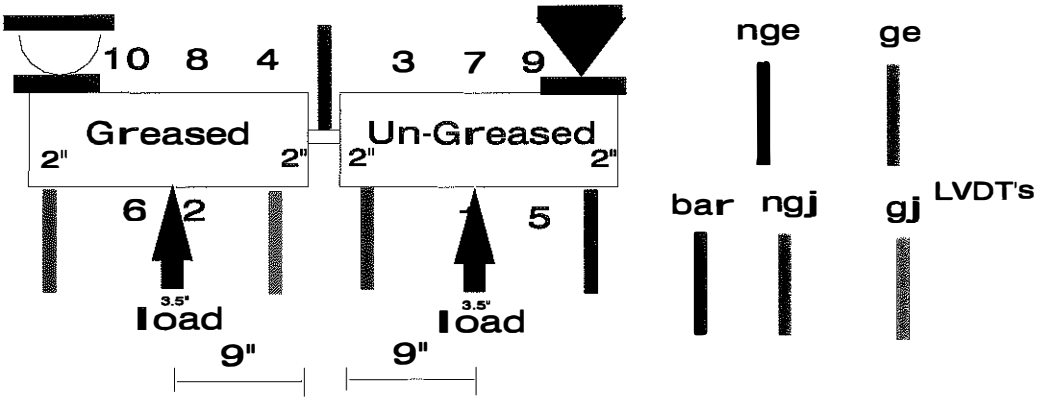
10 8 4
3 7 9
Greased
Un-Greased
2"
2"
2"
2"
6 2
5
3.5"
load
9"
9"
3.5"
load
nge
ge
bar
ngj
gj
LVDT's

B9

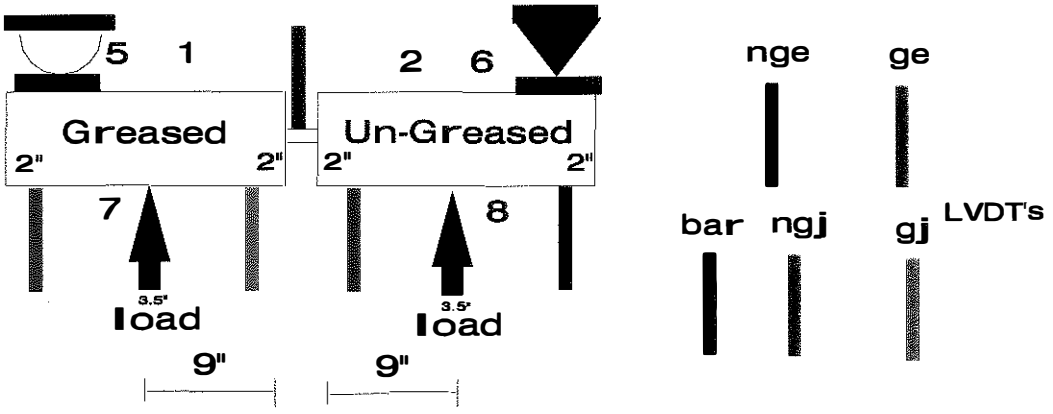
5 1
2 6
Greased
Un-Greased
2"
2"
2"
2"
7
8
3.5"
load
9"
9"
3.5"
load
nge
ge
bar
ngj
gj
LVDT's

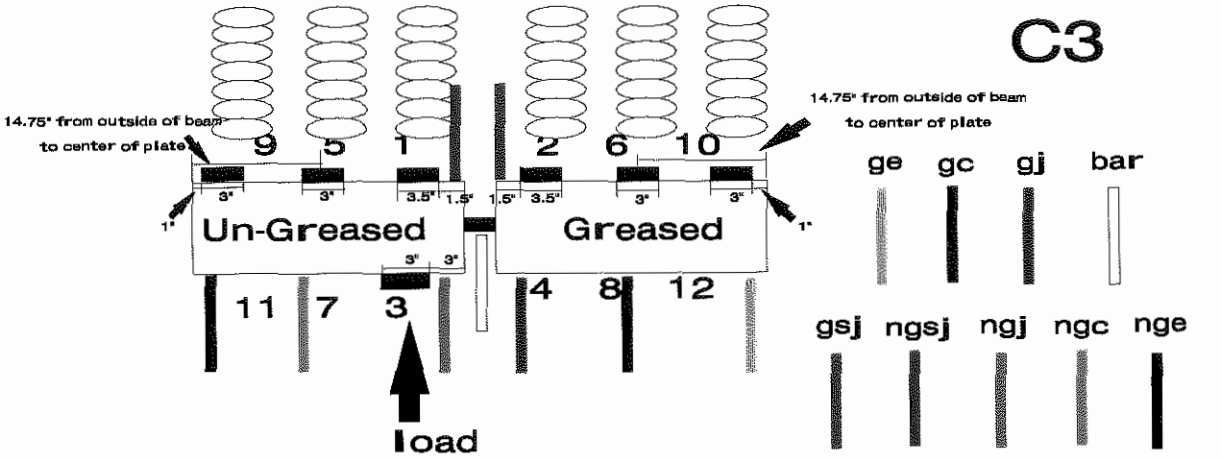
C3
14.75" from outside of beam
to center of plate
14.75" from outside of beam
to center of plate
9 5 1 2 6 10
11 7 3 4 8 12
Un-Greased
Greased
load
ge gc gj bar
gsj ngsj ngj ngc nge

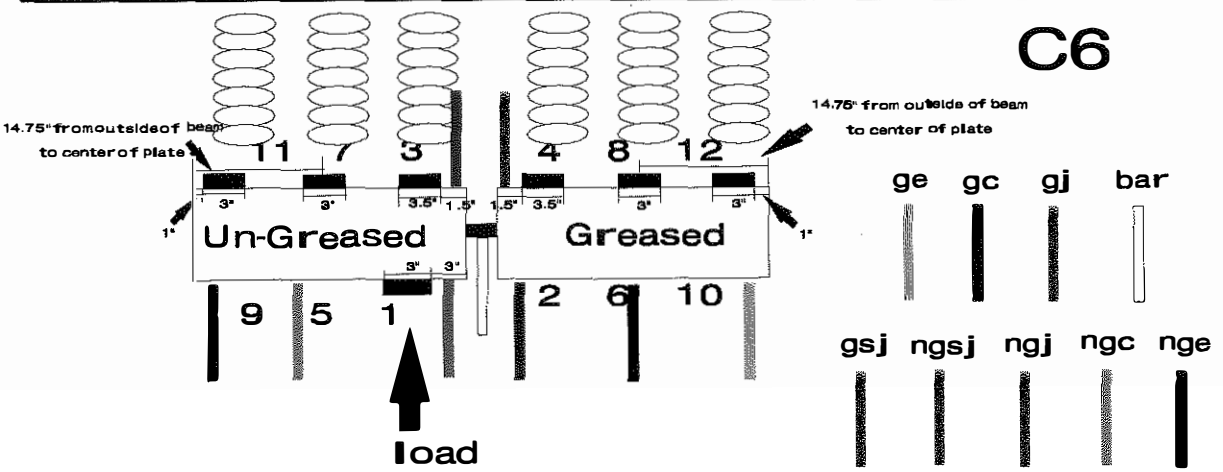
C6
14.75" from outside of beam
to center of plate
14.75" from outside of beam
to center of plate
11 7 3 4 8 12
9 5 1 2 6 10
Un-Greased
Greased
load
ge gc gj bar
gsj ngsj ngj ngc nge

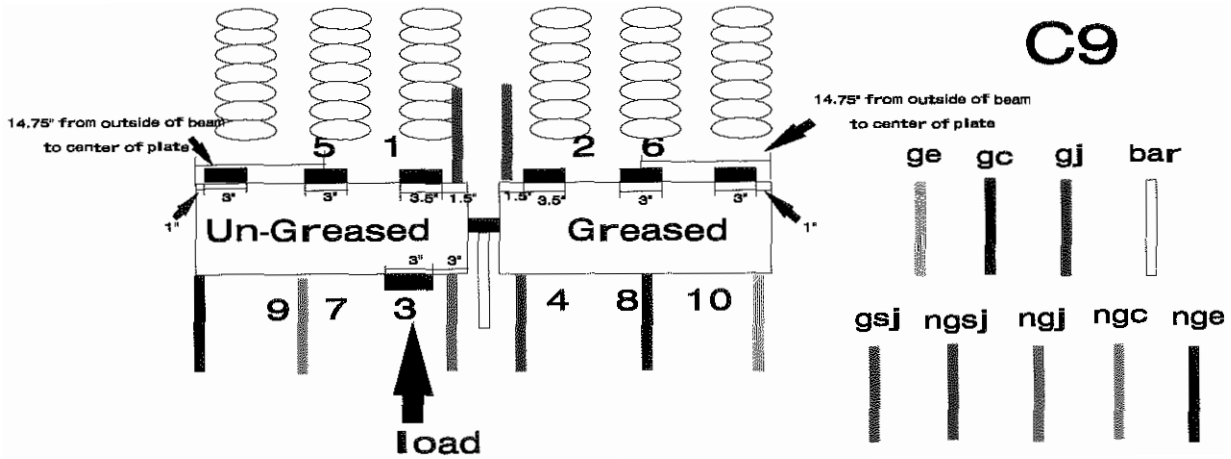
C9
14.75" from outside of beam
to center of plate
14.75" from outside of beam
to center of plate
5 1 2 6
9 7 3 4 8 10
Un-Greased
Greased
load
ge gc gj bar
gsj ngsj ngj ngc nge

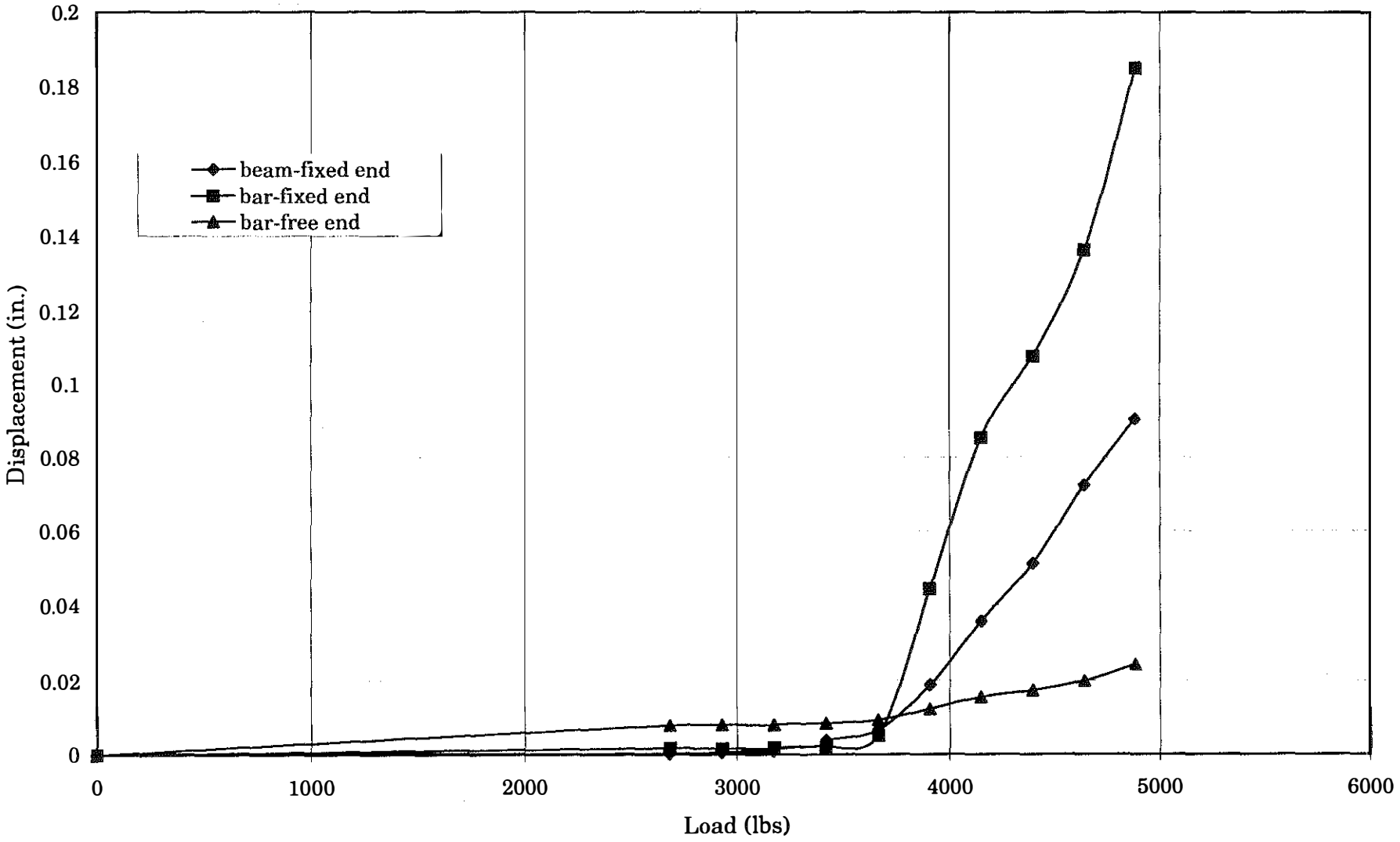

Figure I.1 Load - Displacement Relationship for the Specimen S1

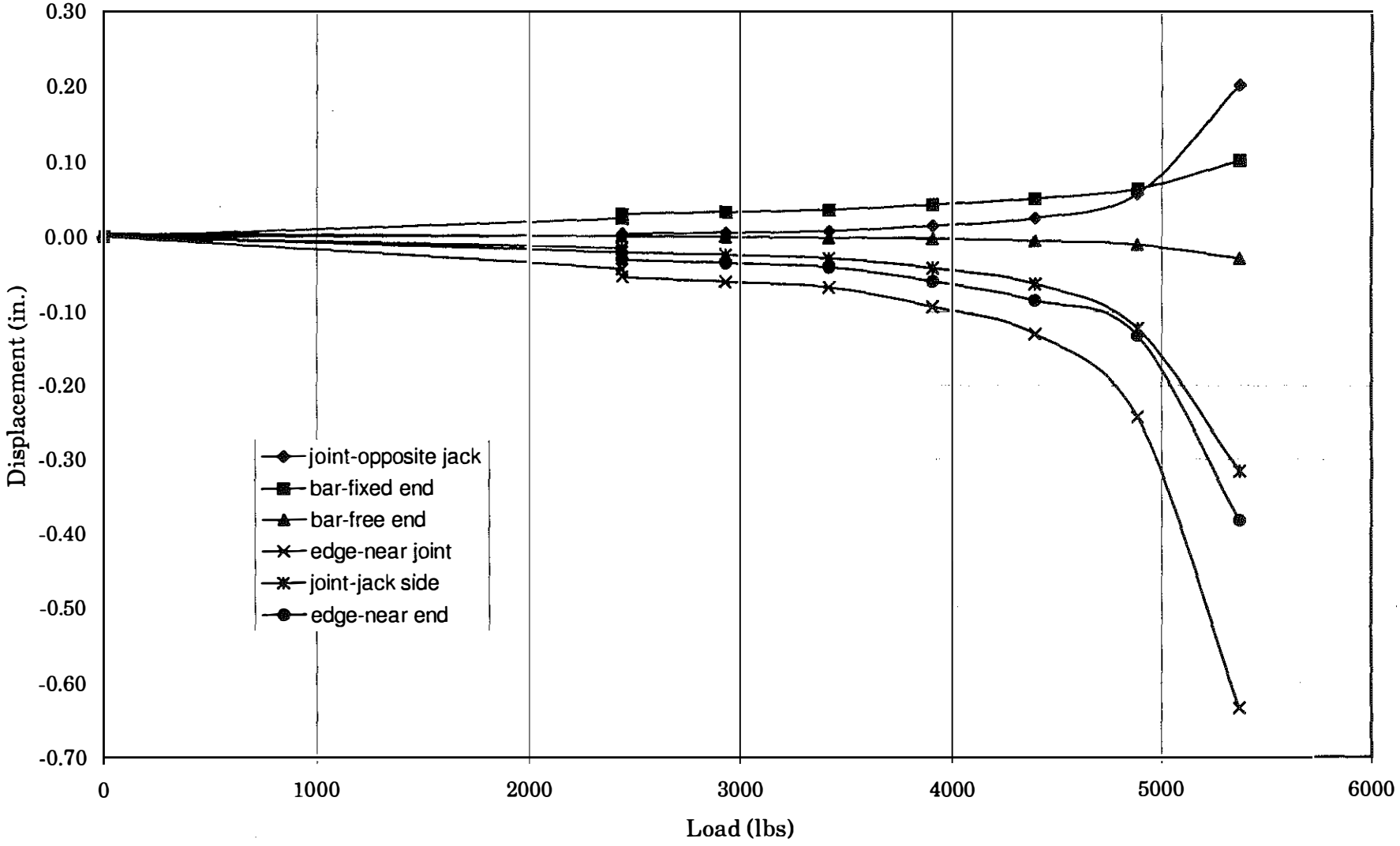

Figure I.2 Load-Displacement Relationship for the Specimen S2

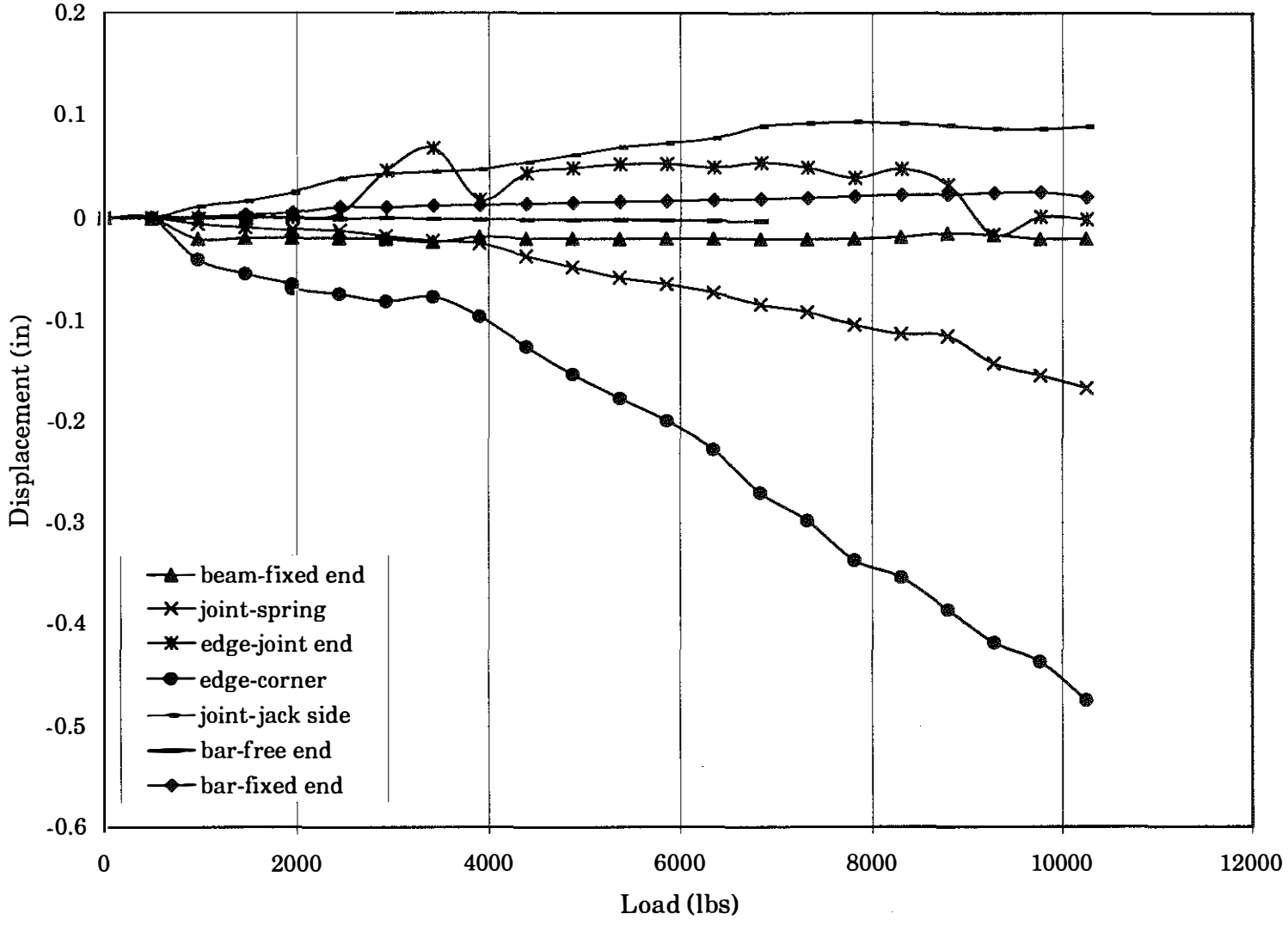

Figure I.3 a Load-Displacement Relationship for the Specimen S3

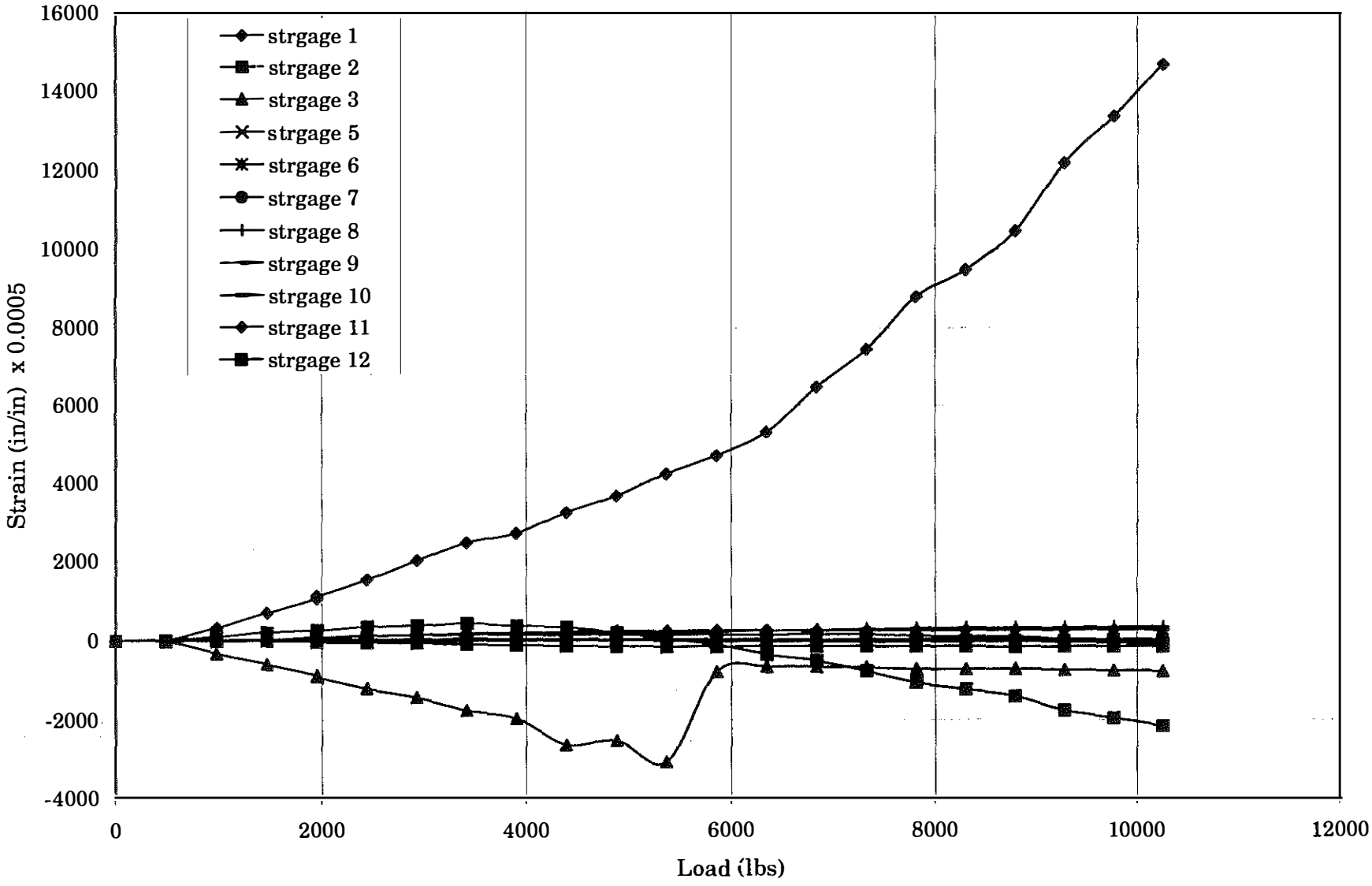

Figure I.3b Load-Strain Relationship for the Specimen S3

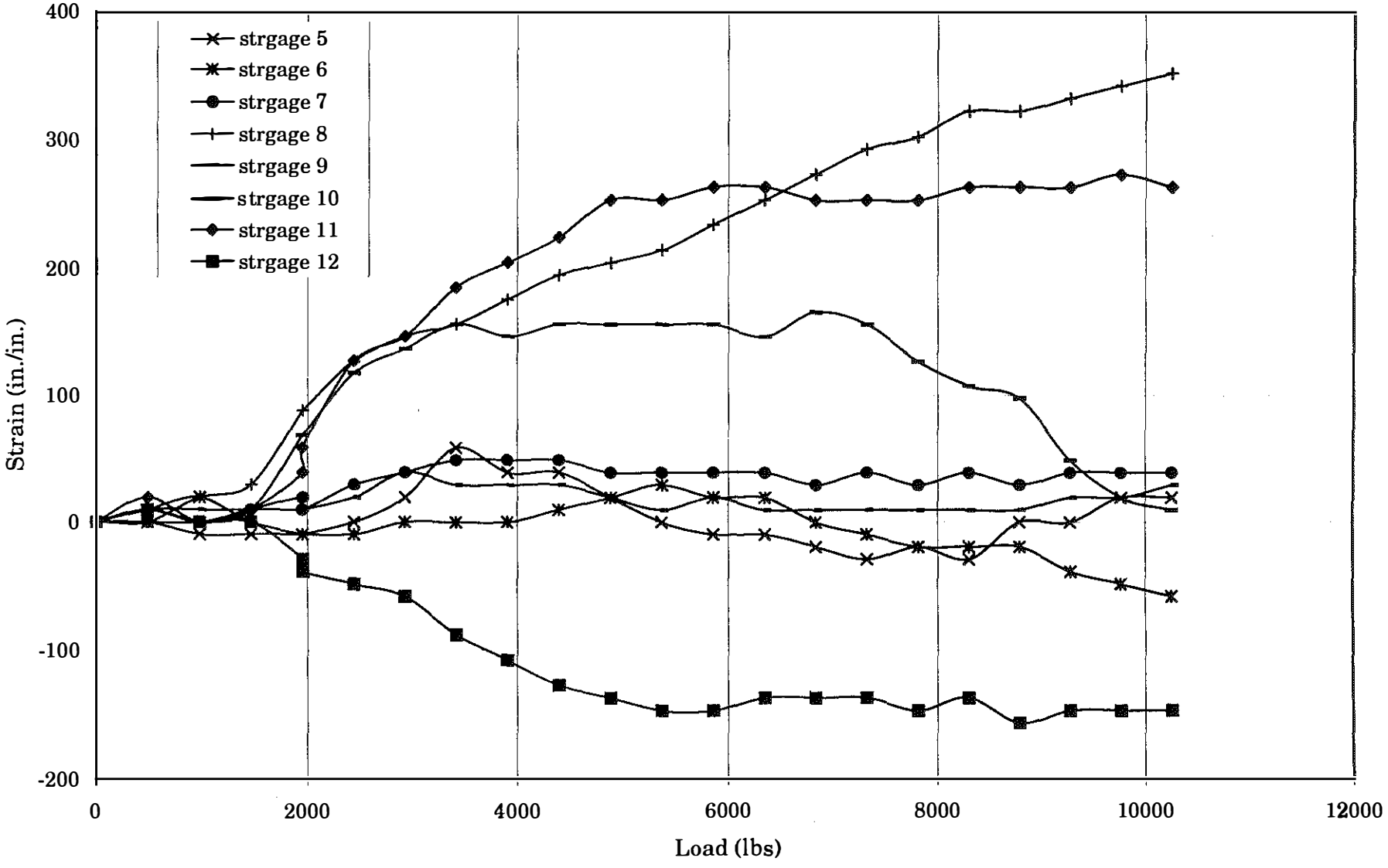

Load-Strain Relationship for the Specimen S3

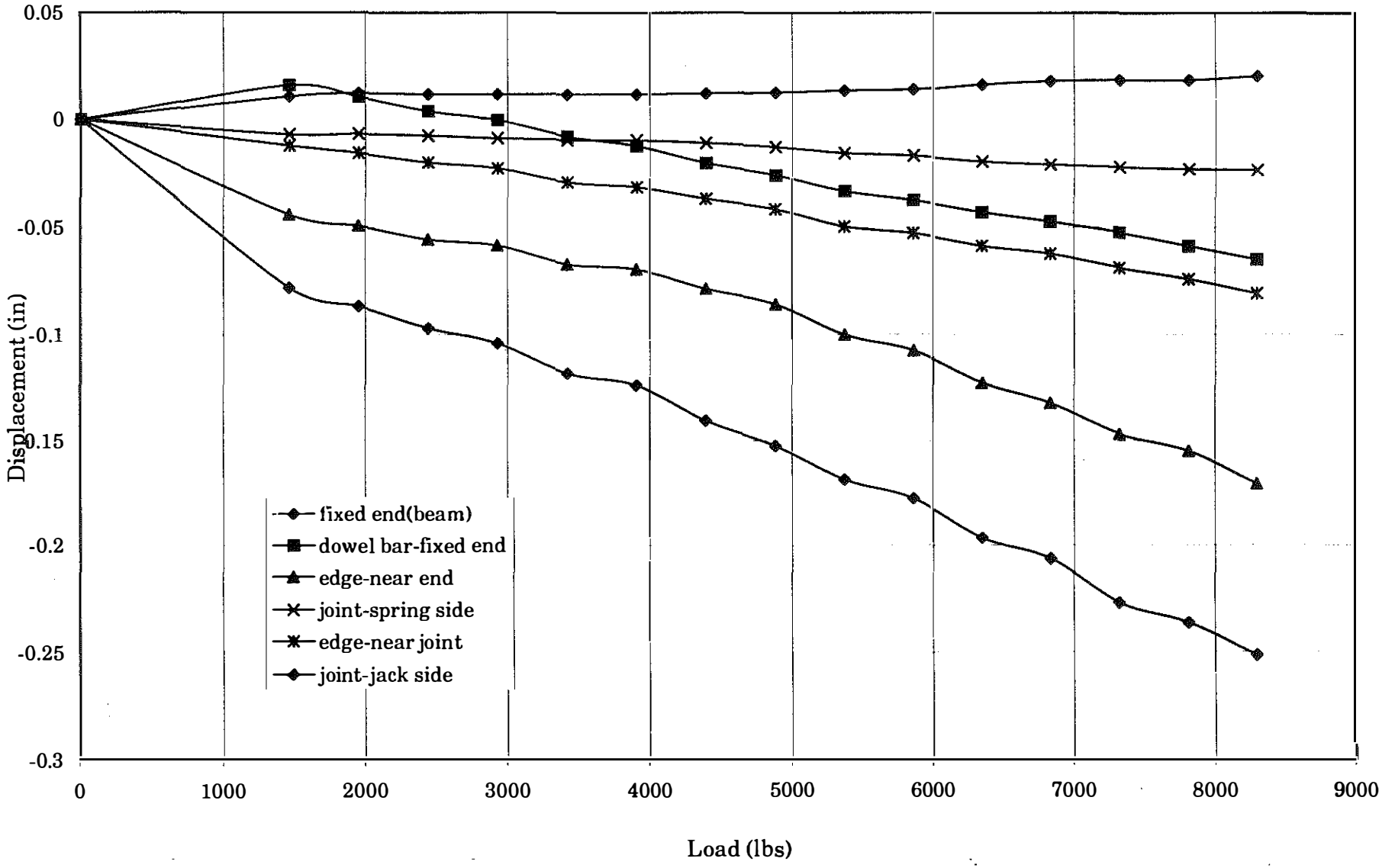

Figure I.4 Load-Displacement Relationship for the Specimen S4

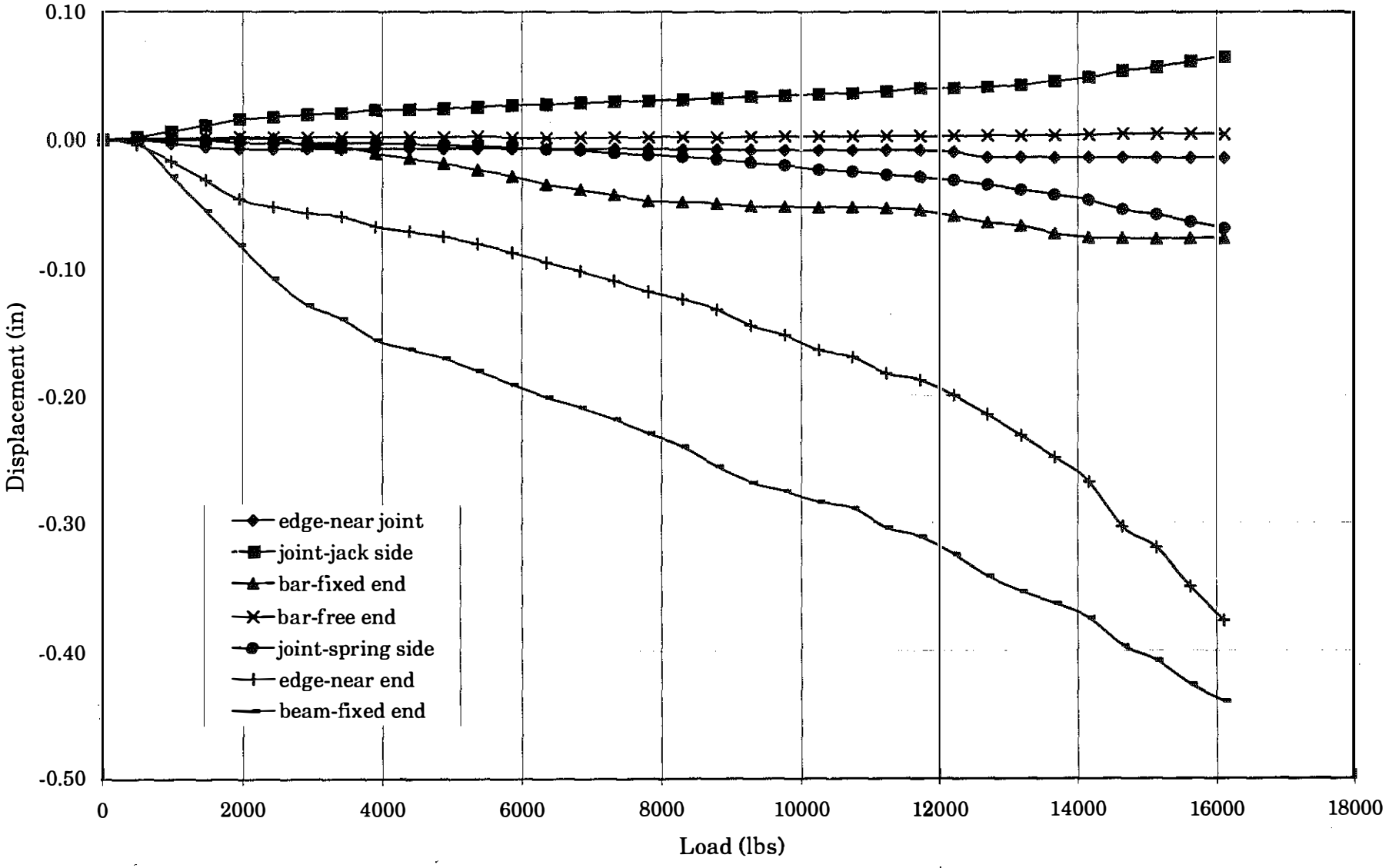

Figure I.5 Load-Displacement Relationship for the Specimen S5

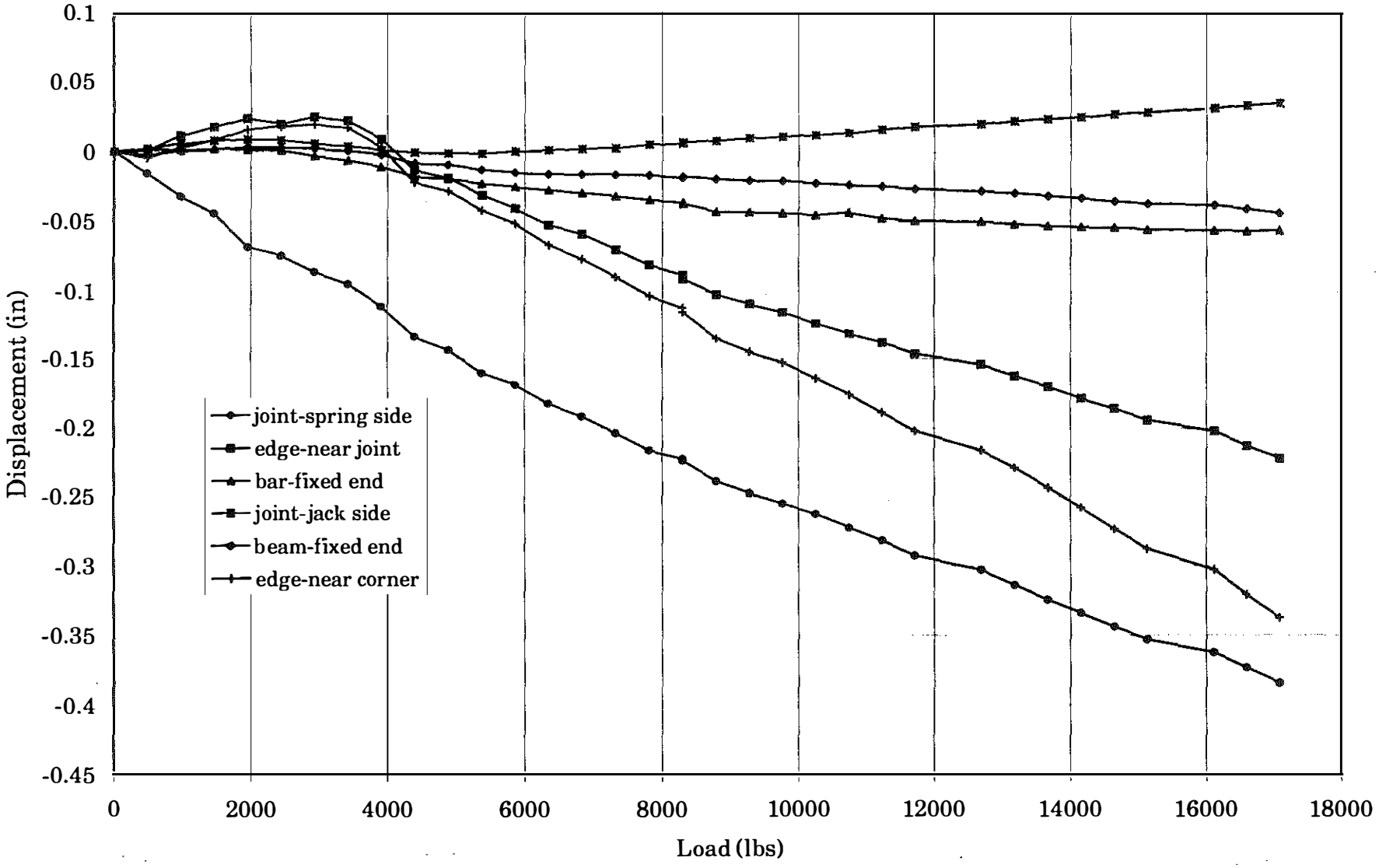

Figure I.6a Load-Displacement Relationship for the Specimen S6

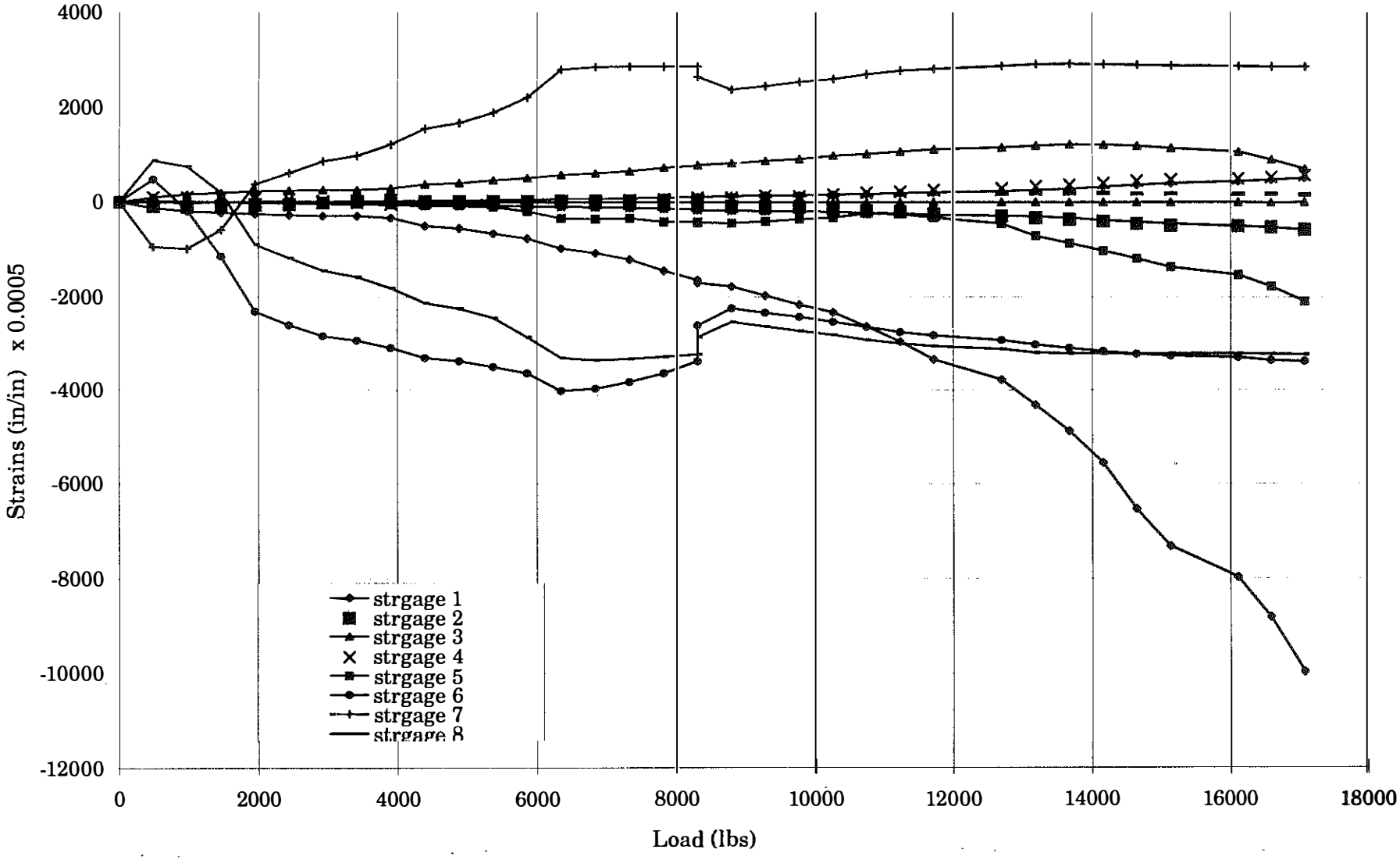

Figure I.6b Load-Strain Relationship for the S6 Specimen

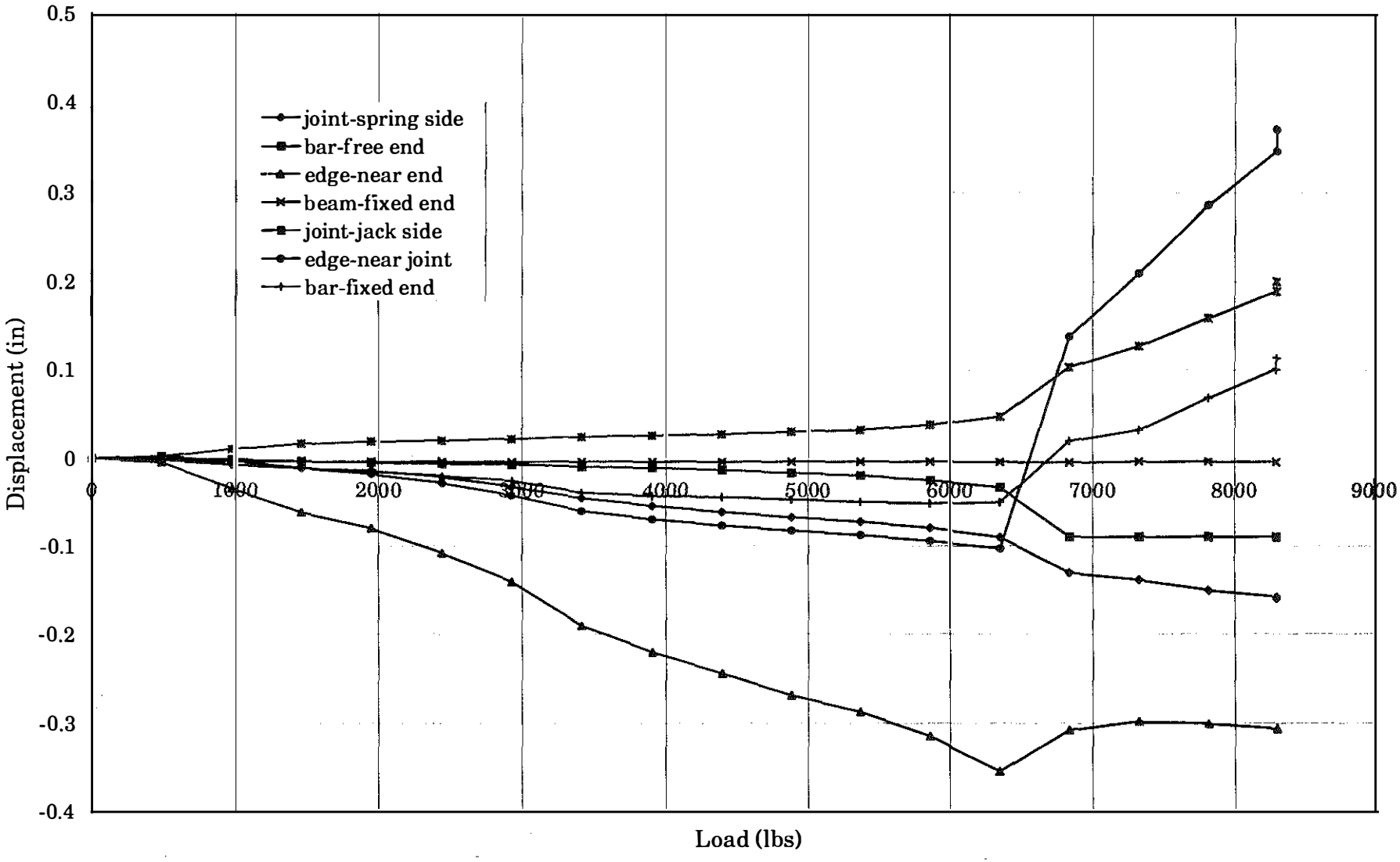

Figure I.7 Load-Displacement Relationship for the Specimen S7

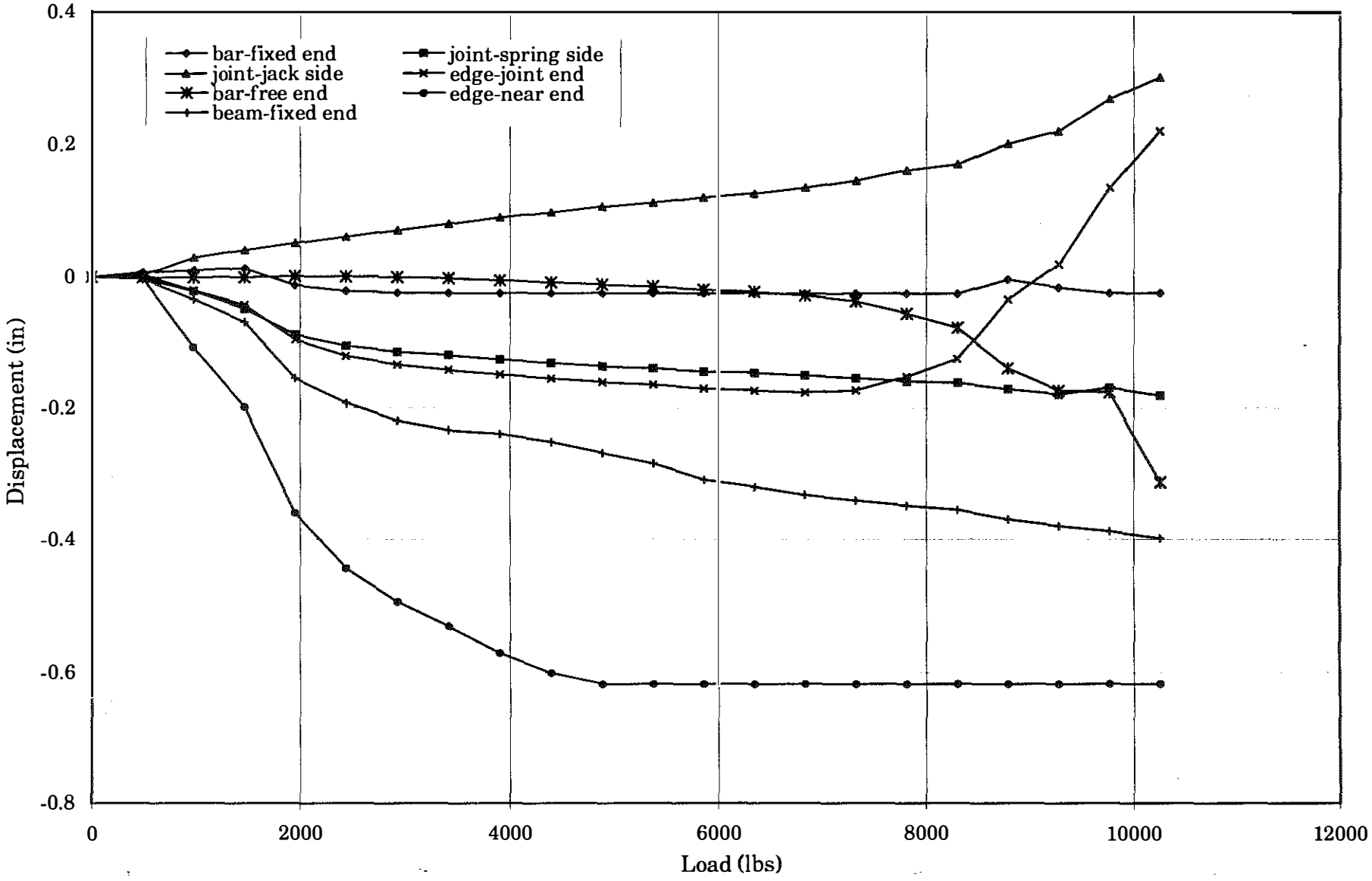

Figure I.8 Load-Displacement Relationship for the Specimen S8

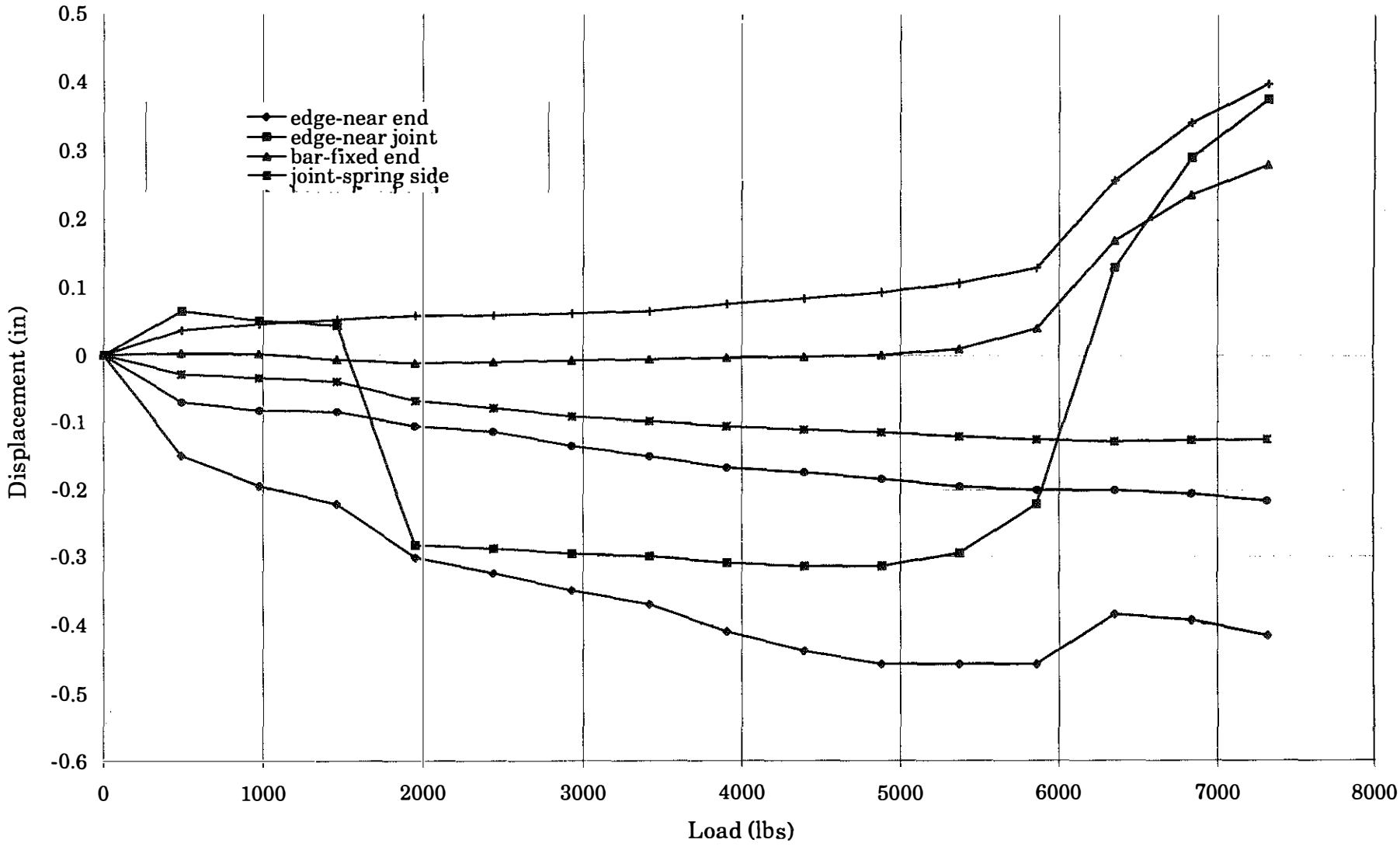

Figure I.9a Load-Displacement Relationship for the Specimen S9

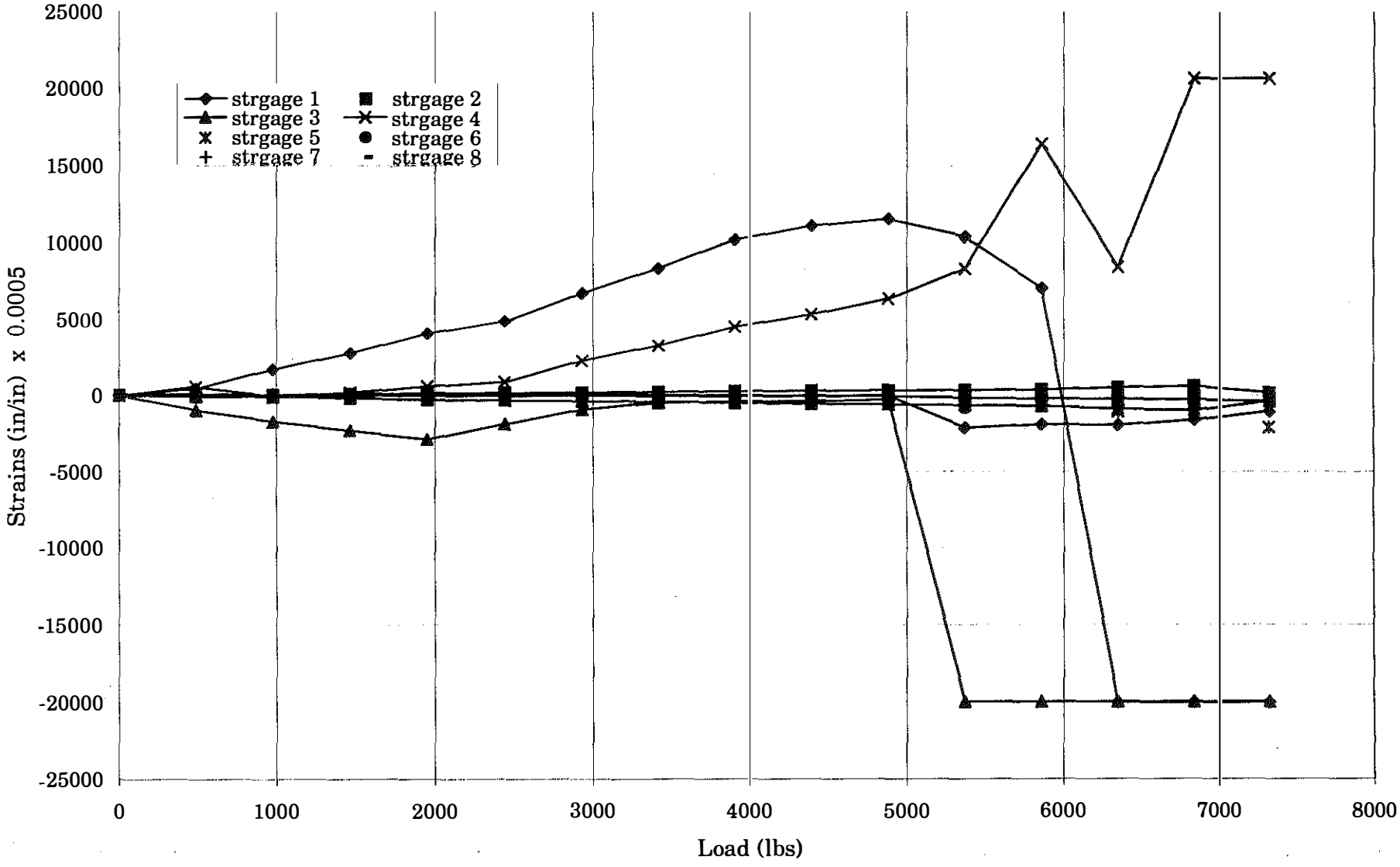

Figure I.9b Load-Strain Relationship for the S9 Specimen

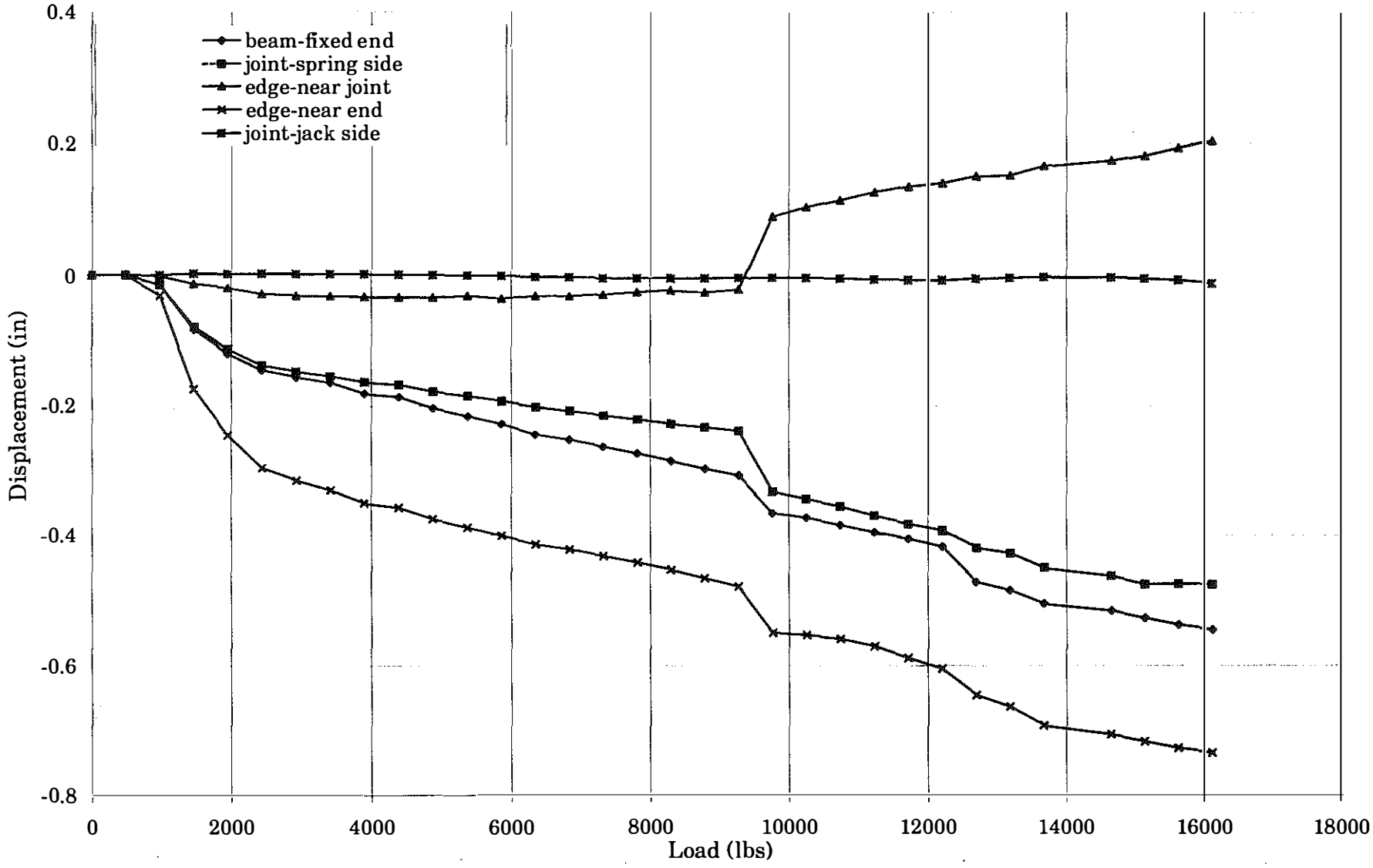

Figure II.1 Load-Displacement Relationship for the Specimen A1

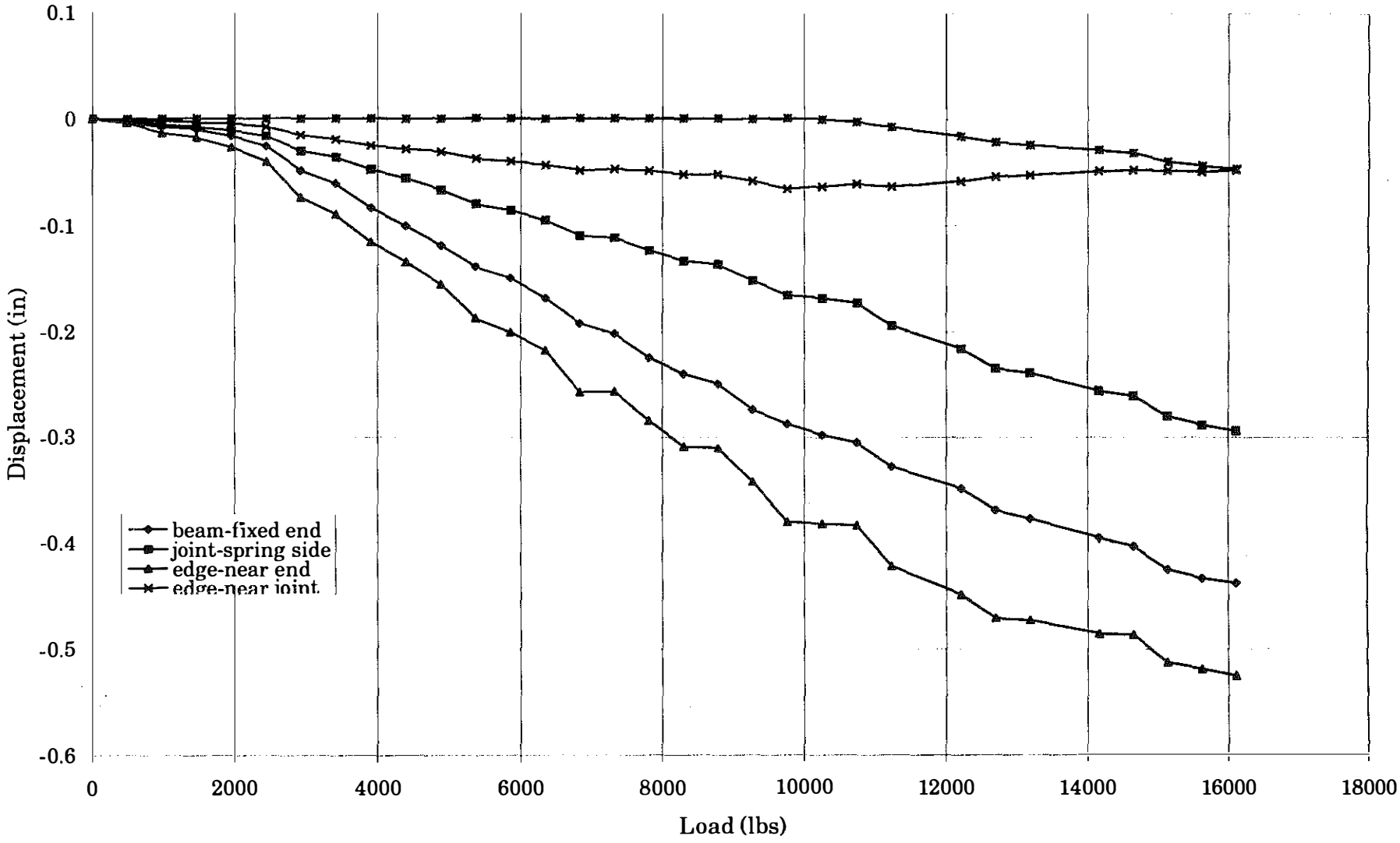

Figure II.2 Load-Displacement Relationship for the Specimen A2 - Run 1

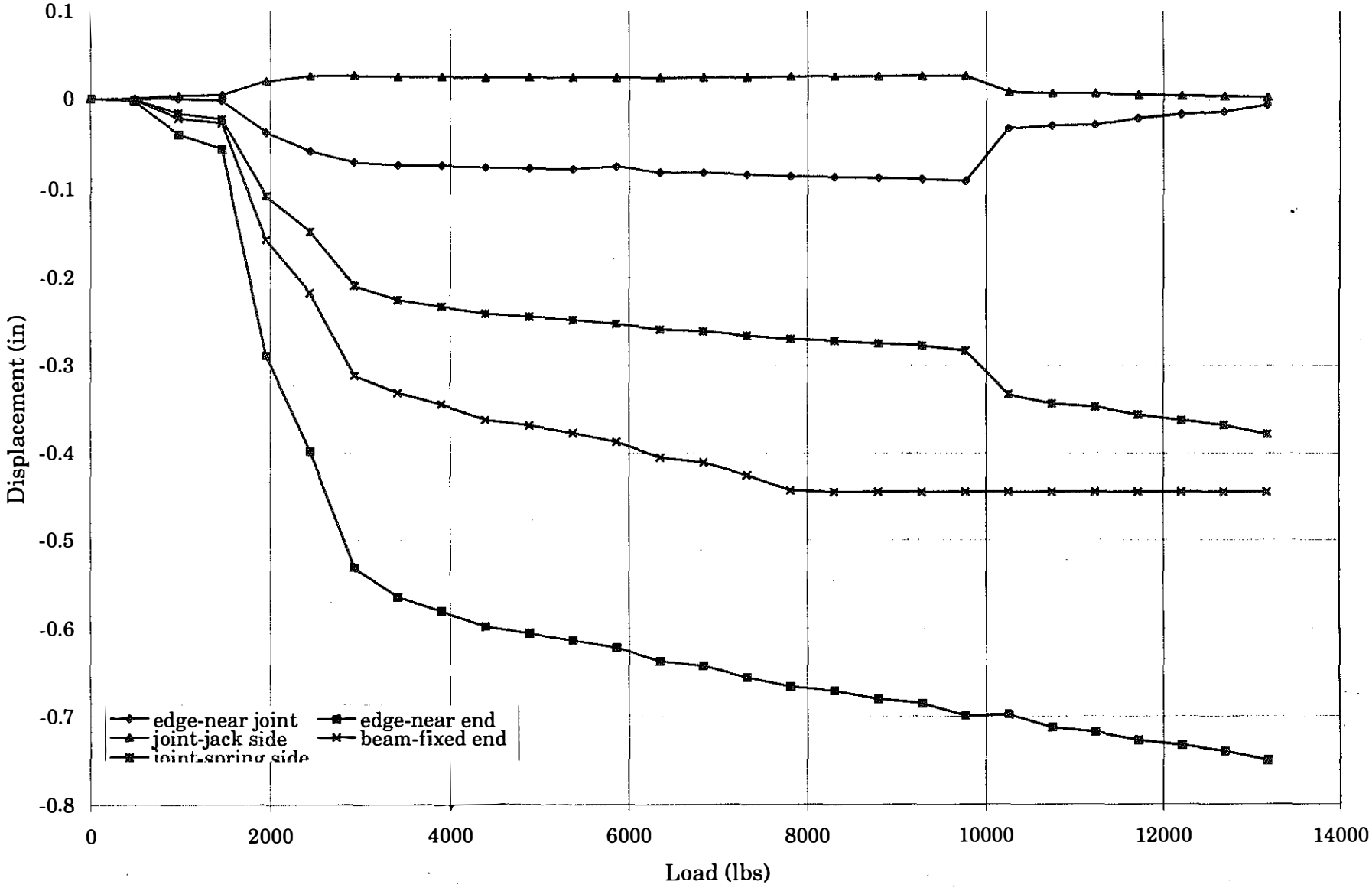

Figure II.3 Load-Displacement Relationship for the Specimen A3

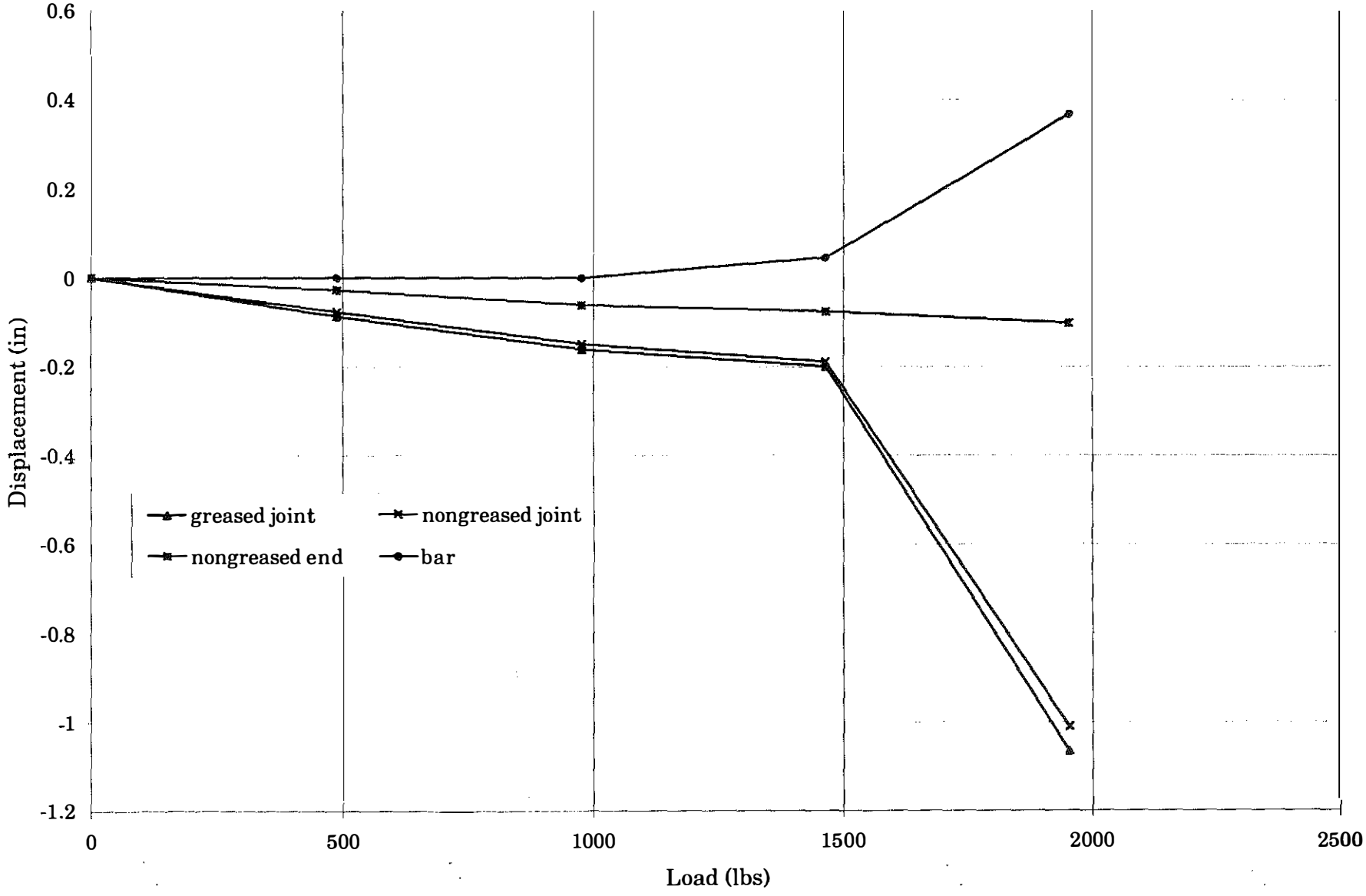

Figure III.1a Load (at Nongreased side)-Displacement Relationship for the B1 Specimen

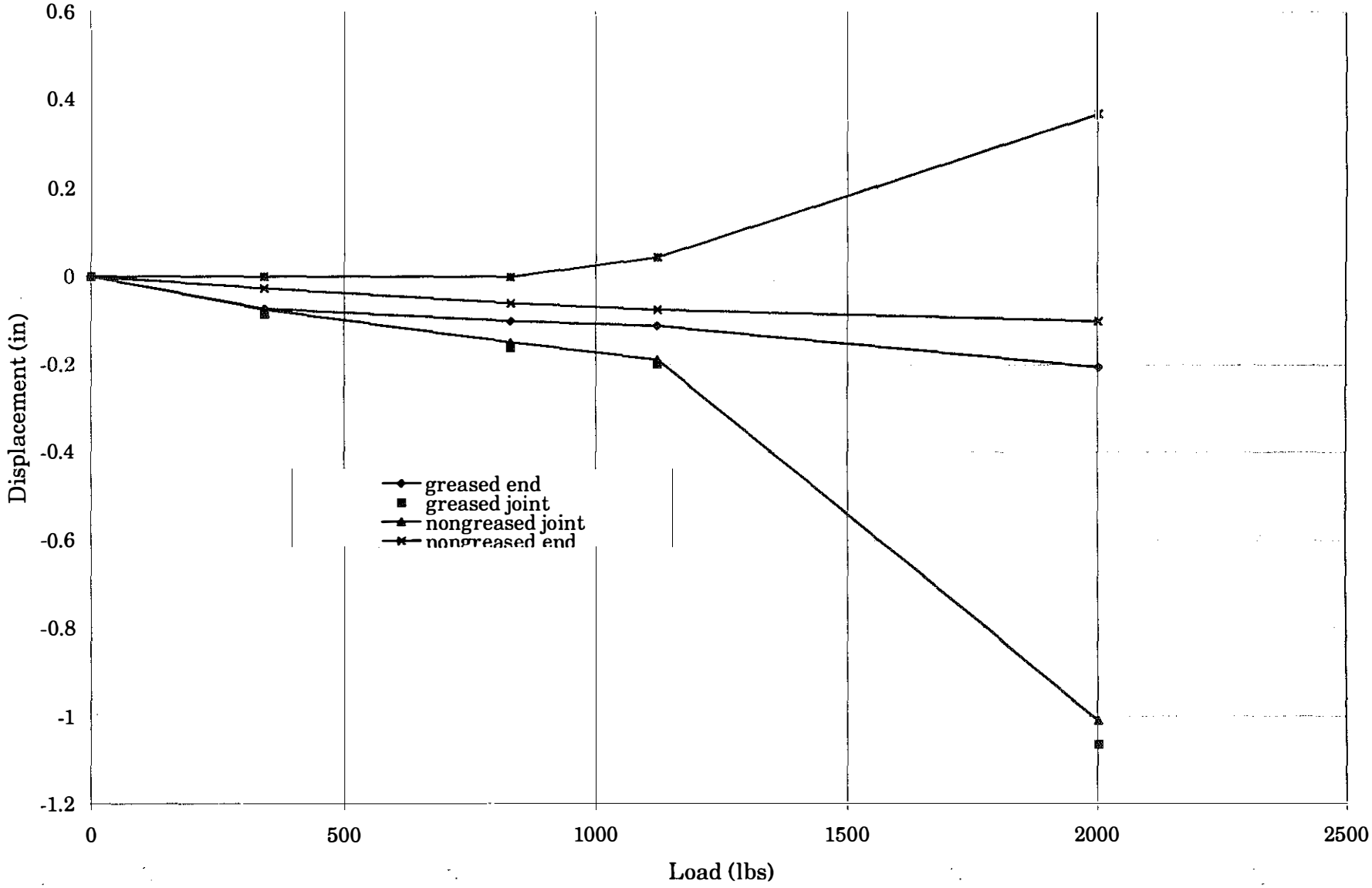

Figure III.1b Load (at Greased Side) -Displacement Relationship for the B1 Specimen

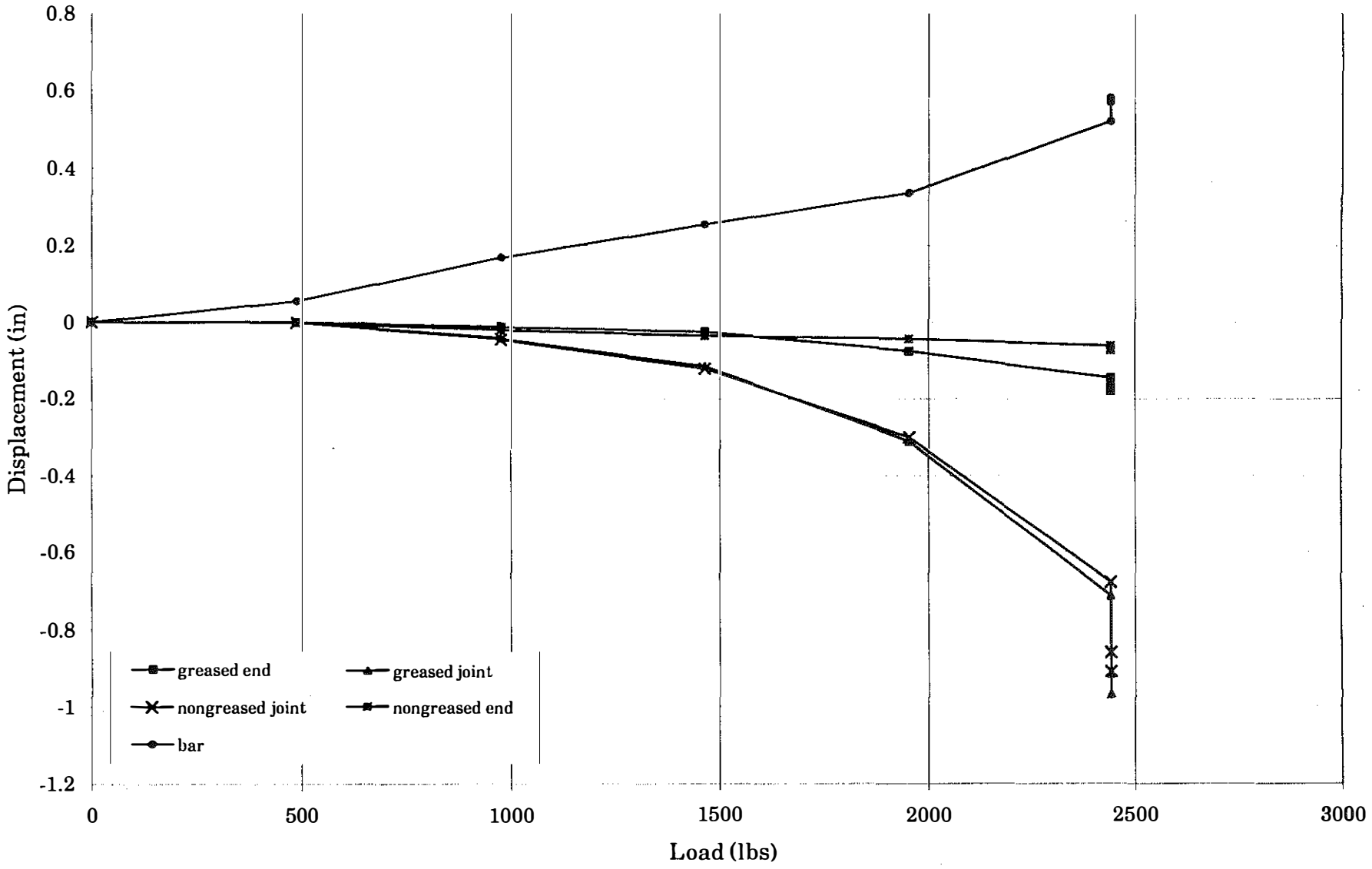

Figure III.2a Load (nongreased side)-Displacement Relationship for the Specimen B2 - Load at Non-greased side

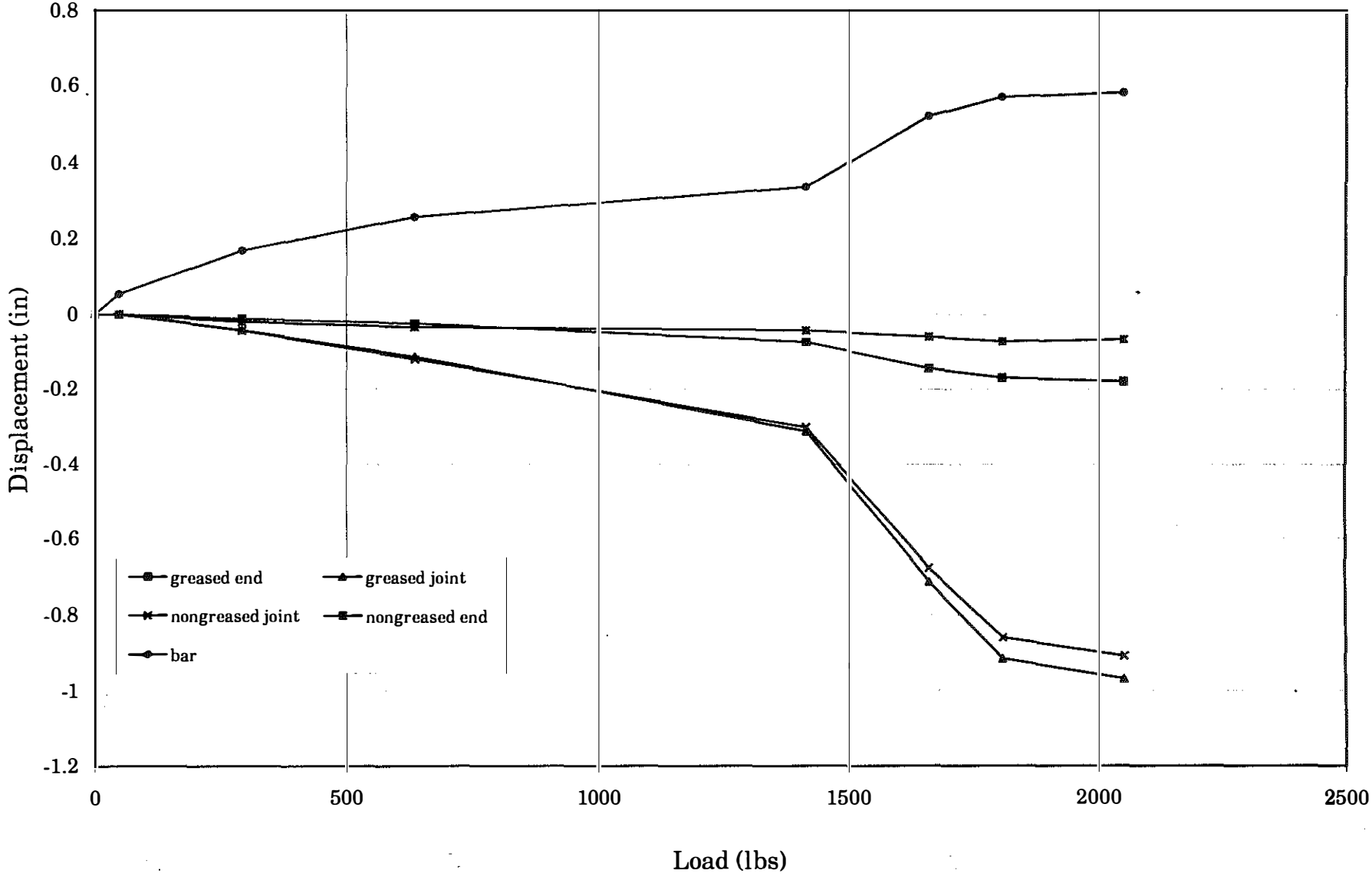

Figure III.2b Load (at Greased Side)-Displacement Relationship for the Specimen B2

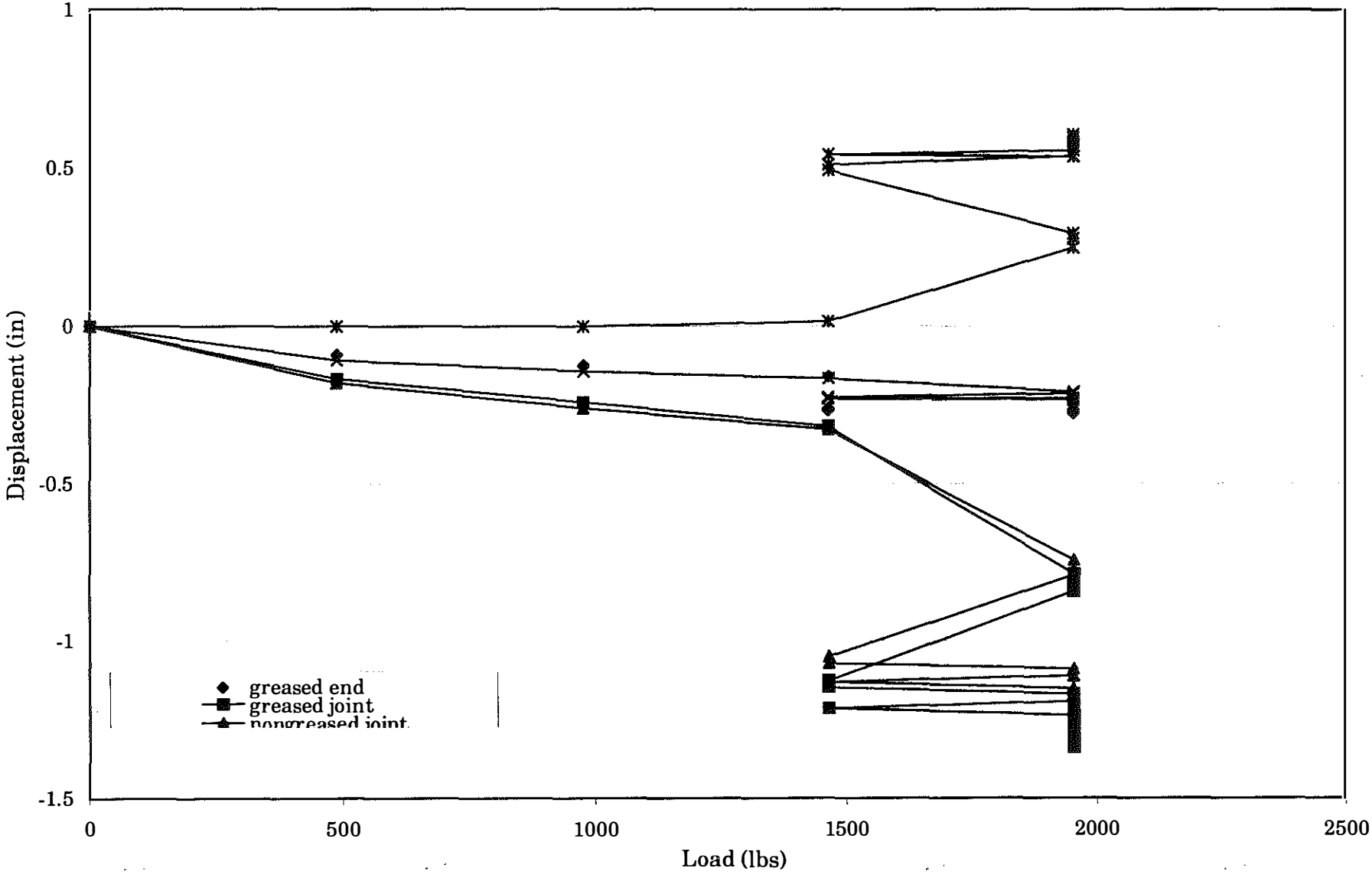

Figure IIII.3a Load (at Nongreased Side) -Displacement Relationship for the Specimen B3

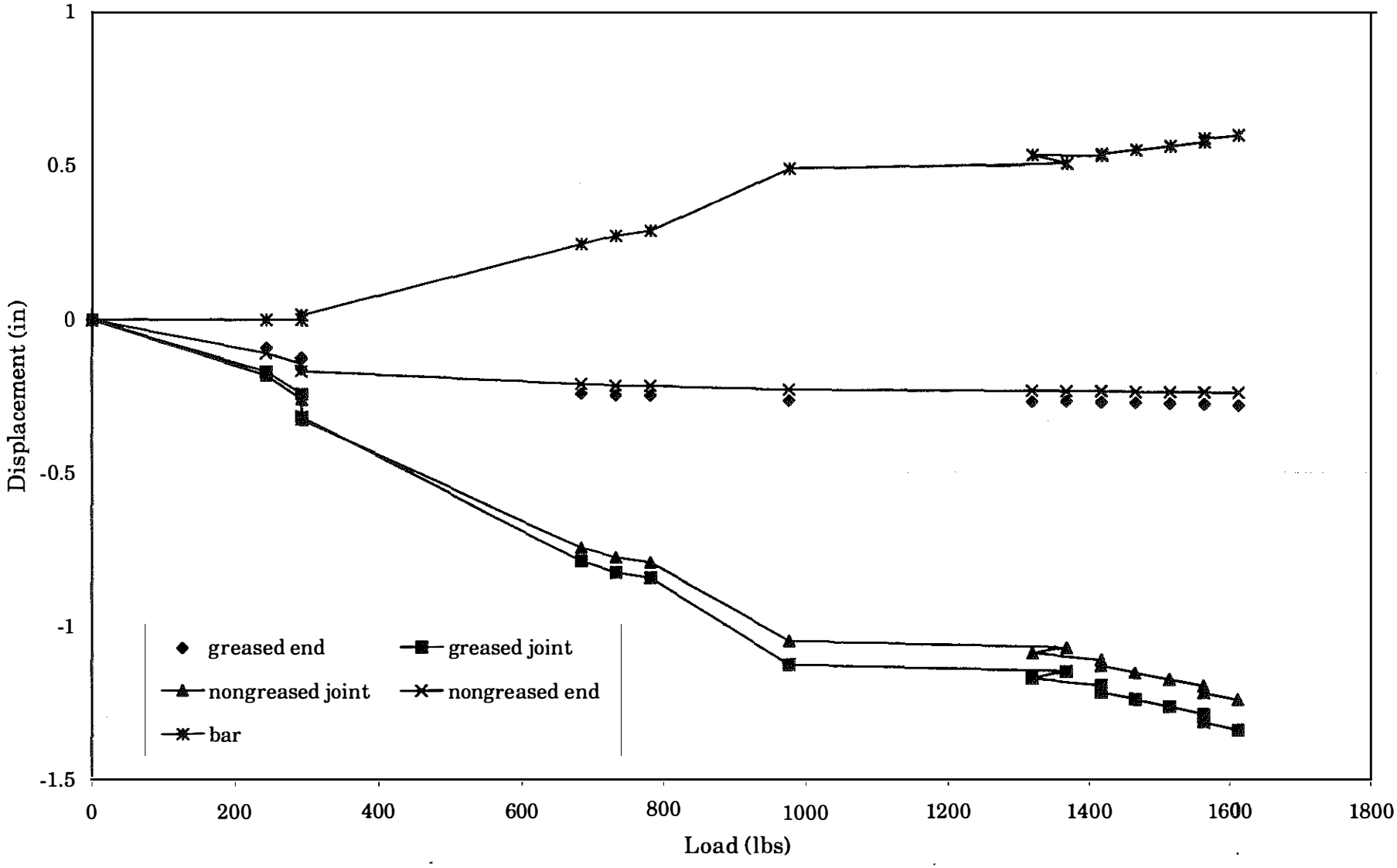

Figure III.3b Load (Greased Side)-Displacement Relationship for the Specimen B3

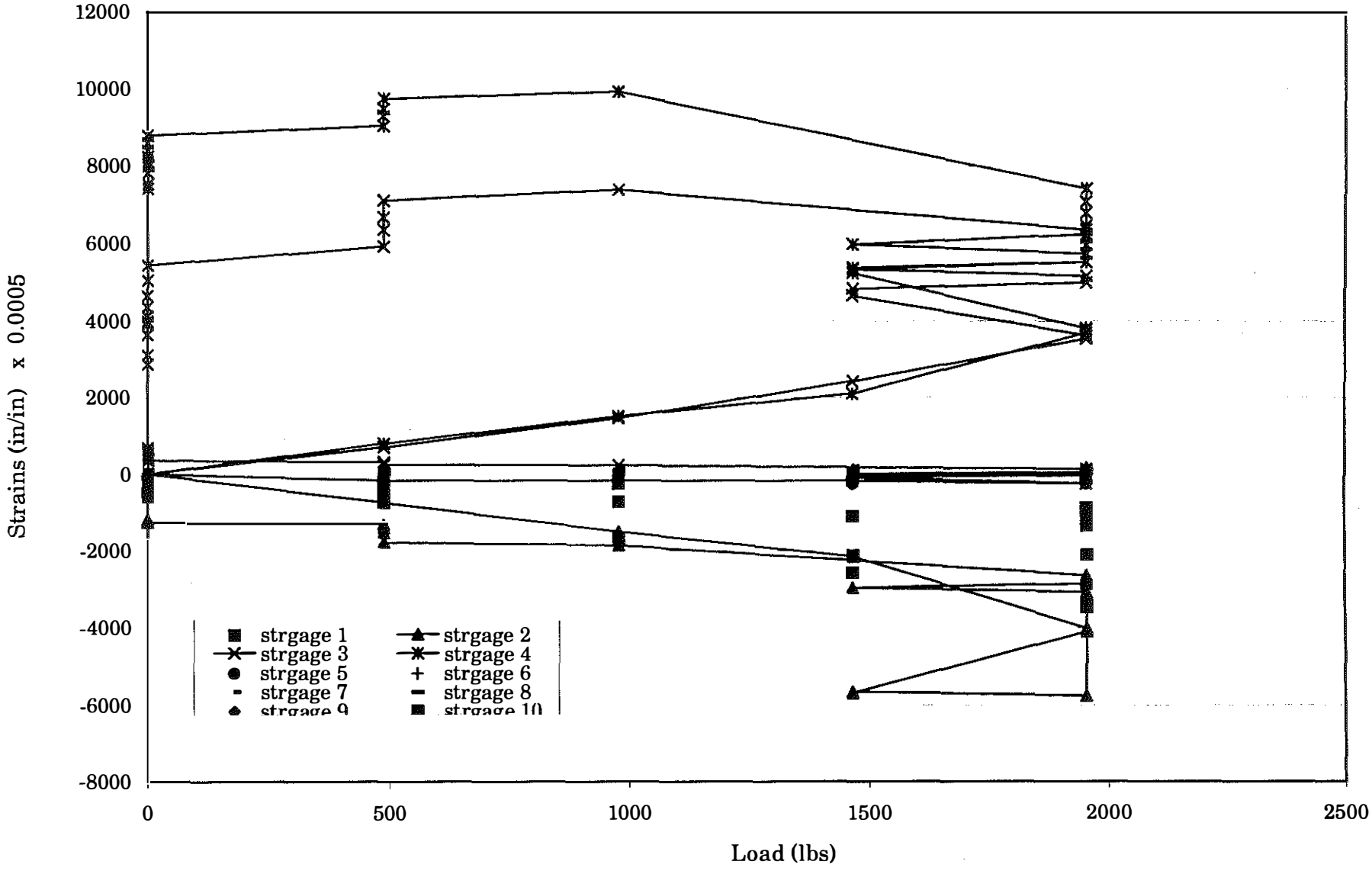

Figure III.3c Load (at Non-greased Side)-Strain Relationship for the Specimen B3

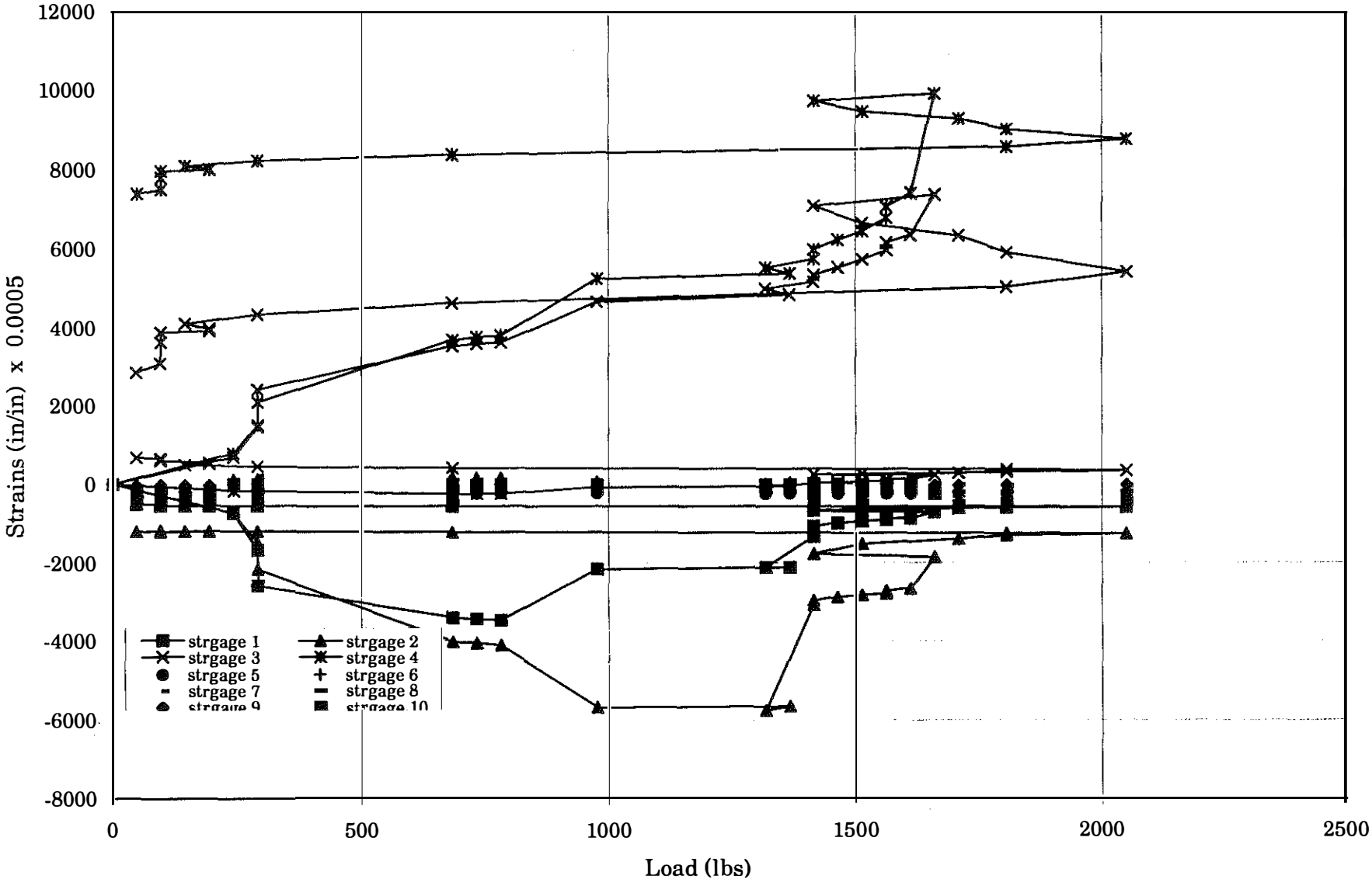

Figure III.3d Load (at Greased Side)-Strain Relationship for the Specimen B3

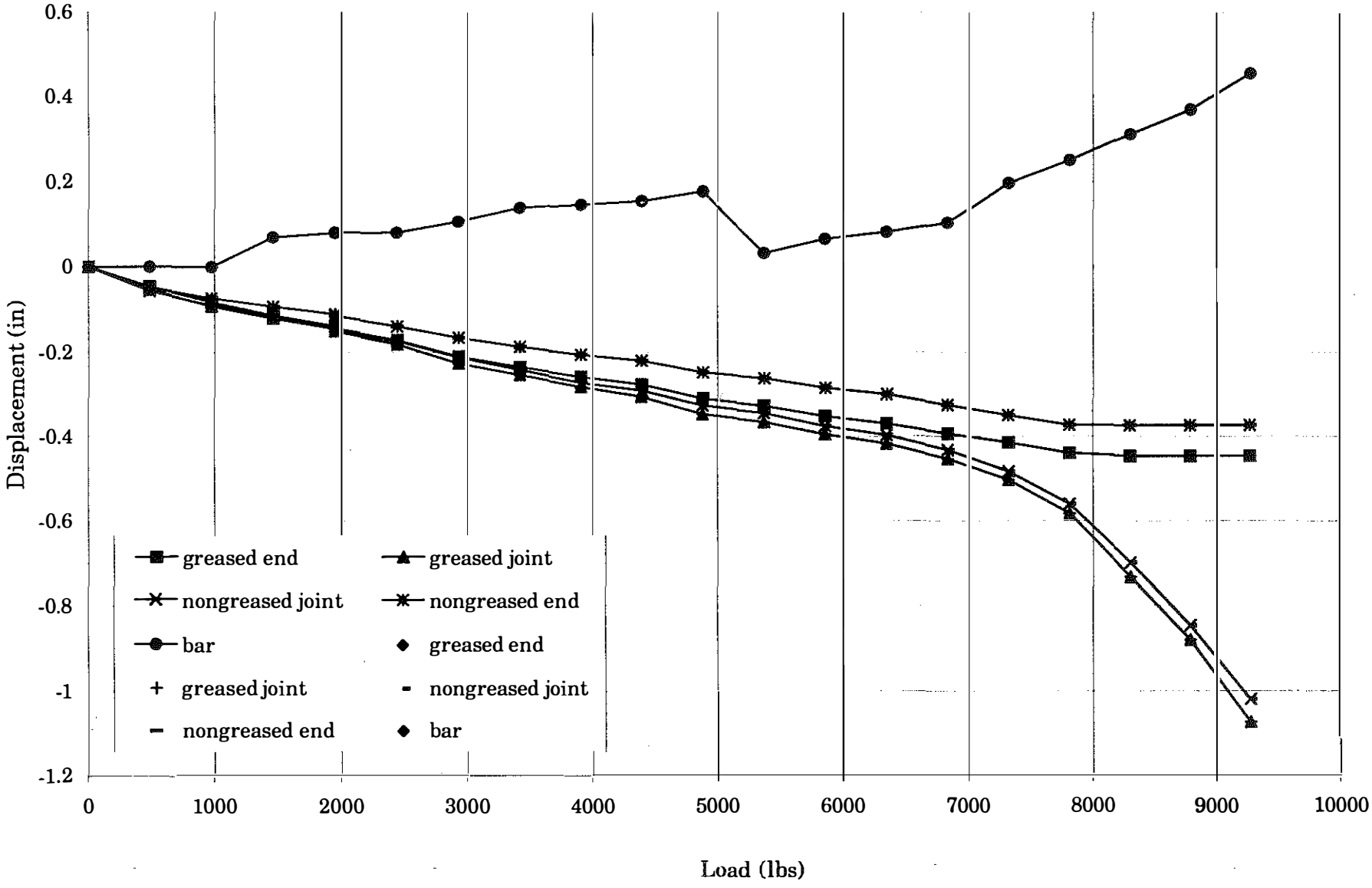

Figure III.4a Load (at Non-greased Side)-Displacement Relationship for the Specimen B4

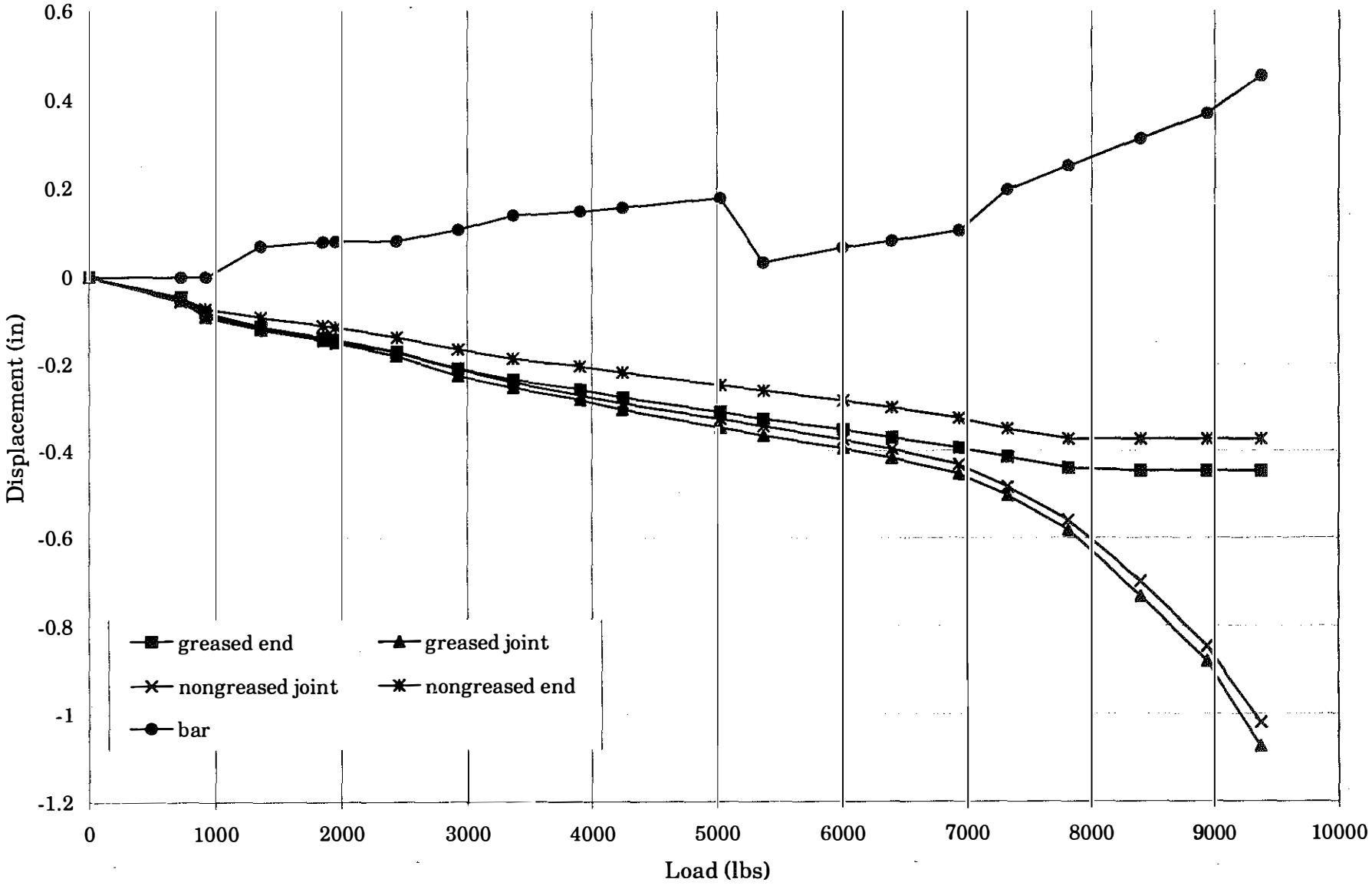

Figure III.4b Load (at Greased Side)-Displacement Relationship for the Specimen B4

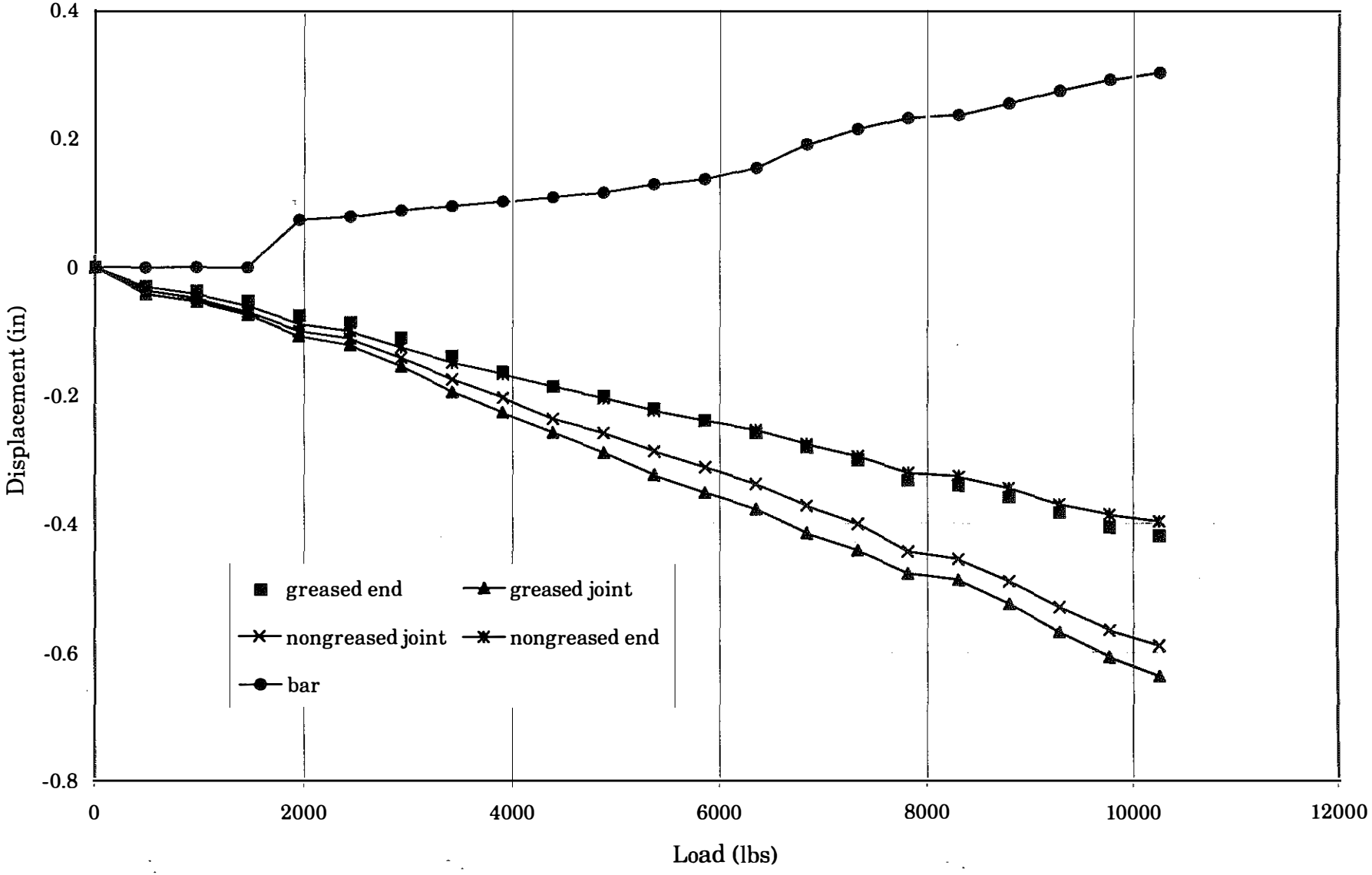

Figure III.5a Load (at Non-greased side)-Displacement Relationship for the Specimen B5

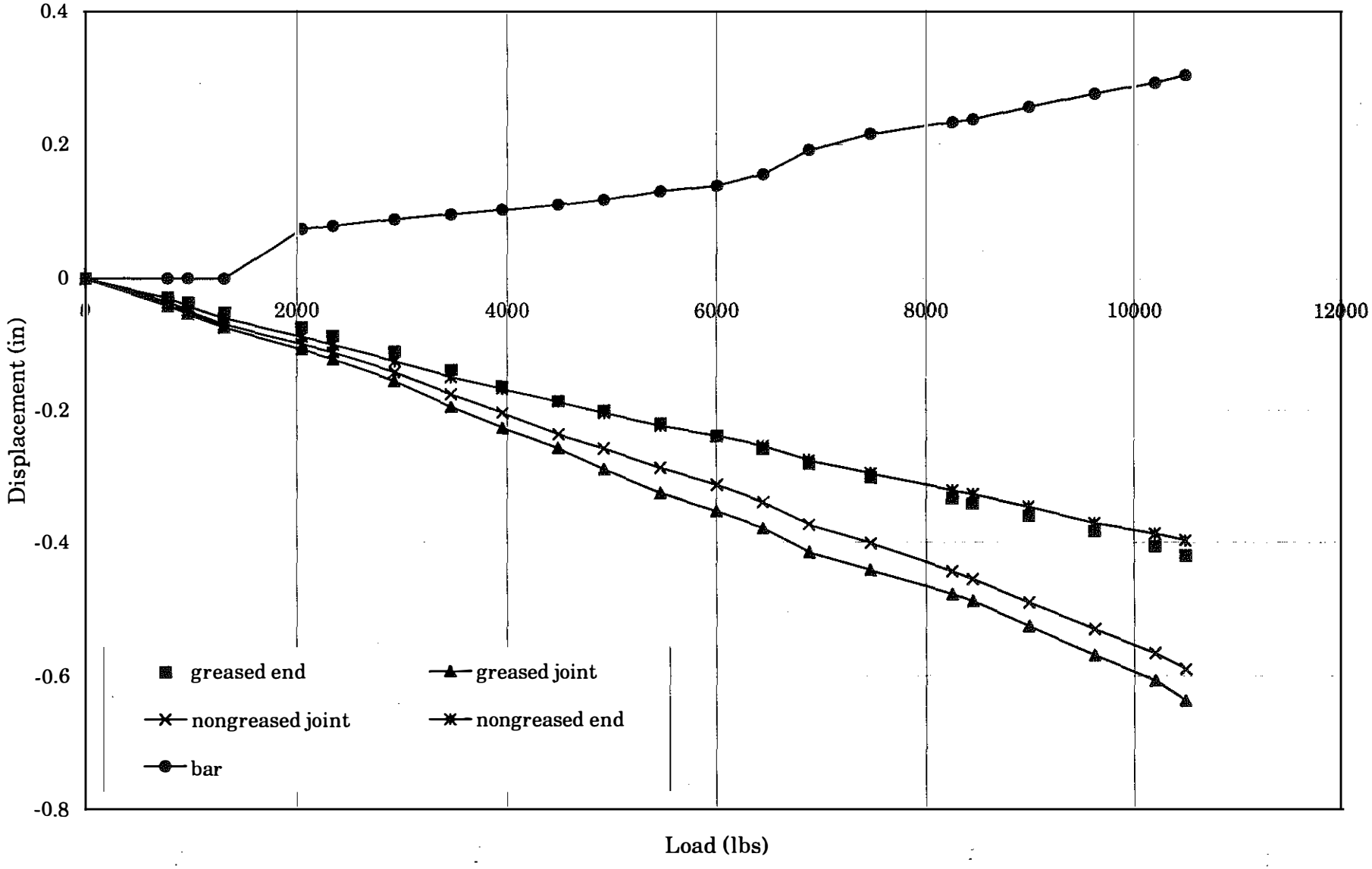

Figure III.5b Load (at Greased Side)-Displacement Relationship for the Specimen B5

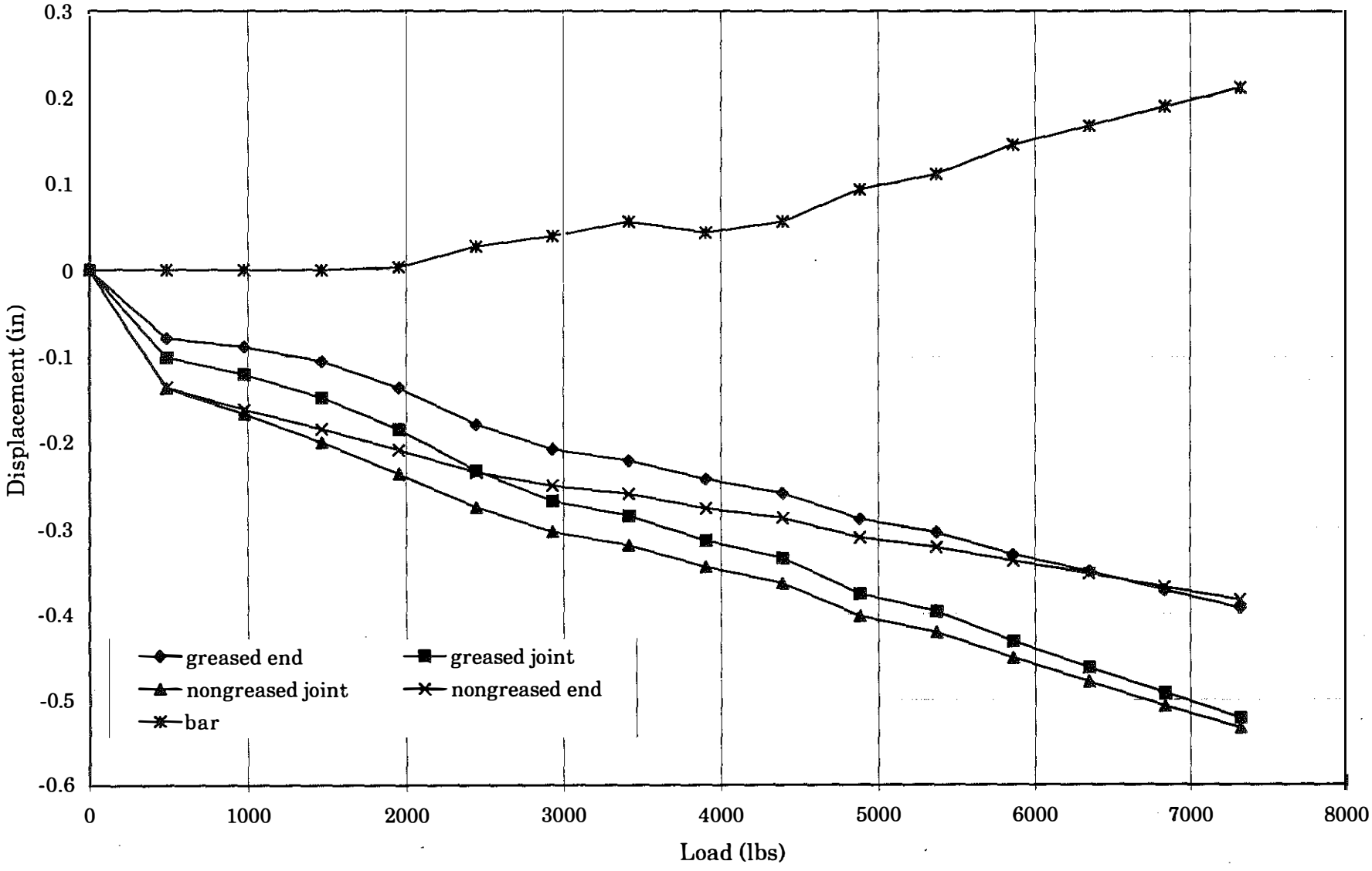

Figure III.6a Load (Nongreased Side)-Displacement relationship for the Specimen B6

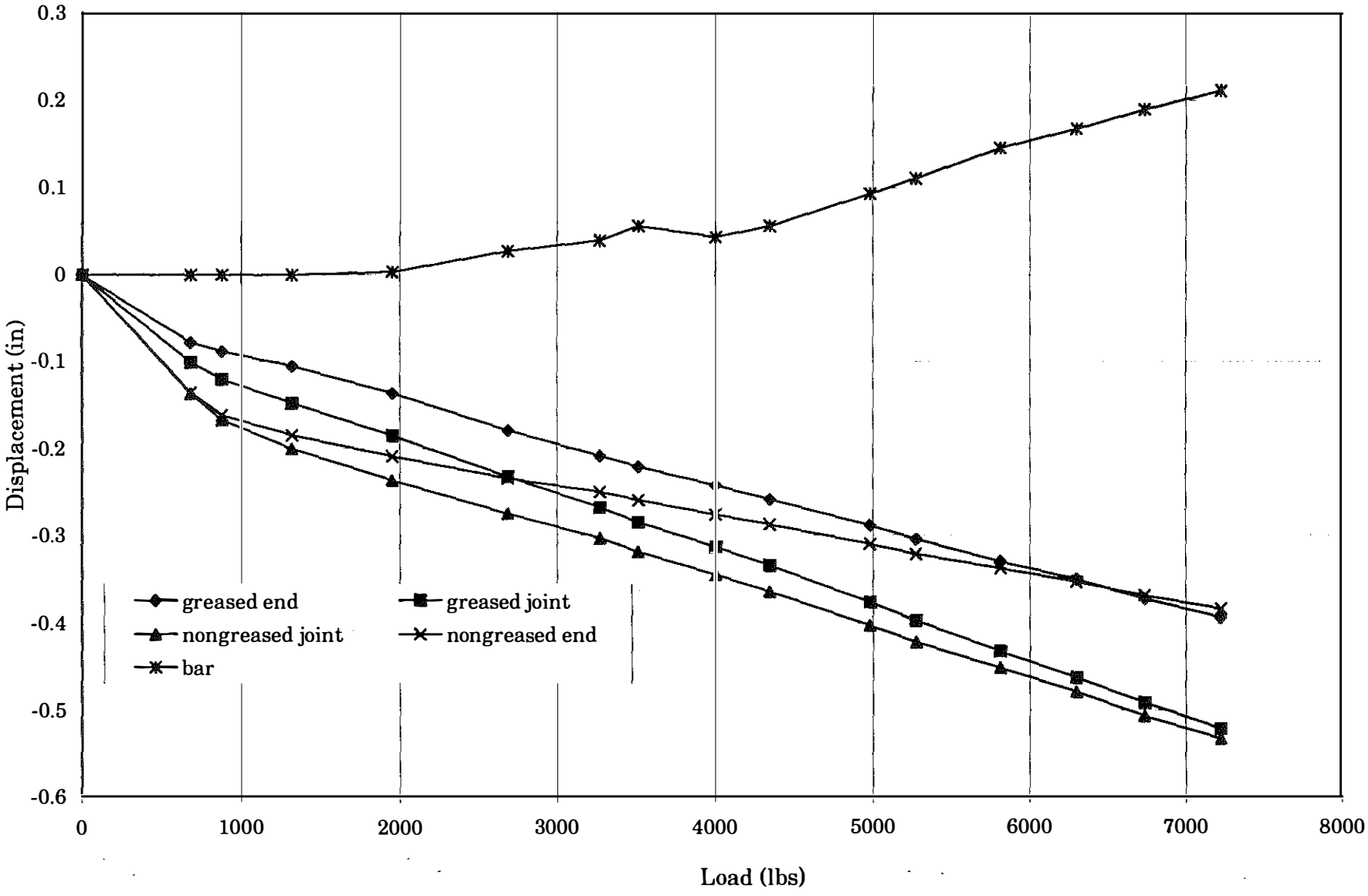

Figure III.6b Load (Greased Side)-Displacement Relationship for the Specimen B6

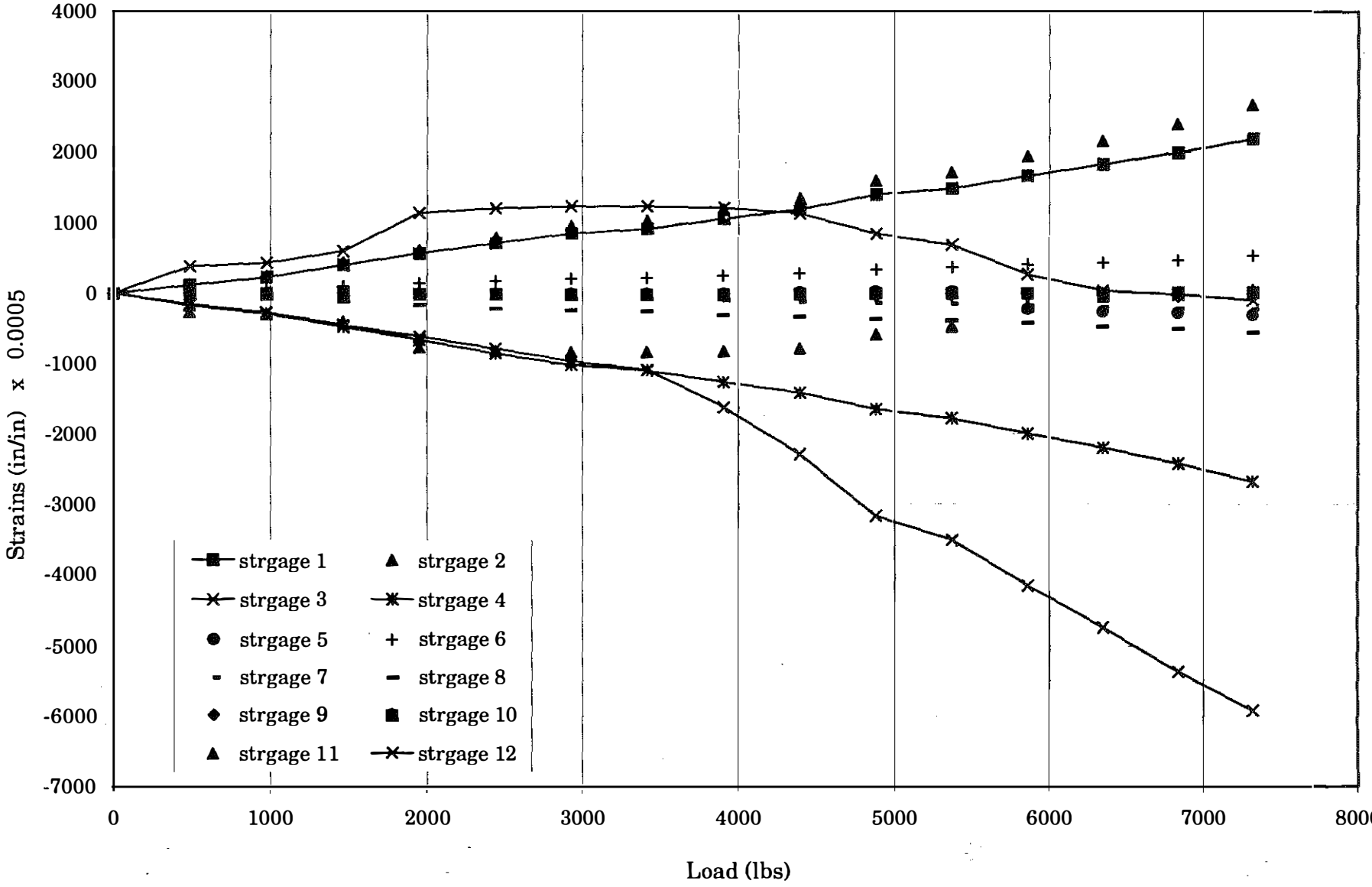

Figure III.6c Load (at Nongreased Side)-Strain Relationship for the Specimen B6

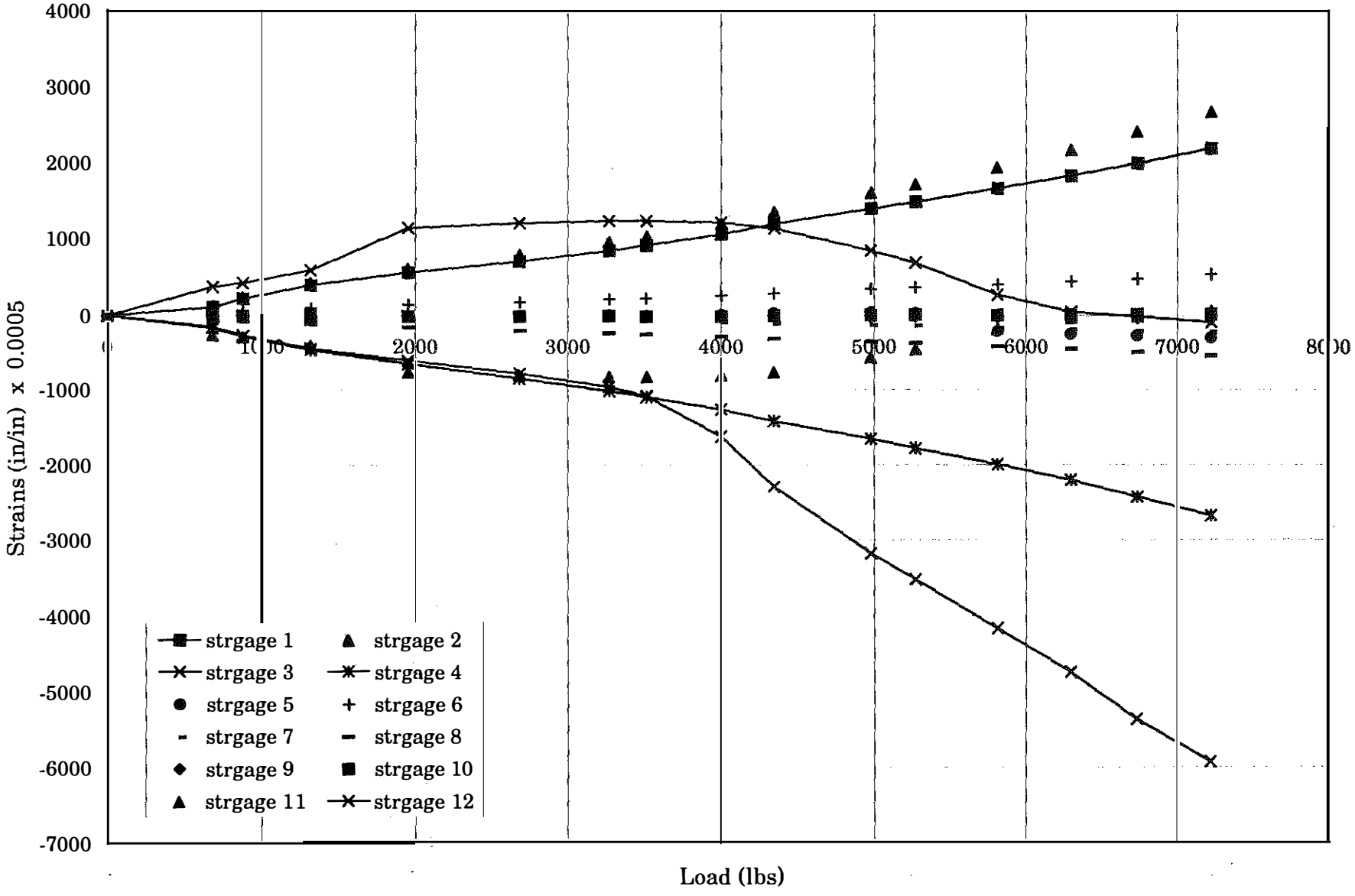

Figure III.6d Load (Greased Side)-Strain Relationship for the Specimen B6

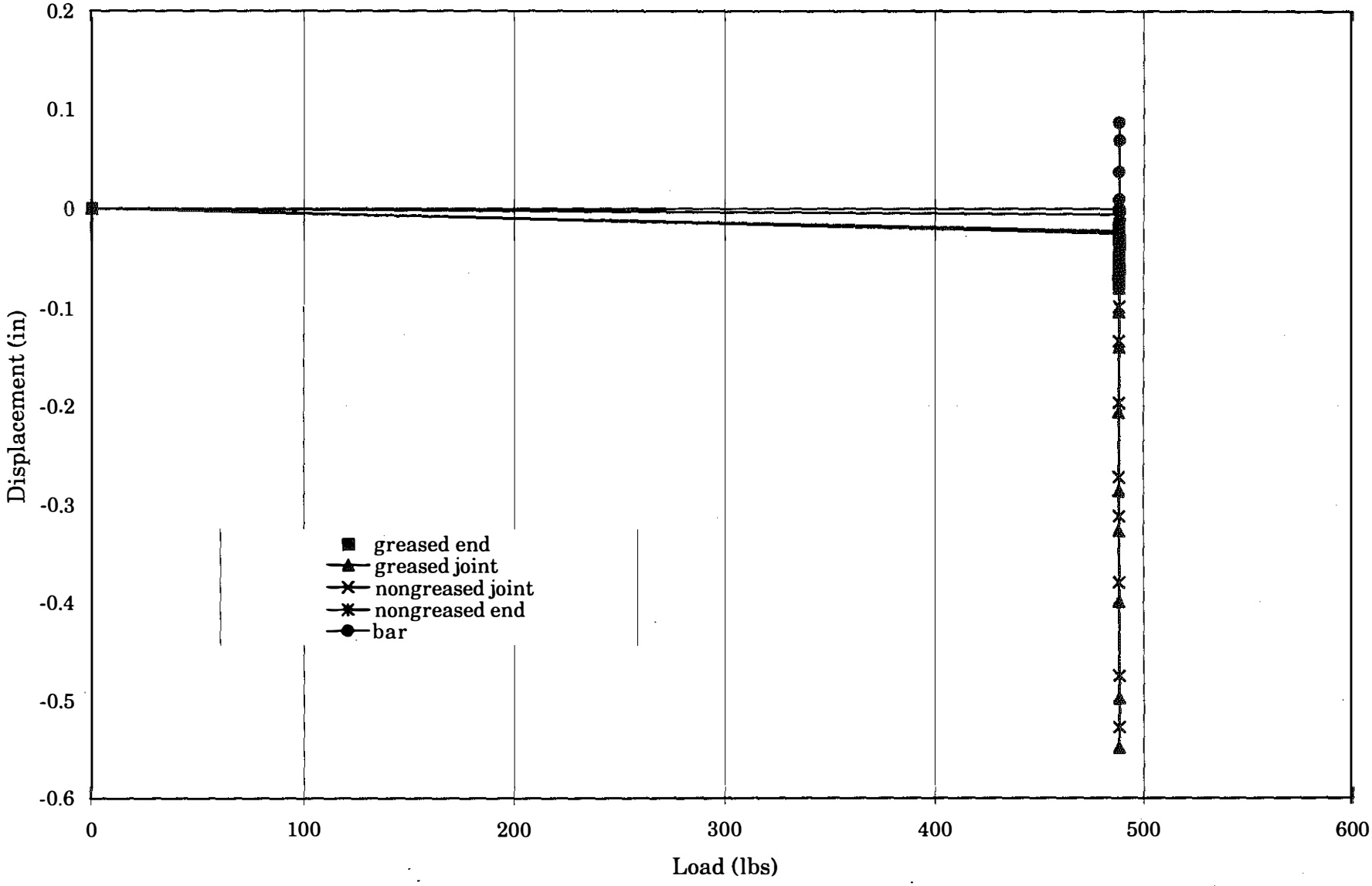

Figure III.7a Load (Nongreased Side)-Displacement Relationship for the Specimen B7

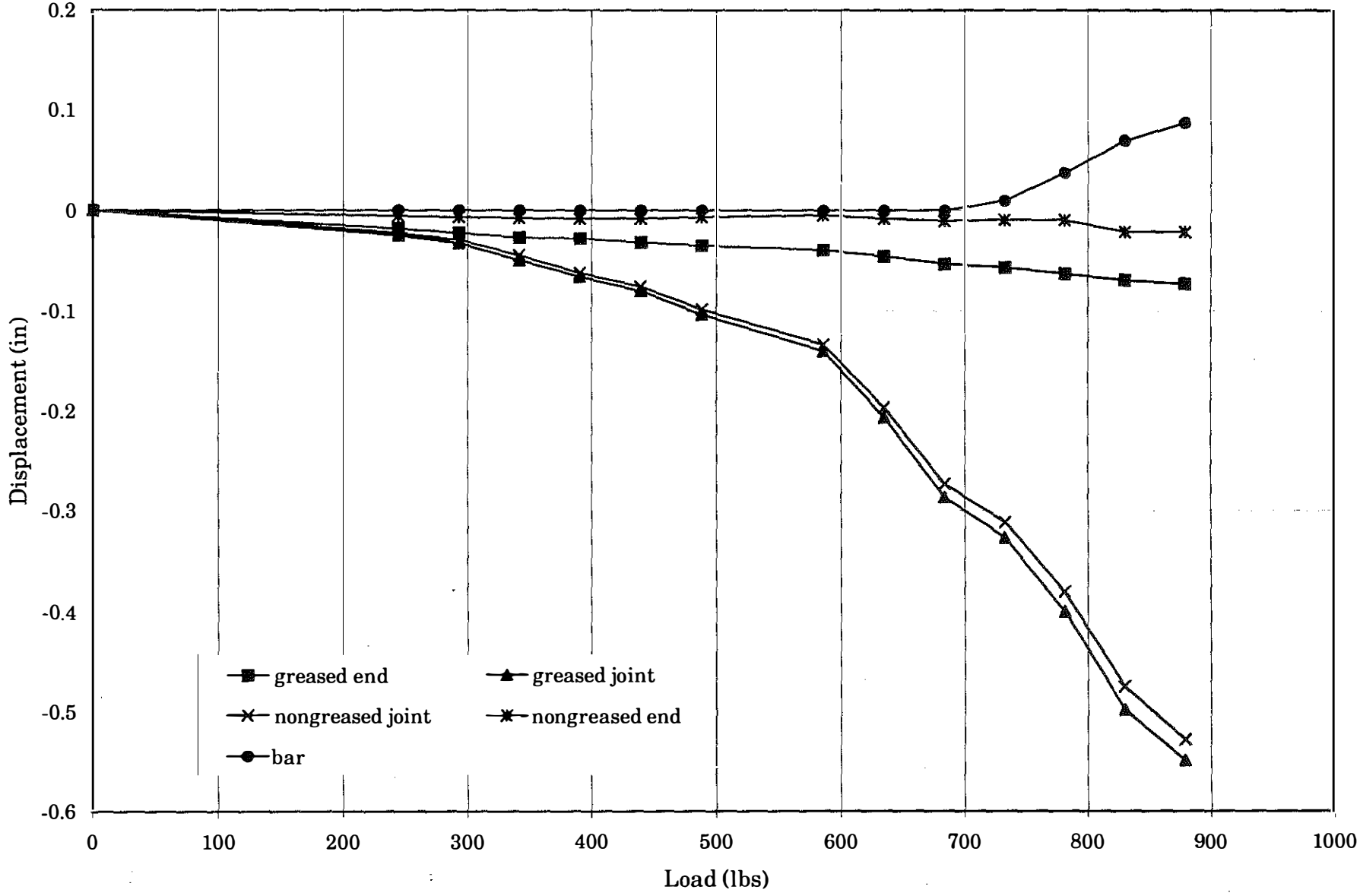

Figure III.7b Load (greased side)-Displacement Relationship for the Specimen B7

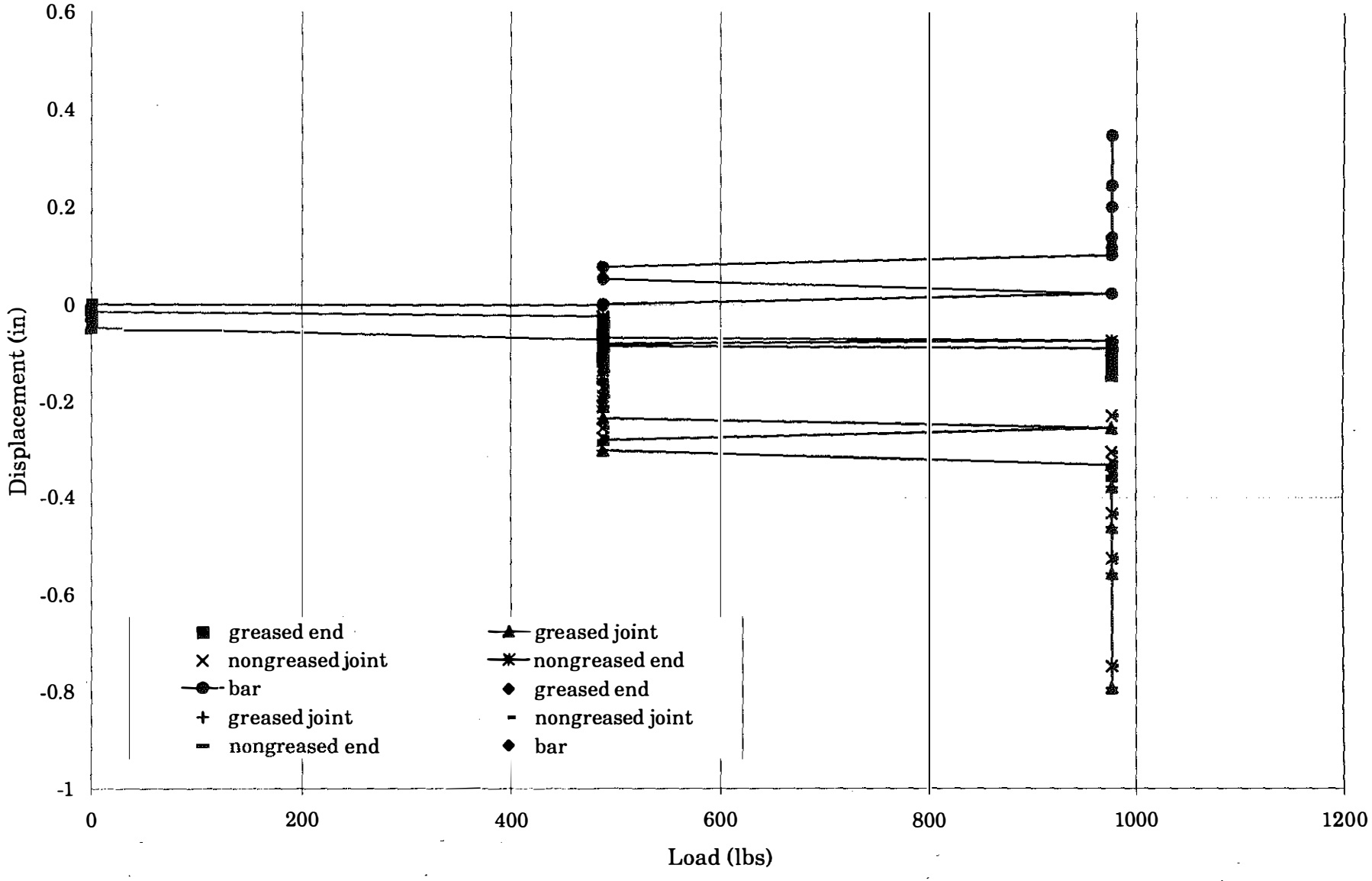

Figure III.8a Load(Nongreased side)-Displacement Relationship for the Specimen B8

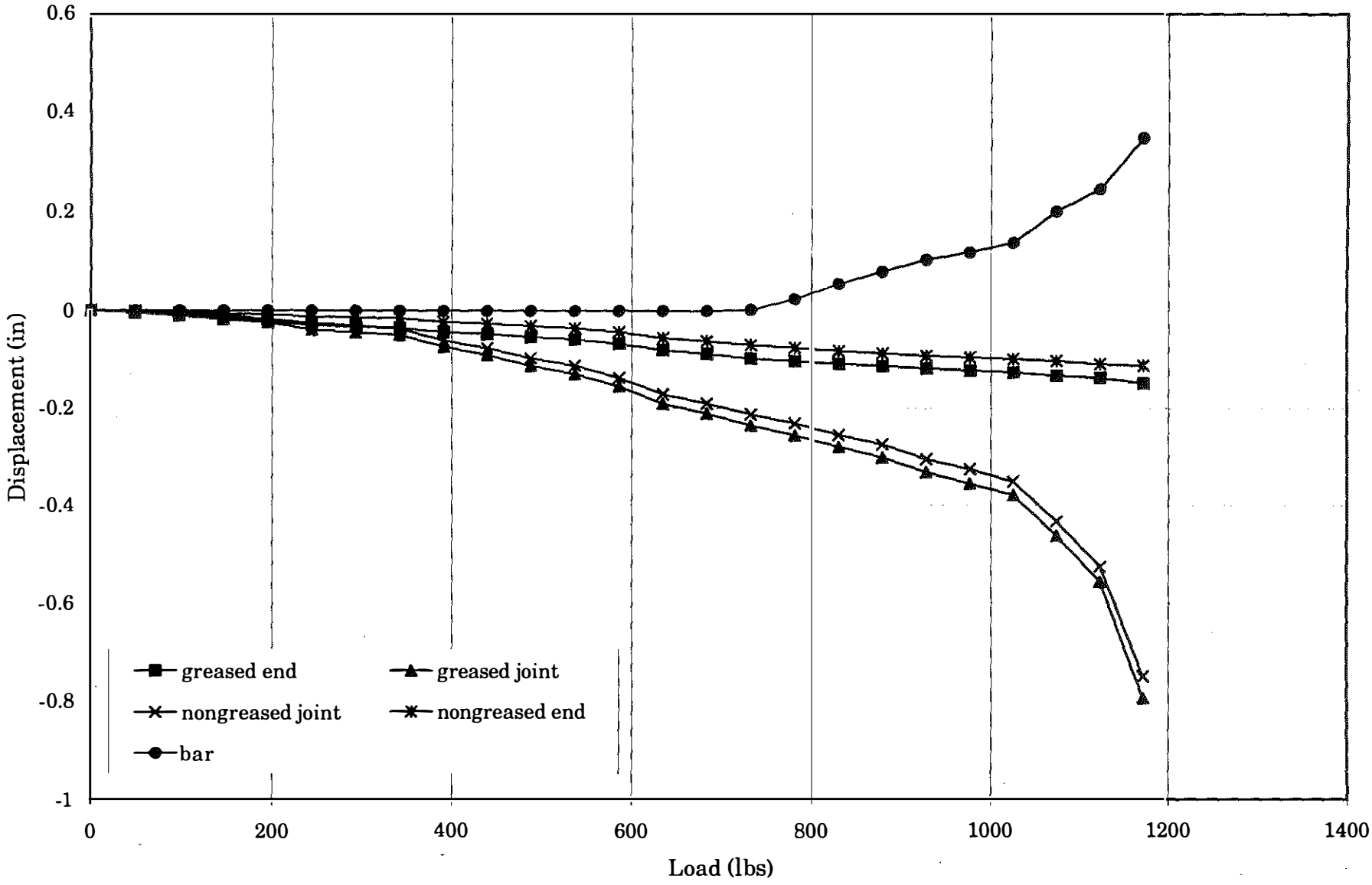

Figure III.8b Load (greased side)-Displacement Relationship for the Specimen B8

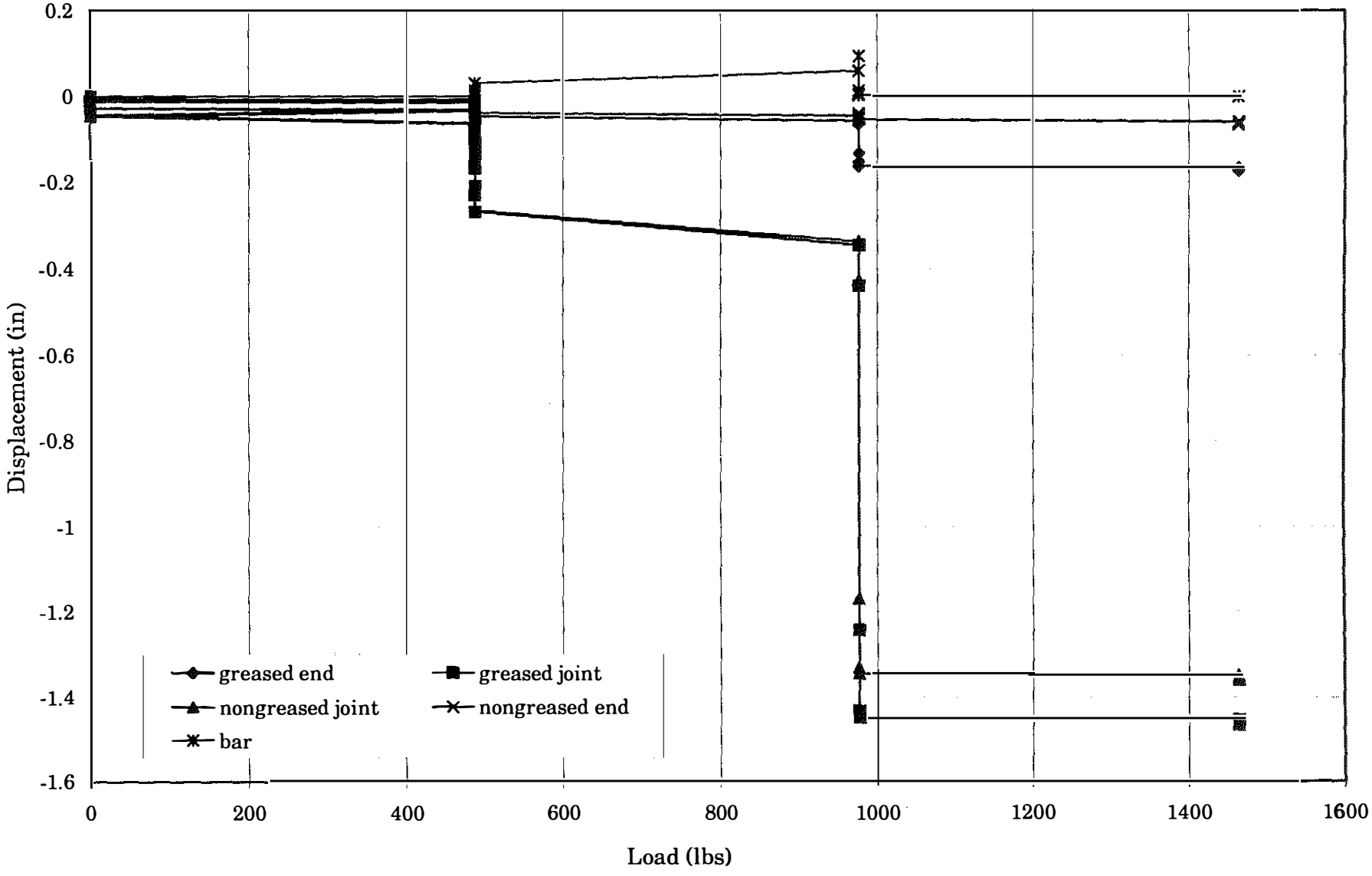

Figure III.9a Load (Nongreased side)-Displacement Relationship for the Specimen B9

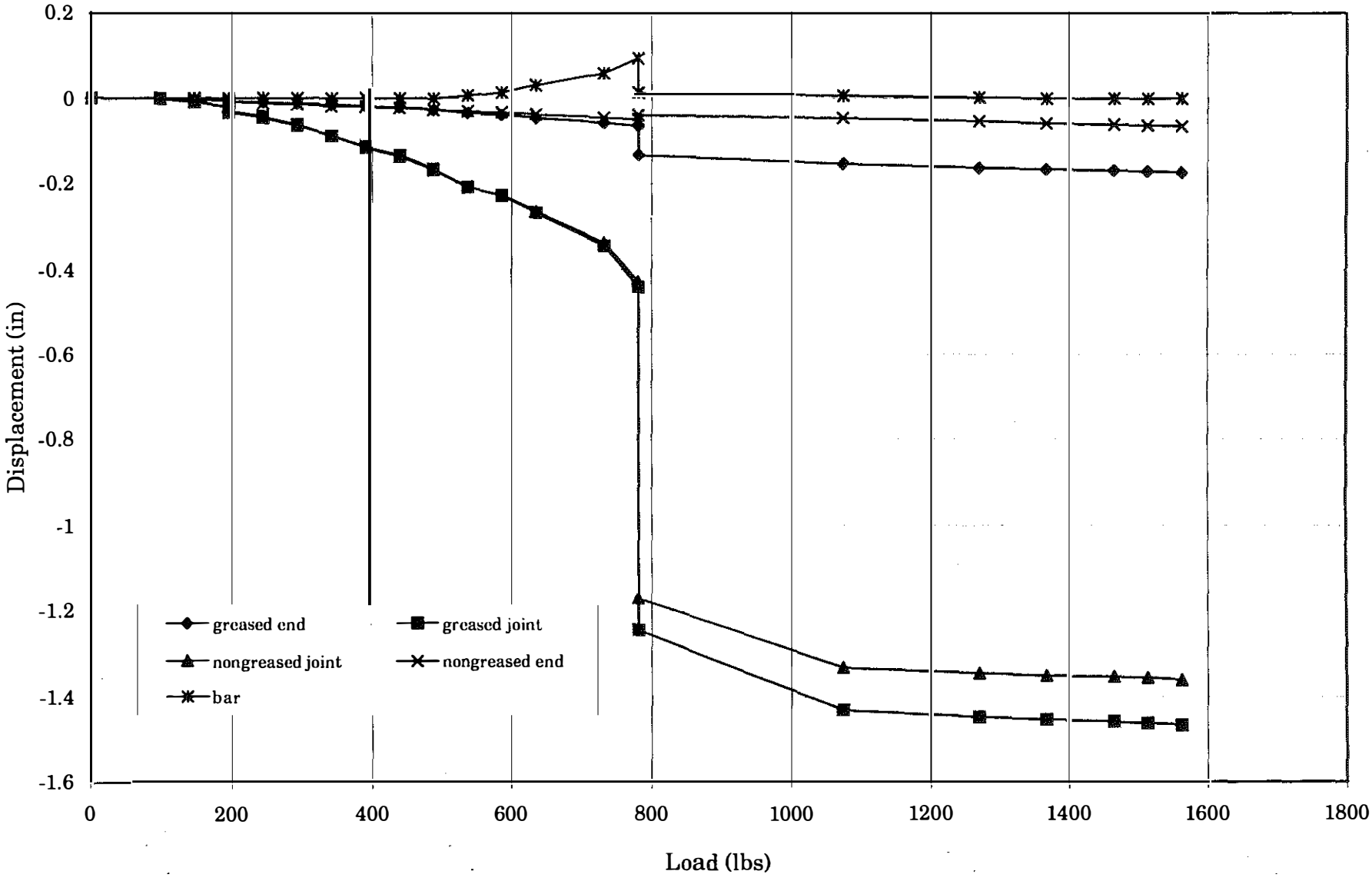

Figure III.9b Load (Greased Side)-Displacement Relationship for the Specimen B9

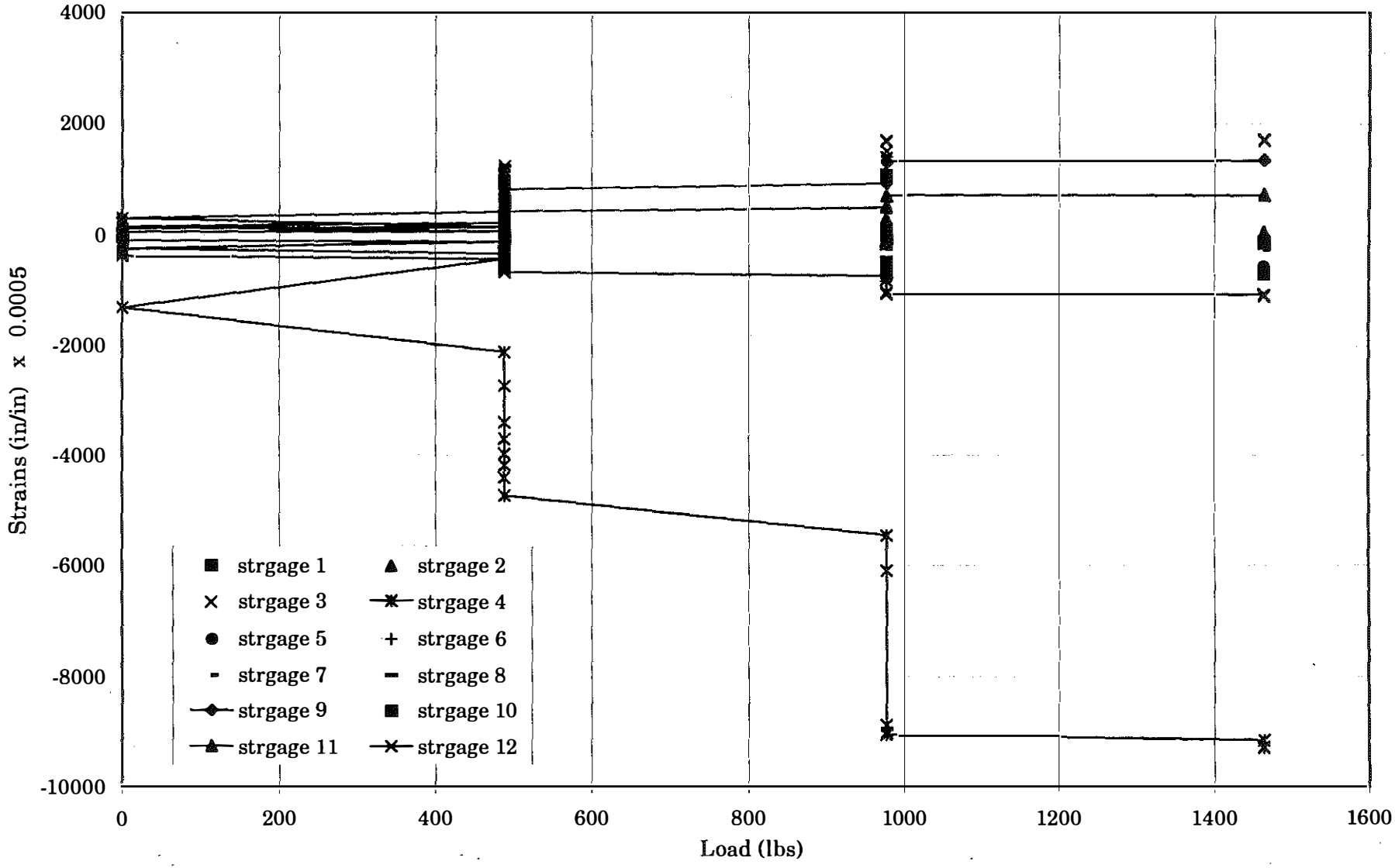

Figure III.9c Load (Nongreased Side)-Strain Relationship for the Specimen B9

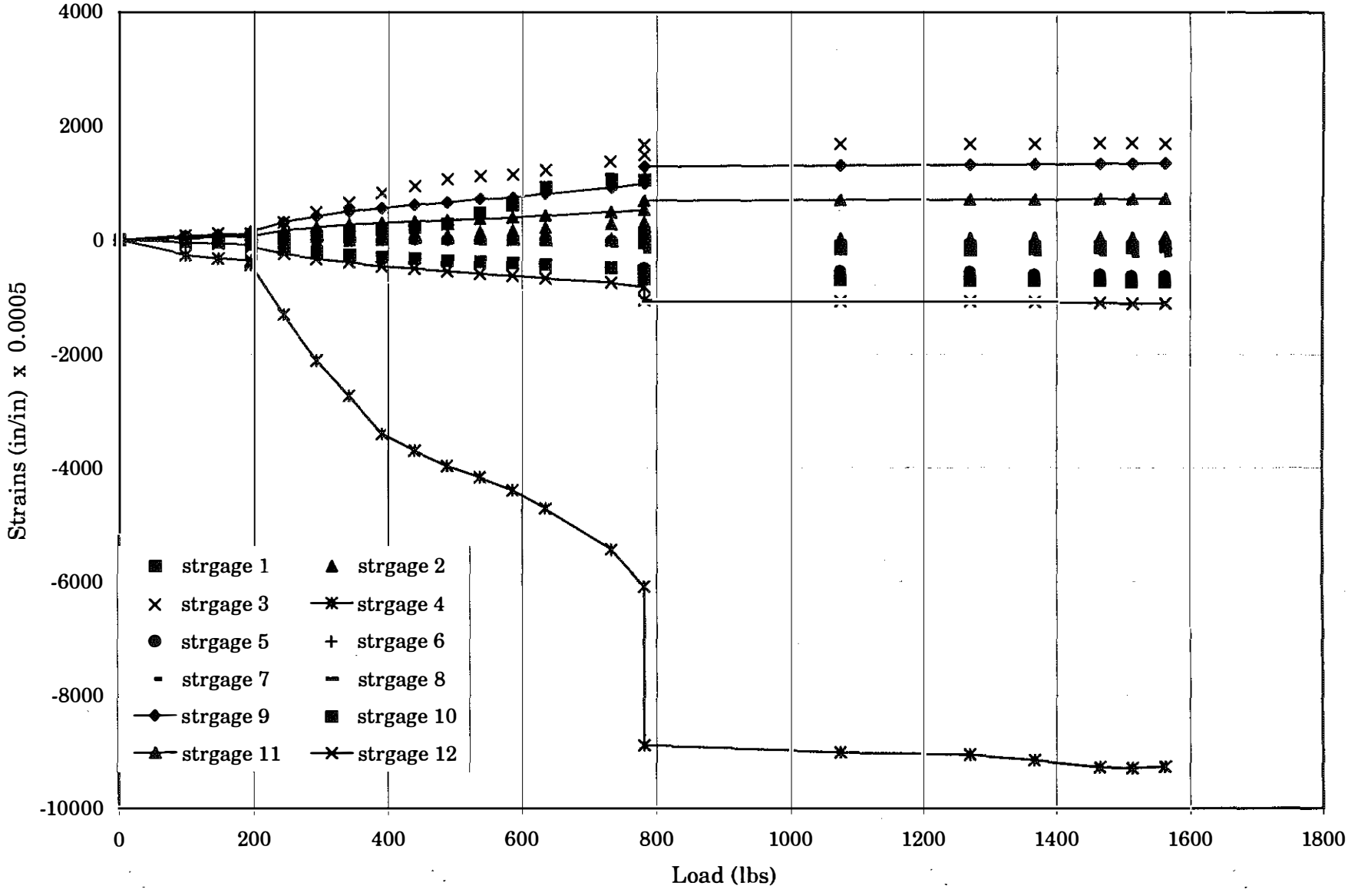

Figure III.9d Load (Greased side)-Strain Relationship for the Specimen B9

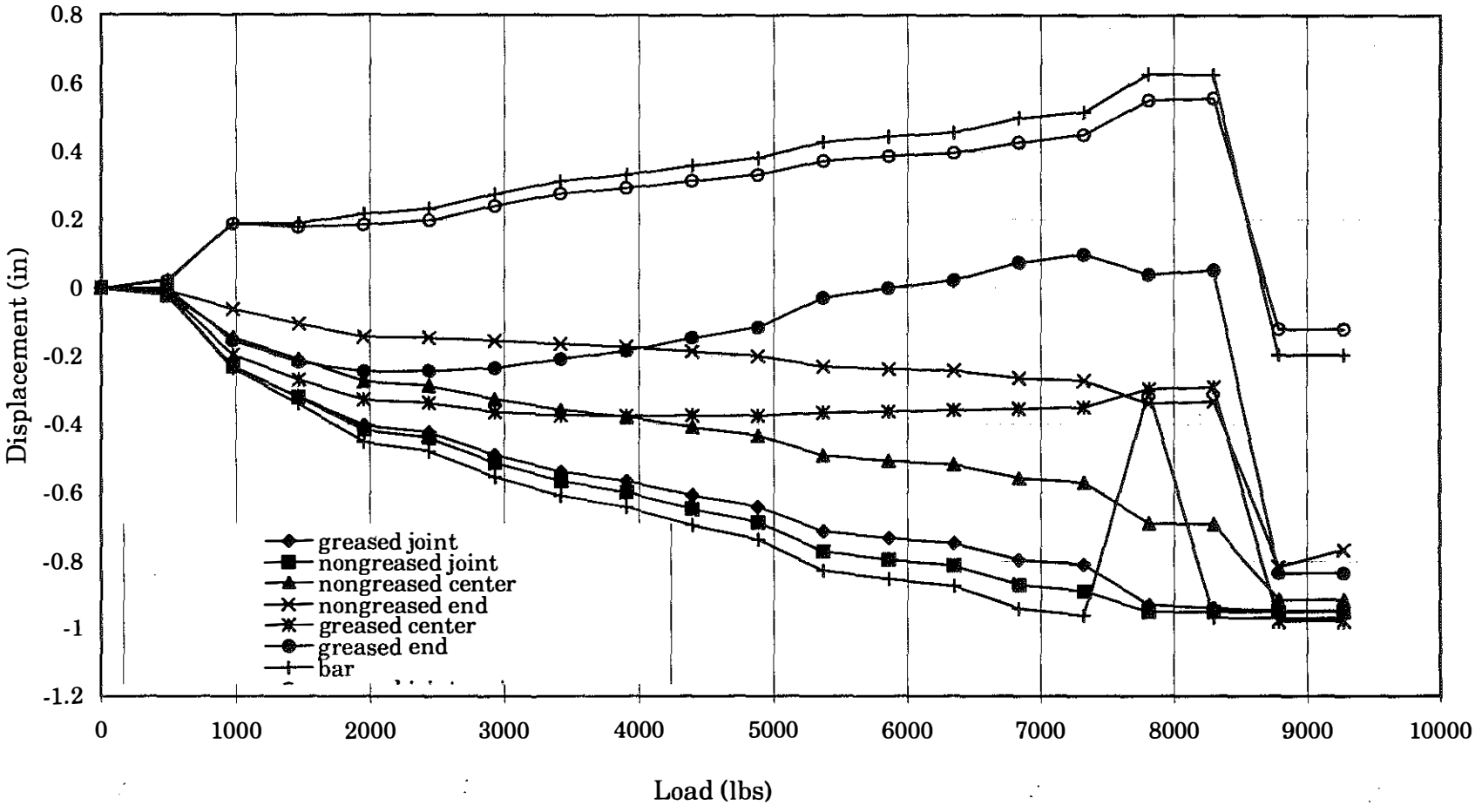

Figure IV.1 Load-Displacement Relationship for the C1 Specimen

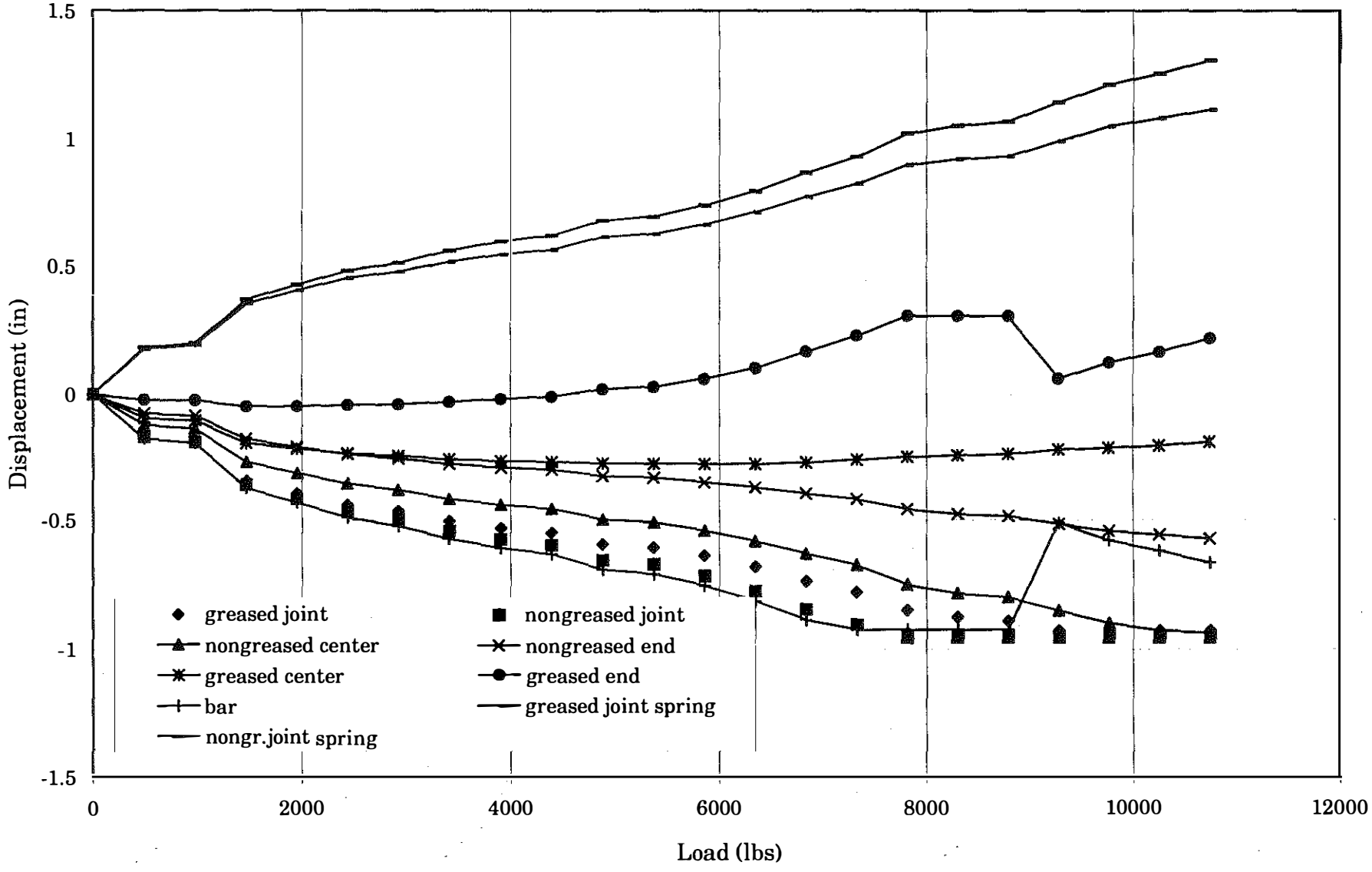

Figure IV.2 Load-Displacement Relationship for the Specimen C2

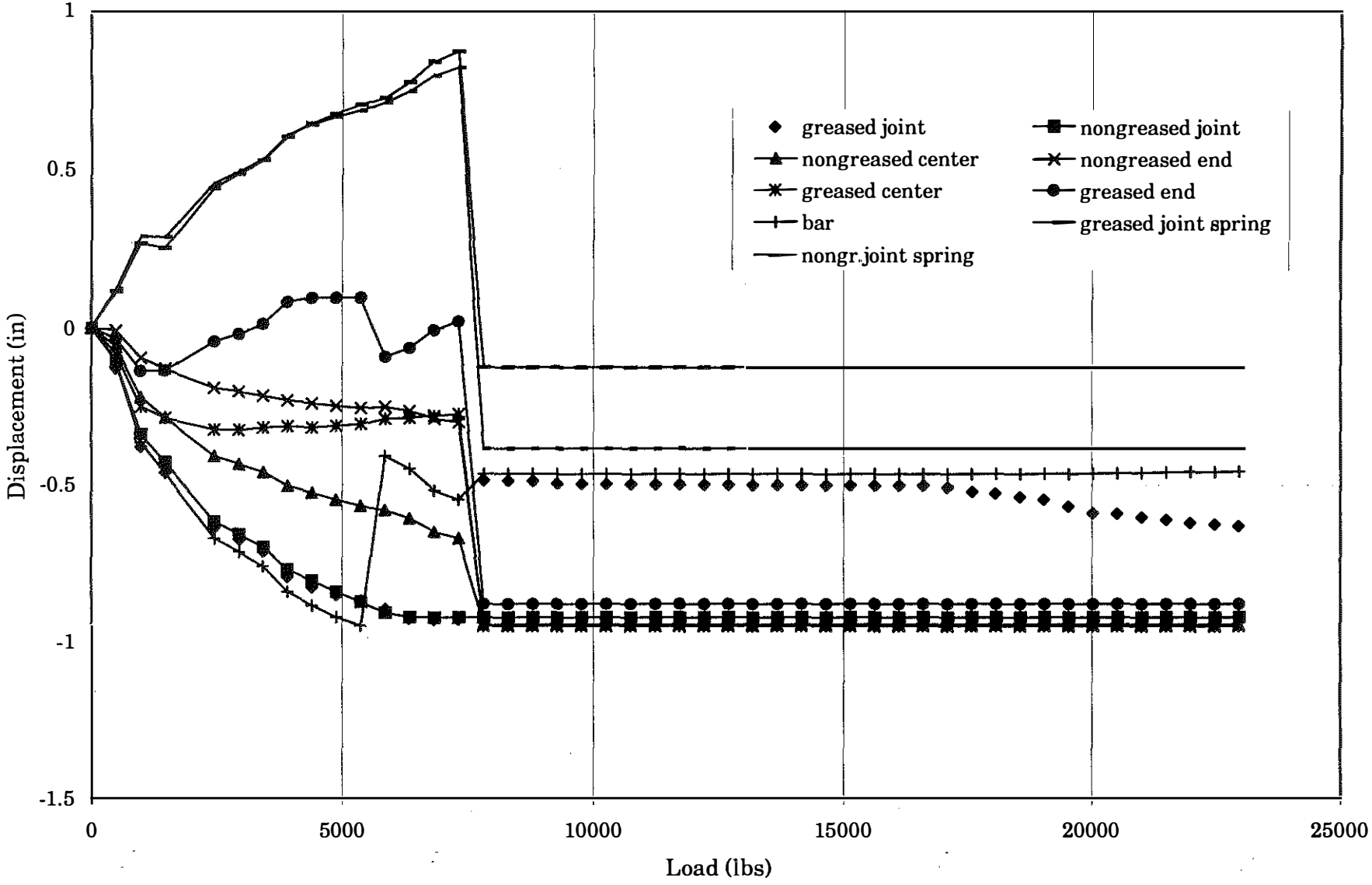

Figure IV.3a Load-Displacement Relationship for the Specimen C3

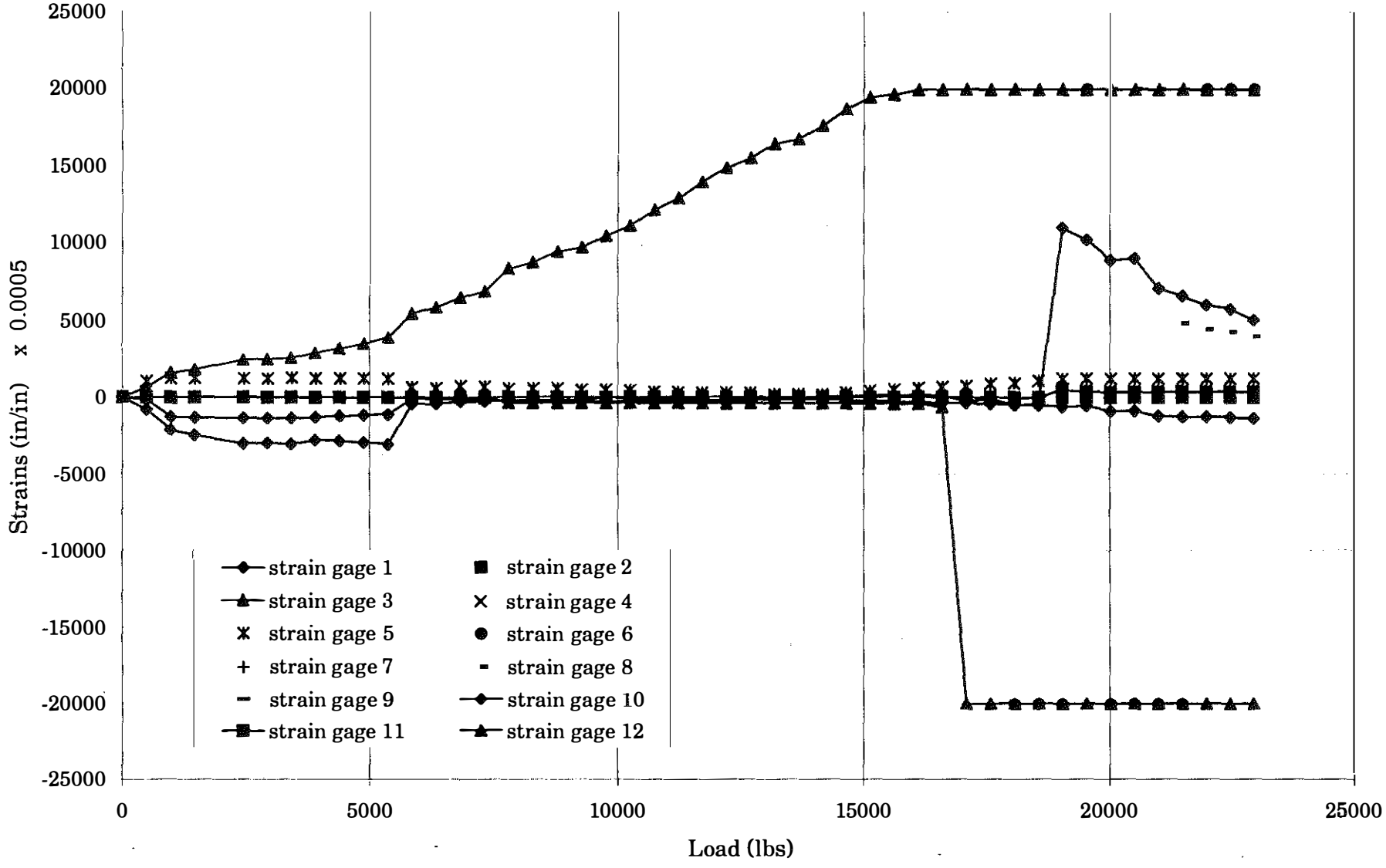

Figure IV.3b Load-Strain Relationship for the Specimen C3

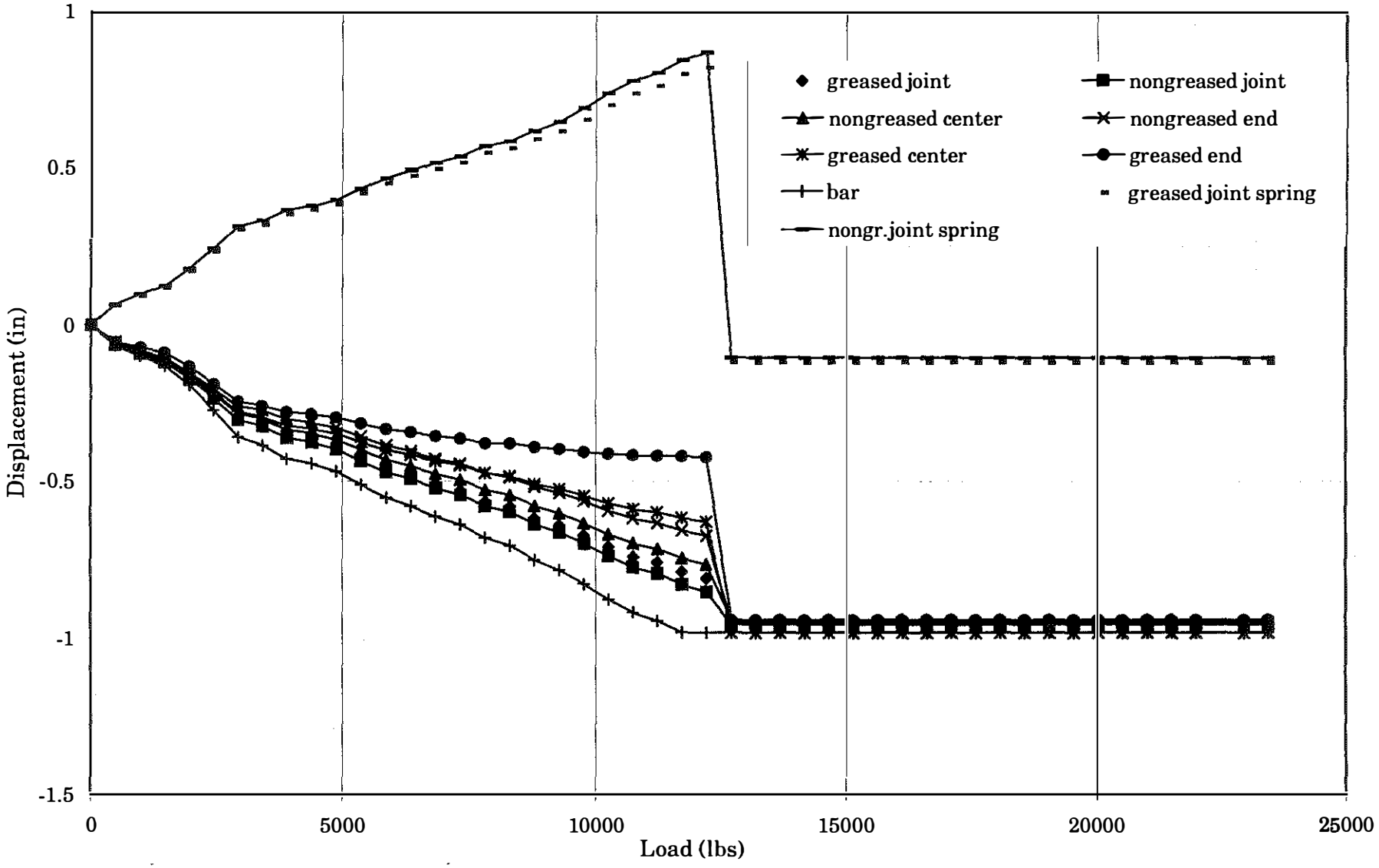

Figure IV.4 Load-Displacement Relationship for the C4 Specimen

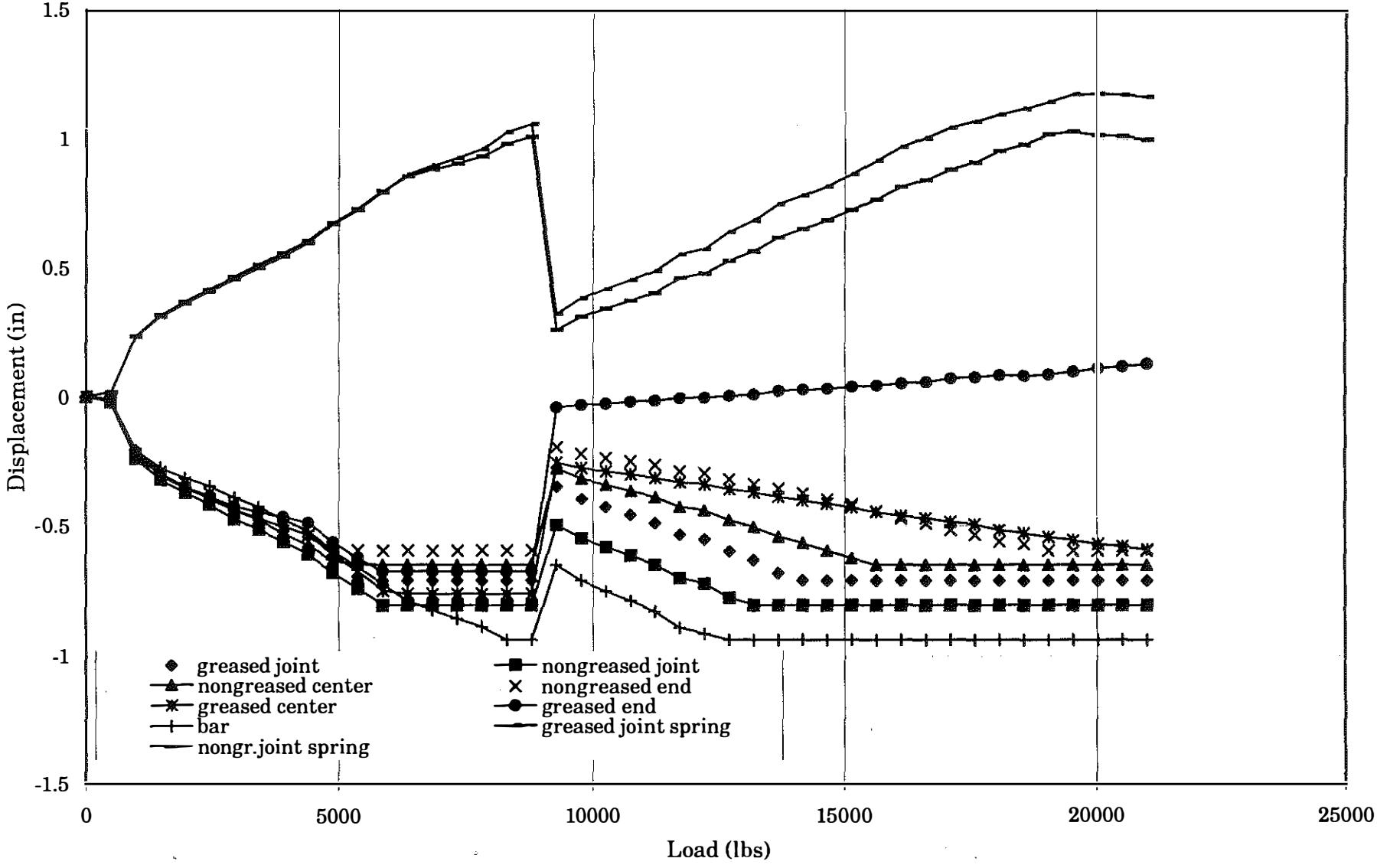

Figure IV.5 Load-Displacement Relationship for the Specimen C5

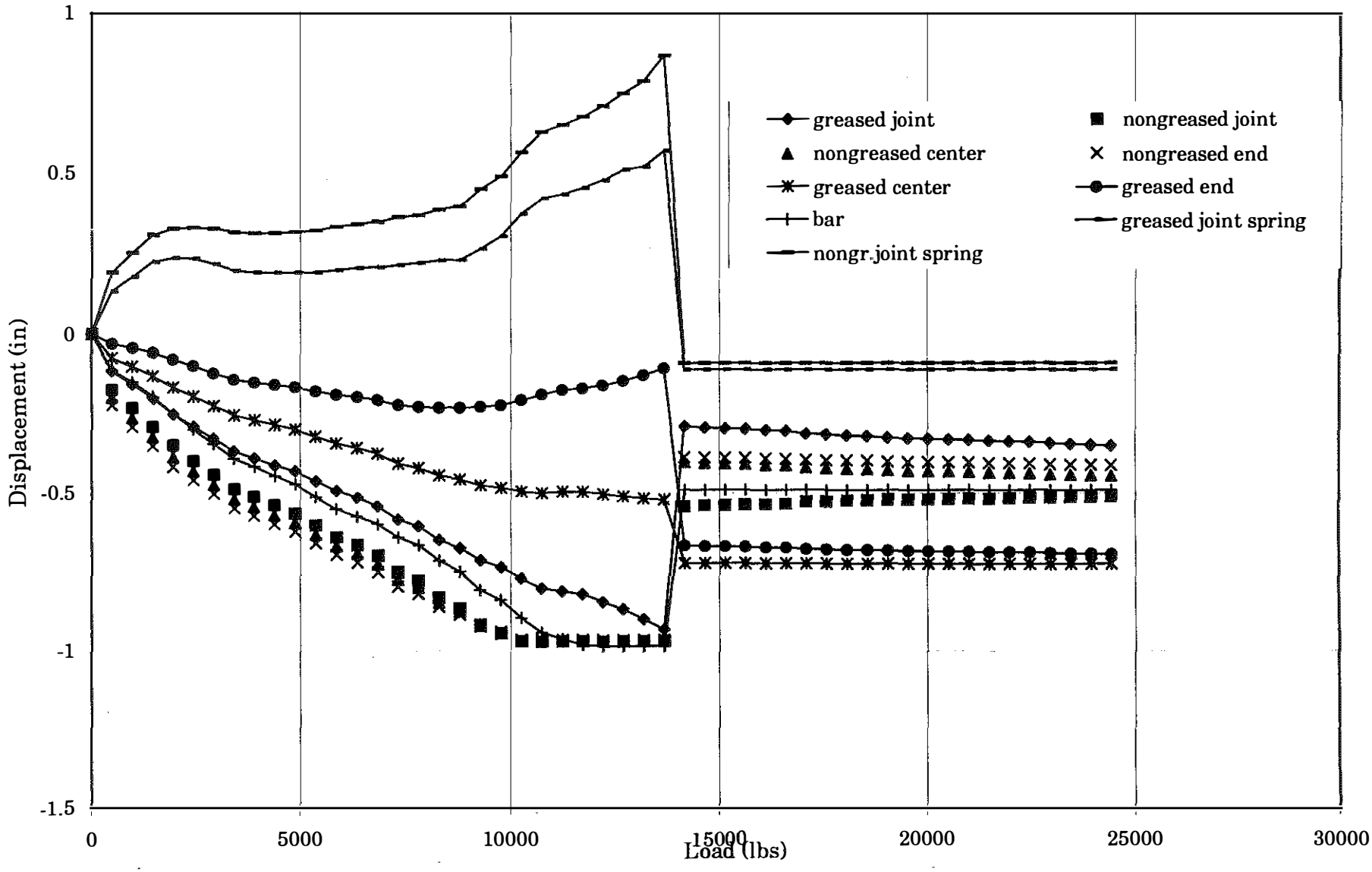

Figure IV.6a Load-Displacement Relationship for the Specimen C6

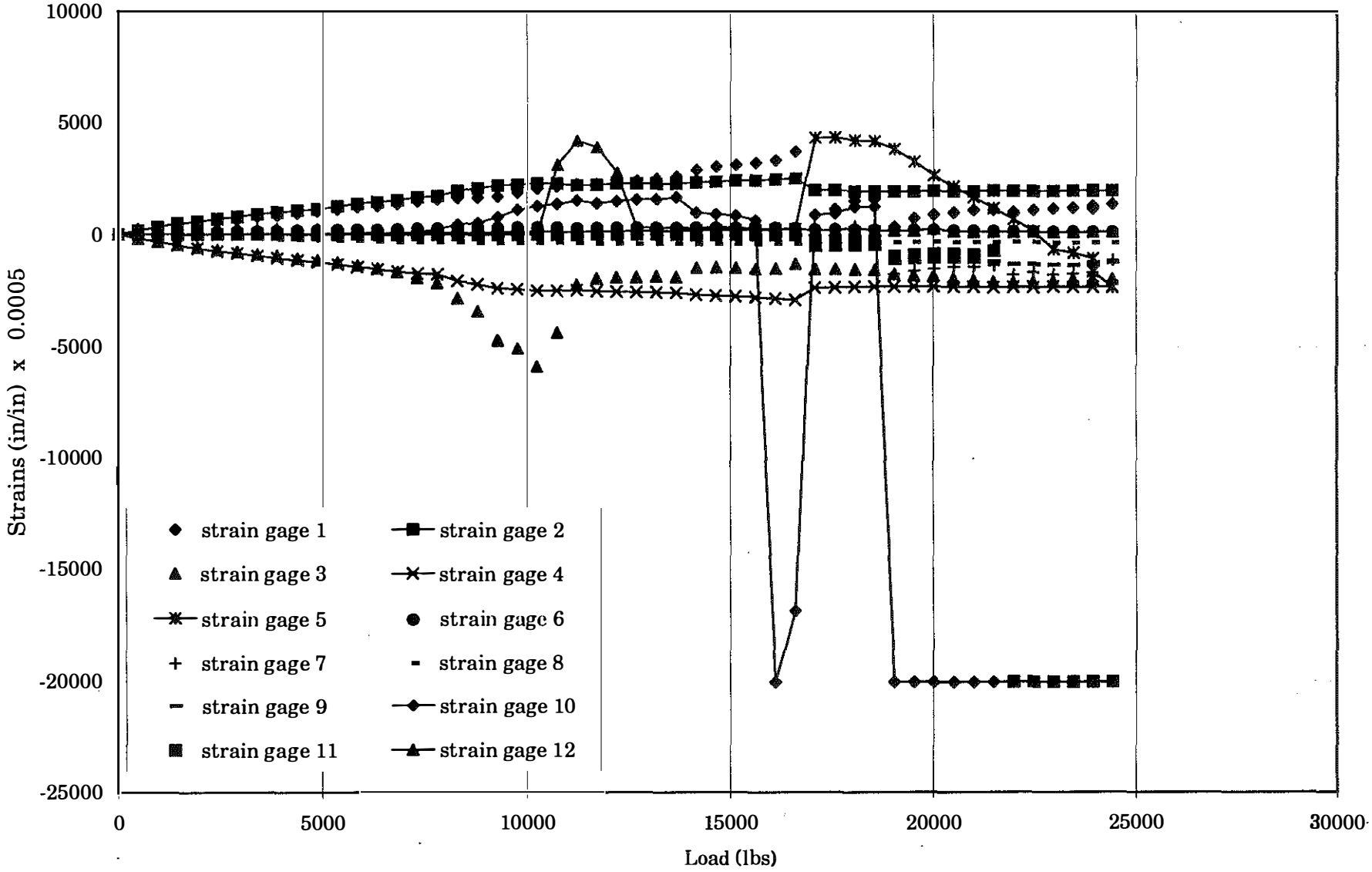

Figure IV.6b Load-Strain Relationship for the Specimen C6

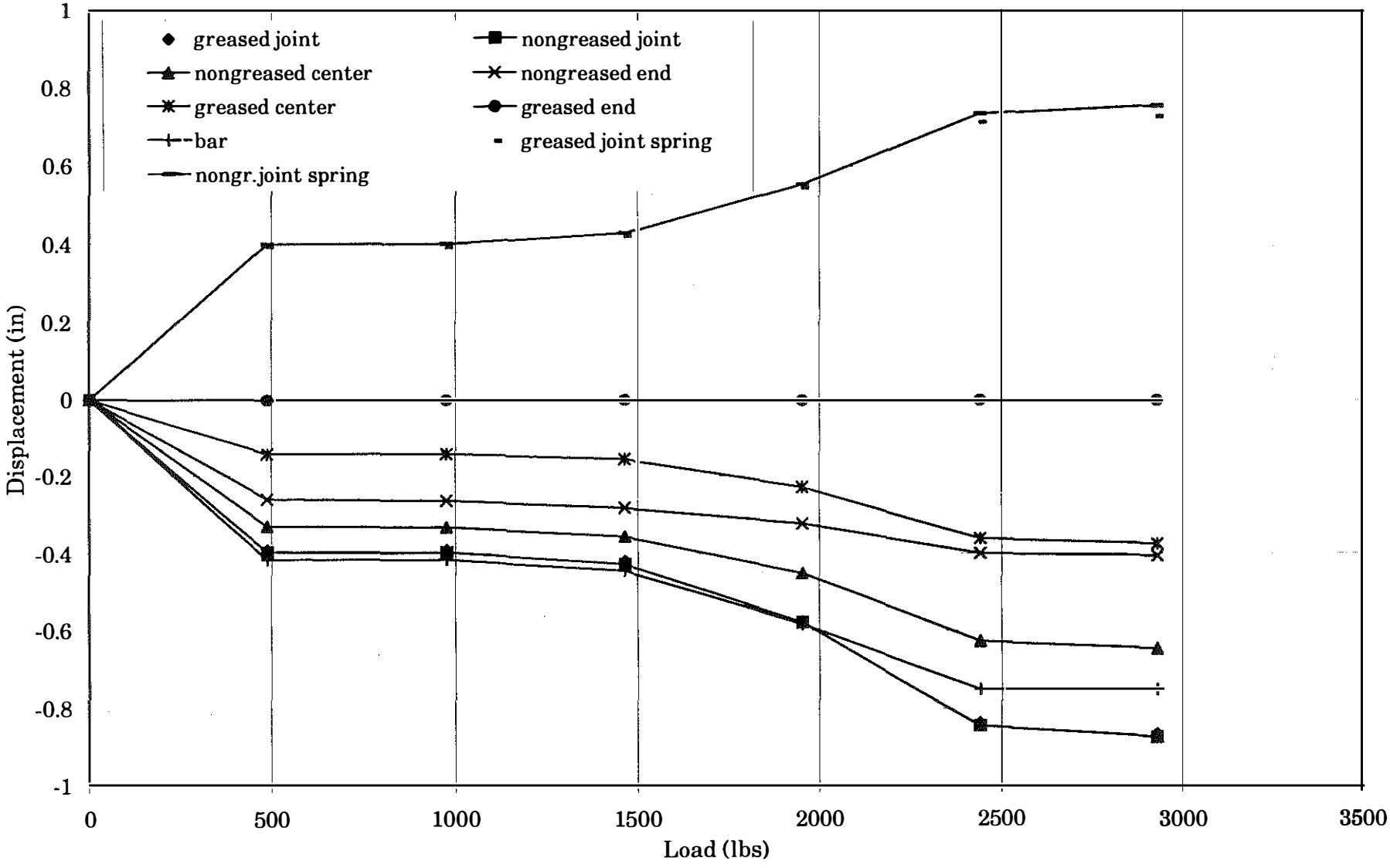

Figure IV.7 Load-Displacement Relationship for the Specimen C7

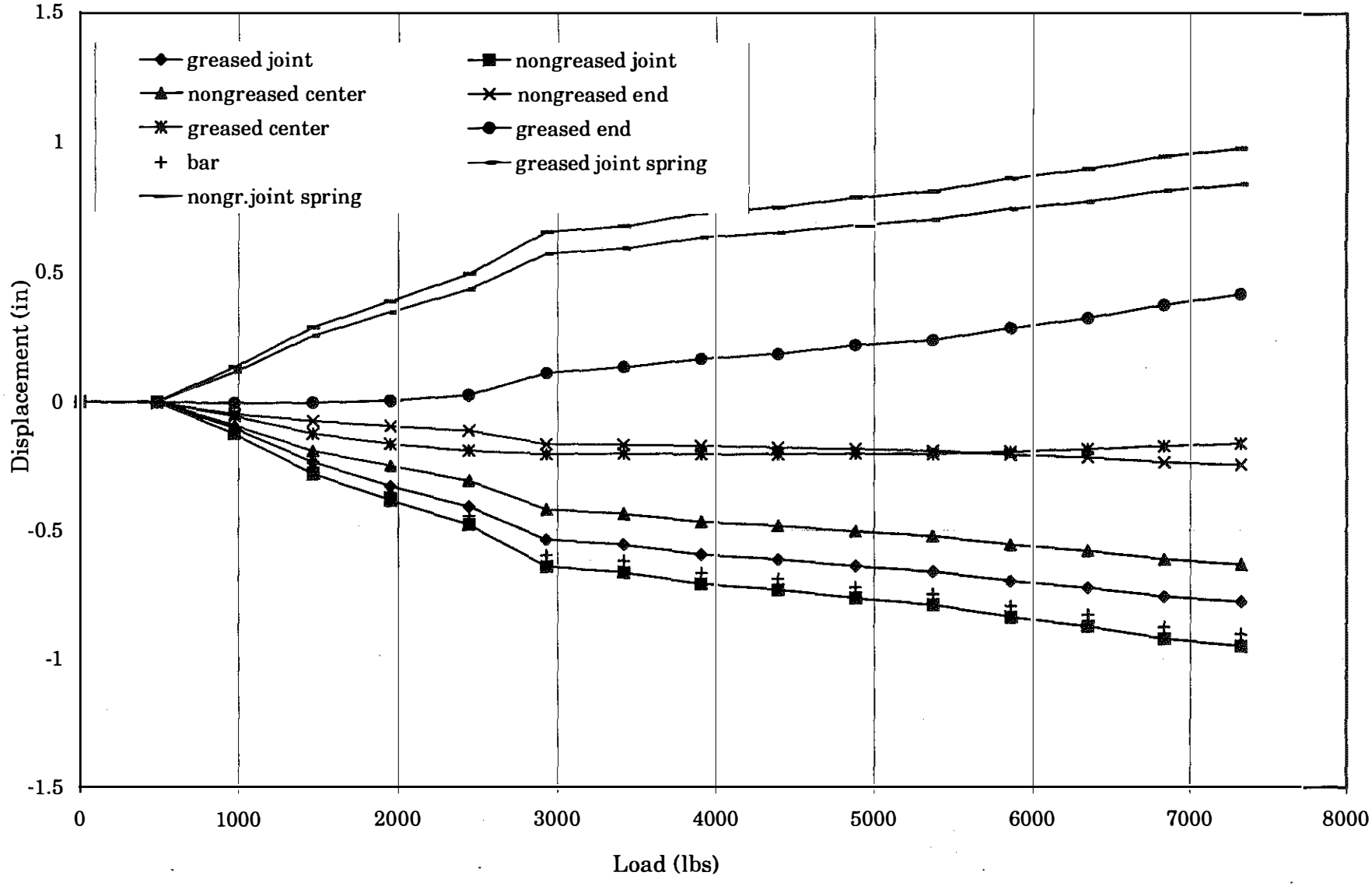

Figure IV.8 Load-Displacement Relationship for the Specimen C8

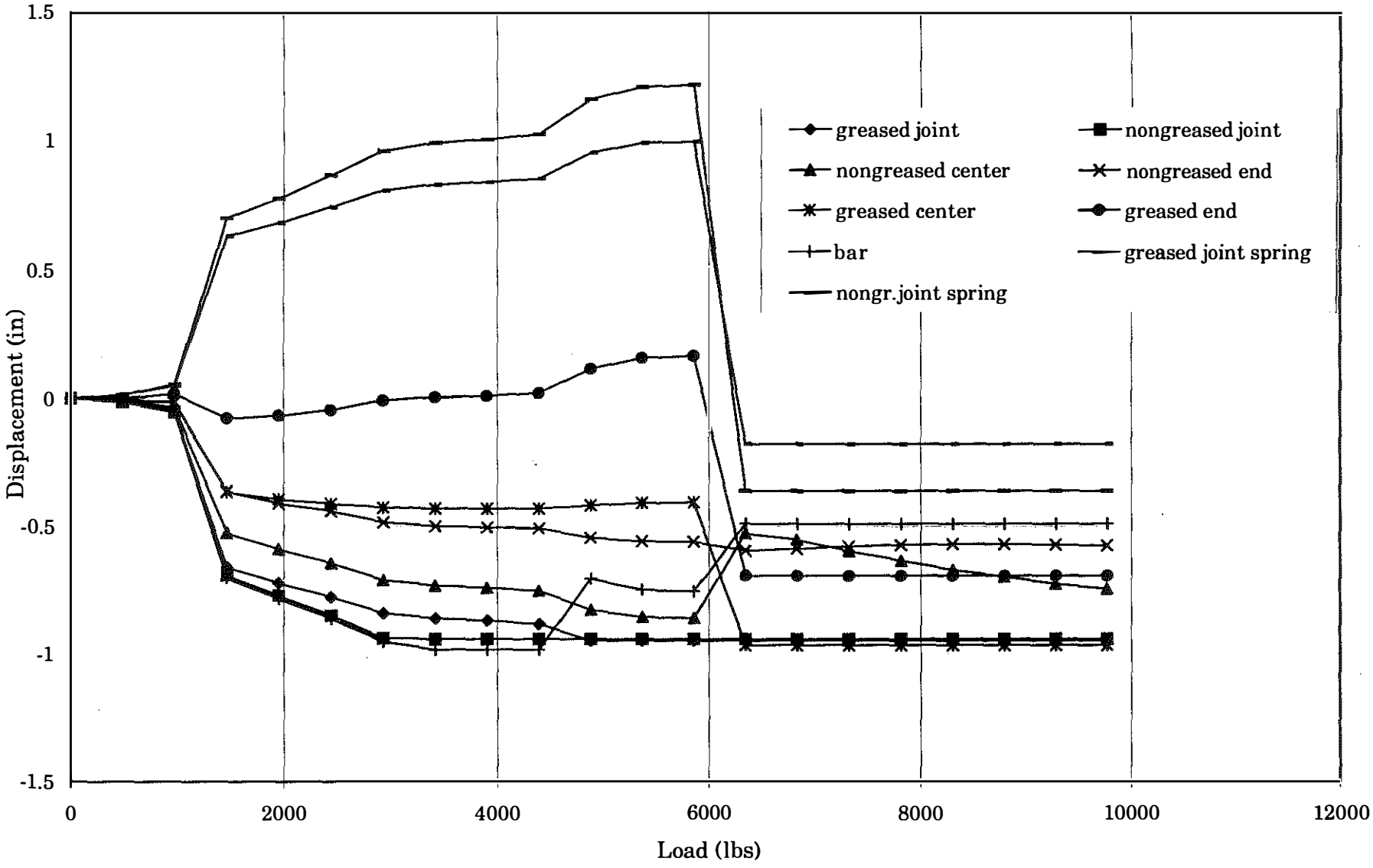

Figure IV.9a Load-Displacement Relationship for the Specimen C9

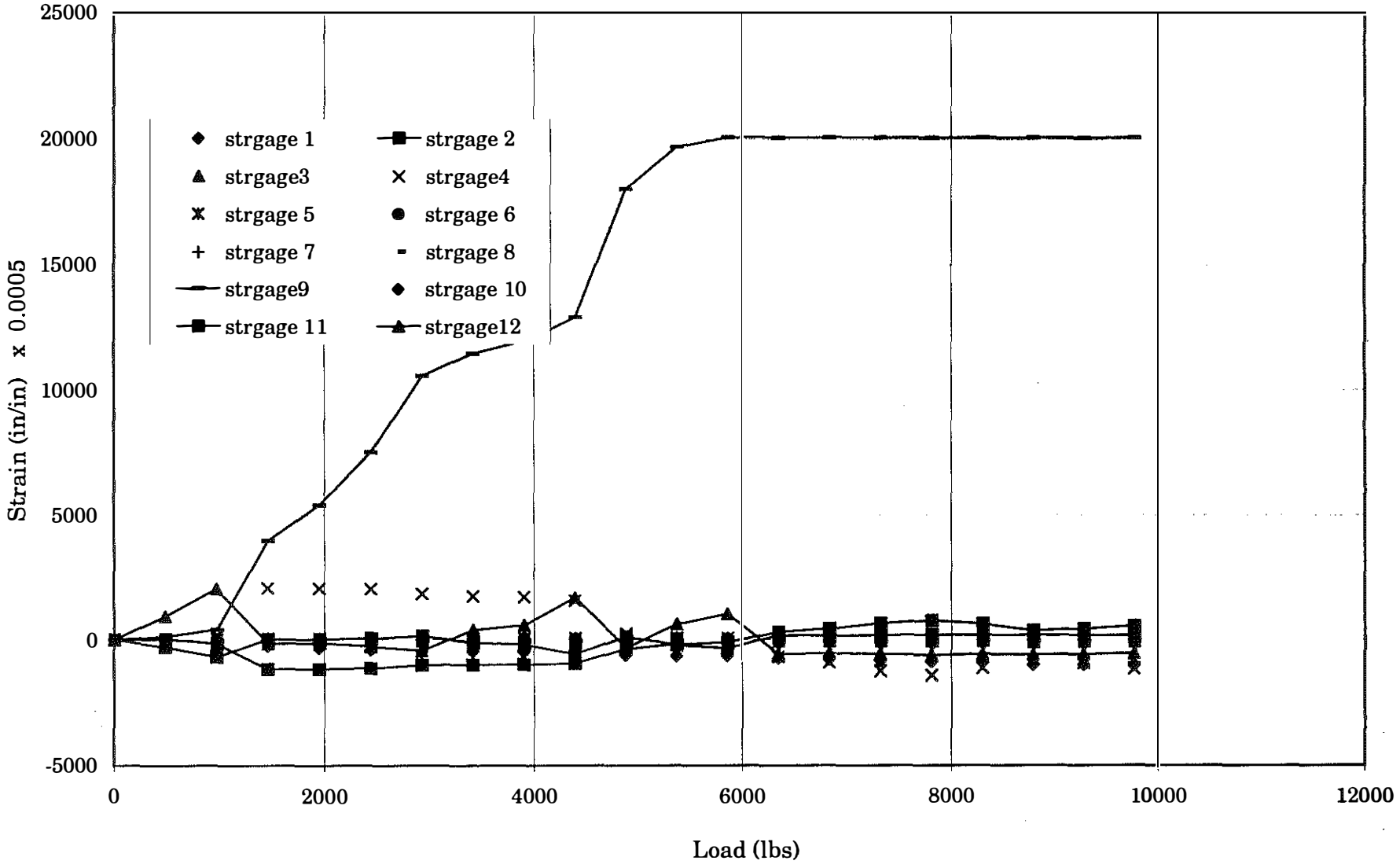

Figure IV.9b Load-Strain Relationship for the Specimen C9